

THE MANY-FACETED LIGHT CURVES OF YOUNG DISK-BEARING STARS IN UPPER SCO AND ρ OPH OBSERVED BY *K2* CAMPAIGN 2

ANN MARIE CODY^{1,2}, LYNNE A. HILLENBRAND³

Draft version June 28, 2018

ABSTRACT

The *K2* Mission has photometrically monitored thousands of stars at high precision and cadence in a series of \sim 80-day campaigns focused on sections of the ecliptic plane. During its second campaign, *K2* targeted over 1000 young stellar objects (YSOs) in the \sim 1–3 Myr ρ Ophiuchus and 5–10 Myr Upper Scorpius regions. From this set, we have carefully vetted photometry from *WISE* and *Spitzer* to identify those YSOs with infrared excess indicative of primordial circumstellar disks. We present here the resulting comprehensive sample of 288 young disk-bearing stars from B through M spectral types and analysis of their associated *K2* light curves. Using statistics of periodicity and symmetry, we categorize each light curves into eight different variability classes, notably including “dippers” (fading events), “bursters” (brightening events), stochastic, and quasi-periodic types. Nearly all (96%) of disk-bearing YSOs are identified as variable at 30-minute cadence with the sub-1% precision of *K2*. Combining our variability classifications with (circum)stellar properties, we find that the bursters, stochastic sources, and the largest amplitude quasi-periodic stars have larger infrared colors, and hence stronger circumstellar disks. They also tend to have larger H α equivalent widths, indicative of higher accretion rates. The dippers, on the other hand, cluster toward moderate infrared colors and low H α . Using resolved disk observations, we further find that the latter favor high inclinations, apart from a few notable exceptions with close to face-on disks. These observations support the idea that YSO time domain properties are dependent on several factors including accretion rate and view angle.

1. INTRODUCTION

Pre-main-sequence stars are highly variable due to mechanisms operating in or near the stellar photosphere, in the magnetosphere and innermost circumstellar disk regions, or in the disk atmosphere over a broader range of stellocentric radii. Specific processes include: rotation of hot and cold photospheric star spots, fluctuations in the accretion flow from the circumstellar disk onto the star (the rate and/or the geometry), and asymmetry in the density or the geometry of the disk material that traverses our line-of-sight as the star, magnetosphere, and inner disk all co-rotate. Variability thus probes a diverse set of physical processes. While the phenomenology and interpretation of young star variability has received attention since the work of Joy (1945), followed by, e.g., Herbig (1954) and Walker (1954), it is only in the last several years that high-quality light curves have become commonplace for young stars. Multi-week duration and high cadence observations (e.g. Cody & Hillenbrand 2010, 2011; Cody et al. 2014) complement work spanning longer multi-year duration but at much lower cadence (e.g. Findeisen et al. 2015; Parks et al. 2014; Rice et al. 2012).

The Cody et al. (2014) study of 1–3 Myr old stars in NGC 2264, based on high-quality space-based photometry from *CoRoT* Baglin et al. (2006), established the light curve morphology infrastructure that we use as the basis for this work. Metrics established therein enable ranking

of sources along two axes: one a scale ranging from pure periodicity to complete stochasticity in terms of pattern repetition within the light curve, and the other a scale of flux asymmetry, ranging from predominantly fading or dipping (exhibiting short-term fades) to predominantly rising or bursting (exhibiting short-term flux increases).

Subsequent work with Kepler in its *K2* mission (Howell et al. 2014) has further defined and refined sub-categories of young star variability within the basic framework. Specifically, the *K2* Field 2 pointing encompassed the Upper Scorpius region of recent star formation, as well as the molecular cloud near ρ Ophiuchus in which star formation is ongoing. Periodic objects are studied in detail by Rebull et al. (2018) in the context of pre-main sequence rotation evolution. Sub-categories known as “scallop shells” and “persistent/transient flux dips” are discussed by Stauffer et al. (2017) and David et al. (2017), and are interpreted as structures associated with the magnetospheric region in rapidly rotating, diskless, low mass young stars. “Bursters”, discussed by Cody et al. (2017) are interpreted as discrete accretion events lasting hours to about a week, and can be quasi-periodic, while “dippers” are interpreted as obscuring dust clumps that are associated with either disk structure or orbiting bodies and semi-periodically cross the line of sight. Herein we present a comprehensive light curve census for the disk-bearing members of Upper Sco and ρ Oph.

Extinction is quite high towards “ ρ Oph” but some cluster members, typically those of higher mass, are bright enough for study with *K2*. The sizable young “Upper Sco” association (see Preibisch & Mamajek 2008, for a review) is essentially gas free but there is a small amount of dust extinction ($A_V < 1$). The association

¹ NASA Ames Research Center, Moffett Field, CA 94035

² Bay Area Environmental Research Institute, 625 2nd St., Suite 209, Petaluma, CA 94952

³ Department of Astronomy, California Institute of Technology, Pasadena CA 91125

samples a wide range in mass – from mid-B type stars having several to ten solar masses, all the way down to late M-type, very low mass stars and sub-stellar mass objects. Notable studies include the early kinematic work that culminated in Preibisch et al. (2002) as well as contemporaneous x-ray (e.g. Köhler et al. 2000) and wide-field optical (e.g. Ardila et al. 2000) studies, through to the most recent additions to the stellar population by e.g. Rizzuto et al. (2011, 2015). For ρ Oph, Wilking et al. (2008) provides a compilation of accepted members. Based on this literature (plus in a few cases, original unpublished survey work), the young star community generated sets of stars that were submitted for observation with *K2*.

Relative to NGC 2264, which was observed with high precision and cadence photometry by *CoRoT*, the older 3–10 Myr old Upper Scorpius region observed by *K2* offers a somewhat more evolved disk population to investigate. The younger 1–3 Myr old ρ Oph region that is adjacent to Upper Sco should be comparable to the NGC 2264 population in terms of disk fraction, though the population is more heavily extinguished. We consider both Upper Sco and ρ Oph together when defining the sample for investigation and categorizing the variability, but do assess the distribution among the different light curve families separately, in comparing to NGC 2264.

The outline of the paper is as follows. §2 describes the sample selection, beginning with all objects proposed for observation in the *K2* Field 2 Campaign and down-selecting to consider only disk-bearing sources, similar to in Cody et al. (2014). §3 discusses the *K2* data processing and photometry, and §4 the selection of variable light curves. The variability classes are assigned in §5 based on the “Q” and “M” metrics for periodicity and flux asymmetry, respectively. §6 presents and the relationship between light curve morphology and circumstellar disk properties. Finally, §7 presents comparison of the present results to other recent studies of *K2/C2* data, and §8 our summary and discussion.

2. SAMPLE

To parallel our efforts in NGC 2264, we aimed to assemble and analyze as complete a set of light curves as possible for young, low-mass disk-bearing stars among the *K2* Campaign 2 targets. We initially selected objects submitted under programs GO2020, GO2047, GO2052, GO2056, GO2063, and GO2085, all specifically targeting Upper Scorpius and ρ Ophiuchus members or candidate members. At a later point, we became aware that aperiodic variability is exhibited among some of the targets in additional programs observing cool dwarf stars, suggestive of young star behavior. As a result, we added objects from programs GO2104, GO2051, GO2054, GO2069, GO2029, GO2106, GO2089, GO2092, GO2049, GO2045, GO2107, GO2075, and GO2114 to our sample, but only if their proper motions were suggestive of membership in the Upper Sco region. This resulted in a set of 2072 potential young stars, upon which we made further cuts based on WISE photometry. One eliminated likely field star interlopers (as described in §2.1 with 587 stars removed) and another selected only the warm inner-disk-bearing systems (see §2.2 with 1137 stars removed). The set of light curves considered in this work (Table 1) includes 340 young stars with presumably primordial cir-

cumstellar disks, of which 288 are considered to have suitably good quality light curves for further analysis.

We spatially divided this sample into ρ Oph and Upper Sco sets by considering the coordinates of each star. There is an overdensity of *K2* sources in a $1.2^\circ \times 1.2^\circ$ square surrounding the position RA=146.79, Dec=−24.60. The square shape is likely an artifact of target selection for various *K2* programs. Nevertheless, we have used it as our boundary to roughly separate the young stars near the ρ Oph core from the older ones in the less nebulous surrounding regions (see further discussion in Cody et al. (2017)). We find that this method yields a similar sample than that generated with an $A_V > 2$ extinction contour.

2.1. Selection of young stars in Upper Sco and ρ Oph

Known members of Upper Sco and ρ Oph regions have already been vetted by, e.g., Ardila et al. (2000); Slesnick et al. (2006); Luhman & Mamajek (2012); Lodieu (2013); Rizzuto et al. (2015). However, the Upper Sco population is known to be incompletely cataloged, and there remain hundreds of photometric and proper motion selected candidate members to be confirmed or rejected. Many of these were included in the *K2* Campaign 2 proposals. For ρ Oph, Wilking et al. (2008) provide a compilation of accepted members which is thought to be relatively complete given the more compact distribution on the sky and the decades of deep infrared survey work in this region.

To assess which of the (mainly Upper Sco) candidates have photometry consistent with the expected 1–10 Myr old sequence of cluster members, we plotted near-infrared and mid-infrared color-magnitude diagrams for all objects with prior reports of being young and/or having proper motions consistent with membership in the Sco-Cen region, and compared them with the *K2* samples (Figures 1 and 2). Infrared data from the 2MASS and WISE missions is available for nearly all of the stars in our sample. Over 65% of these candidates do *not* appear in Luhman & Mamajek’s (2012; LM12) work. We therefore queried the IRSA database⁴ to match objects to infrared and near-infrared counterparts, using a 6'' matching radius to account for the large WISE pixels. This photometry is provided with flags, and we eliminated measurements for which the WISE band 1 or 2 signal-to-noise ratio (SNR) was less than 10, or for which the band 3 SNR was less than 7. In addition, we discarded photometry reported as affected by diffraction spike contamination, persistence, halo, or optical ghosts. The remaining datapoints were used to clean the *K2* sample of field stars, as described below.

A near-infrared H versus $J - K$ color-magnitude diagram (Figure 1) displays a clean and nearly vertical cluster sequence at low masses, with stars previously vetted by LM12 forming a narrower sequence among the broader set of *K2* observed stars. There are few stars blueward of $J - K = 0.8$, apart from the bright end ($H < 9$). There are many red outliers beyond $J - K = 1.3$ and these are likely disk-bearing objects (see §4). Although contaminants are present, the near-infrared color-magnitude diagram does not appear to have many interlopers.

⁴ <https://irsa.ipac.caltech.edu>

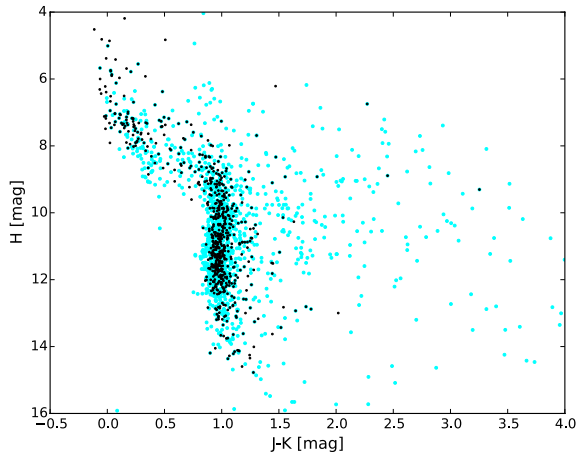


FIG. 1.— A 2MASS near-infrared color magnitude diagram of K2 Campaign 2 young star candidates (cyan) compared to known Upper Sco members from LM12 (black). The distinct sequence of pre-main sequence stars retains some field star contaminants due to the overlap in colors between young pre-main sequence and older post-main sequence stars.

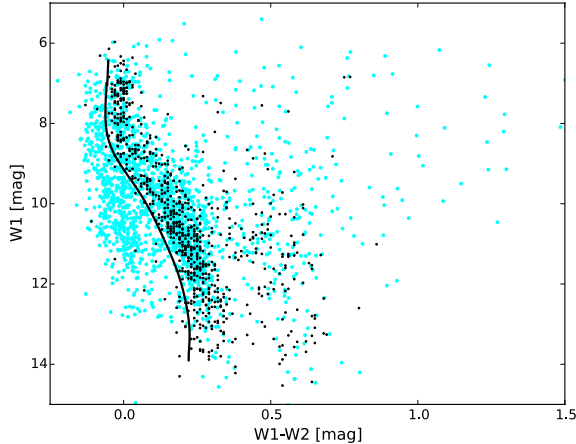


FIG. 2.— Similar to Figure 1, the mid-infrared WISE infrared color magnitude diagram shows all K2 targets in cyan, overlaid with the set of LM12 Upper Sco members in black. A large set of the targeted K2 stars are too blue to be in the Upper Sco region or ρ Oph cluster. The black points blueward of $W1 - W2 = 0.3$ display a distinct sequence, which we have fitted, and subsequently shifted to model the blue boundary. This boundary then serves as the cut-off between likely and unlikely young stars— the latter of which we remove from our sample.

A mid-infrared $W1$ versus $W1 - W2$ color-magnitude diagram (Figure 2), on the other hand, reveals that there is indeed a large population of field objects in the K2 candidate Upper Sco and ρ Oph sample. A clear cluster sequence once again emerges, but now there are many K2 lightcurve sources lying blueward of that sequence. Unlike the near-infrared colors – which become bluer by ~ 0.2 – 0.8 mag during pre-main sequence evolution and redder in the post-main sequence – the mid-infrared colors exhibit little evolution, in fact no more than 0.05 mag at any given mass over the entirety of 1– 1000 Myr of evolution. Furthermore, the range in color with mass is relatively small, < 0.3 mag. This means that at any

given color, sources having the same or similar brightness are at the same distance, essentially regardless of age. Sources at different distances are shifted vertically by the distance modulus, again essentially independent of age. The resulting effect is a cleaner break between age and distance degeneracies in the mid-infrared relative to near-infrared color-magnitude diagrams, where the spread in color at a given magnitude masks the distance modulus effects.

We fit a polynomial to the sequence of disk-less stars from LM12 in the WISE $W1$ versus $W1 - W2$ color-magnitude diagram, and then shifted it until 96% of these points lie on the red side of the curve. All K2 objects blueward of this curve are hereafter removed from the young star sample. This rejection reduces the sample from an initial 2072 to 1485. Remaining field star contaminants are likely older objects with a distance close to that of Upper Sco members.

2.2. Selection of stars with inner disks

With our cleaned young star sample, we then identified objects with evidence of inner, largely primordial, circumstellar disks. We searched for infrared excesses in infrared color-magnitude diagrams utilizing WISE colors versus J -band magnitudes, which exhibit a clearly bimodal sequence of stars with and without excesses, as shown in Figure 3. To define the border between the disk-bearing stars and naked photospheres, we first computed a running median of $W1 - W2$ values as a function of J magnitude, then shifted this median curve upward such that it lay above 84% of the points (i.e., median plus one standard deviation). We took this boundary as the criterion for selecting stars with $W1 - W2$ excesses, identifying 326 likely disk bearing stars in this way. Not all disks will appear as infrared excess sources in the $W1 - W2$ color ($4.5 \mu\text{m}$ excess), however, so we repeated this exercise for $W1 - W3$ ($8 \mu\text{m}$ excess) and $W1 - W4$ ($24 \mu\text{m}$ excess), where the longer wavelength photometry is available. This netted 77 and 65 additional disk-bearing stars, respectively, namely those lacking strong shorter wavelength excesses due to inner cleared regions in their disks.

Our disk selection method includes fairly liberal color-magnitude cut-offs, and we find 158 stars for which a potential infrared excess is seen only in one band. Of these, 11 appear in either LM12 or Dawson et al. (2013). Only three of this set are classified by those authors as disk-bearing; the other eight are all listed as class III. It is difficult to envision a scenario under which a disk could appear as an $W2$ -only excess; debris disks may appear at $W3$ and $W4$, but we are interested only in primordial disks that retain significant gas. Therefore we removed these objects from the sample. We inspected the WISE images for targets with excesses only in $W3$ or $W4$, and of those that were more than $1-\sigma$ above the color-magnitude cut-off, the majority had suspicious nebulous background. Only three had clear $W3$ -band excesses, as seen in the image and SED, and two of those objects were too faint to properly centroid and produce a light curve. We retained the remaining target (EPIC 203440253) in the disk sample. None of the $W4$ -only sources were included in our young disk sample, as they are likely debris disks.

Through further literature searches, we found that

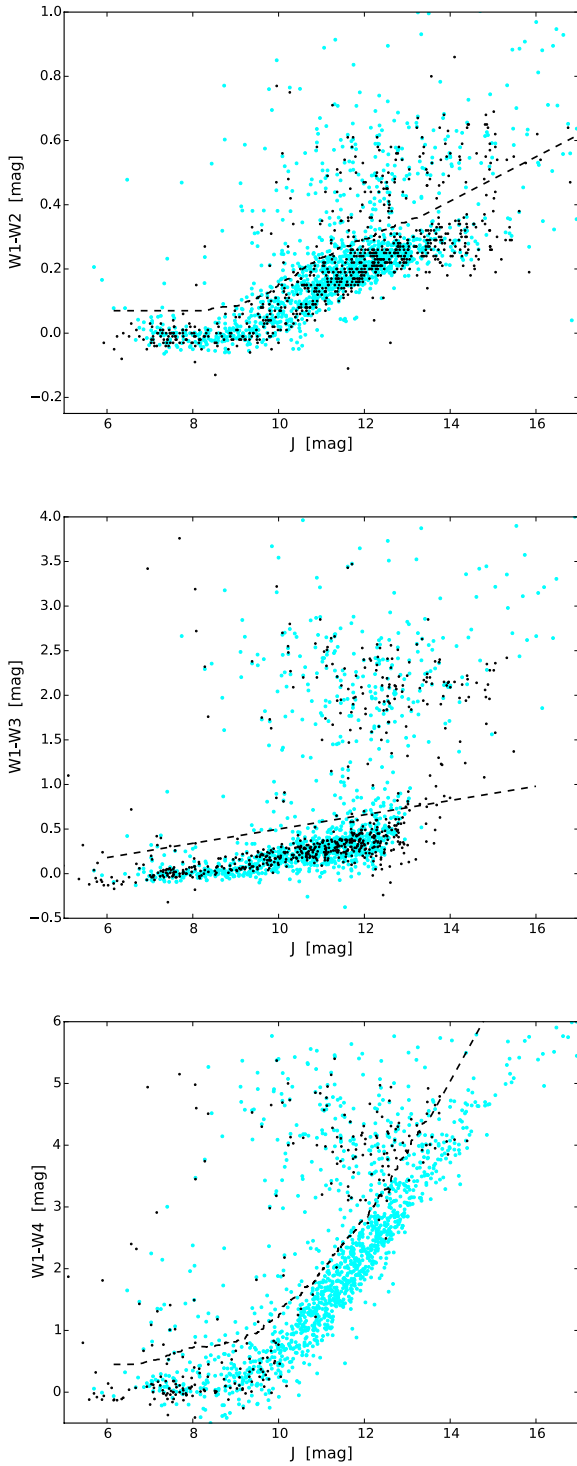


FIG. 3.— We use *WISE* colors, plotted against 2MASS J -band magnitude, to discern which of our young star sample has infrared excesses indicative of circumstellar disks. Shown here are both the K2 sample (cyan), and the LM12 sample (black). For each set of *WISE* colors in the K2 sample, we determine the median trend as a function of J . We then shift that median upward by 1σ to denote the boundary between disk-bearing and diskless stars.

a few asymptotic giant branch (AGB) stars made it into the sample due to their very red colors. We eliminated eight such objects (EPIC ids 203812608, 203871153, 203882149, 203902911, 203962241, 203963116, 203970821, and 204232199) from the disk list based on reported spectroscopic data indicating AGB status or otherwise an M spectral and III luminosity class.

The disk-bearing sample was augmented with some sources that were missing usable *WISE* photometry (e.g., due to source crowding or bright infrared background) but are previously known disk-bearing sources from *Herschel*, *Spitzer* Space Telescope, or submillimeter data that are more sensitive than *WISE* to cool dust. We performed a literature search on all objects with missing *WISE* data to identify potential such cases. As a result, the following stars were added to the disk hosting set: EPIC 203806628 Rebollido et al. (2015), EPIC 203833873 Isella et al. (2009), EPIC 204514546 Honda et al. (2015), EPIC 205684783 Andrews & Williams (2007), and EPIC 210282534 Najita et al. (2015). We augment this list with disk-bearing sources found by Gutermuth et al. (2009) in ρ Oph using *Spitzer*: EPIC 203860592, EPIC 203863066, EPIC 203924502, and EPIC 203934728. In addition, there were four sources (EPIC 204281210, EPIC 204399980, EPIC 205249328, and EPIC 205327575) for which we had declined to use the *WISE* data, but LM12 declared them to be disk bearing.

We created spectral energy distributions (SEDs) with all available photometry for each source, to determine which, if any, of the *WISE*-flagged objects should be retained in the disk-bearing sample. In addition to the four sources named above from LM12, one star with little literature attention showed an SED with an infrared slope consistent with a young star excess: EPIC 203725791. Upon further inspection of its light curve, we opted to add it to the sample.

We have compared our disk selection results with those of LM12, who also identified infrared excess sources using all four *WISE* bands. There are 474 stars in the K2 Campaign 2 young star dataset (of which they list 140 as having a disk). After rejecting sources with excesses in a single band, in no cases do we find evidence of a disk where LM12 do not. Moreover, as noted above there are just four cases for which LM12 report an infrared excess at one of the *WISE* bands, whereas we do not detect it.

We retain our no-disk classifications for these. Thus overall, 99% of our classifications are in agreement with LM12's results.

2.3. Selection of stars with good K2 light curves

After the above adjustments, from the initial set of K2 Campaign 2 targets from which we down-selected to 1485 likely young cluster members, we are left with 340 disk bearing stars; 217 are in Upper Sco, and 123 are in ρ Oph. The resulting composite disk fraction (23%) is consistent with the value of 27% quoted by Erickson et al. (2011) for stars between the embedded ρ Oph core and the more dispersed Upper Sco region. We list the names of each object in Table 1 along with available spectral types. A “blend” flag is given if the K2 photometry contains more than one source. And a “sample” flag indicates whether they source is retained in the final light curve sample

after the further considerations below.

A further, practical limitation to our analysis below comes from considering the quality of the *K2* photometry. Our photometric extraction methods (see Section 3) to produce light curves perform fairly well on bright stars, but they often fail to centroid on low signal-to-noise objects with Kepler magnitudes less than ~ 16 . Many of these are near the sub-stellar limit, and a fraction of them are in our disk-bearing sample. However, we are unable to study the variability properties of those objects missing reliable *K2* photometry. Thus, we were compelled to disregard another 45 faint stars from the disk set. There were a further seven extremely bright stars that were too saturated to produce a systematics-free light curve. We also removed these objects from the disk set.

After removal of the faint members, we were left with 288 disk-bearing stars for analysis of variability properties.

2.4. Present *K2* Upper Sco sample relative to previous *CoRoT* sample in NGC 2264

Considering the 176 young classical T Tauri stars already probed by *CoRoT* in NGC 2264 (Cody et al. 2014), with our sample of 288 identified Upper Sco and ρ Oph members with *K2* data, we increase the set of disk-bearing YSOs with high quality light curves to over 450. Relative to the *CoRoT* NGC 2264 sample, the *K2* Upper Sco and ρ Oph sample has greater breadth in stellar mass. There are 15 stars in the BAF spectral type range (all of these were too bright for *CoRoT* in NGC 2264) and low-mass targets all the way down to M8 (whereas the NGC 2264 set reached only to spectral type of M5). It is also important to keep in mind possible age spreads among the *K2* stars, as compared to previous samples. This is not only because ρ Ophiuchus is significantly younger than Upper Sco, but also because there may be a range of ages in Sco itself (Fang et al. 2017). We explore potential age and mass dependences of variability in §6.

TABLE 1
YOUNG INNER DISK-BEARING STARS IN *K2* CAMPAIGN 2

EPIC id	2MASS id	SpT	Reference	Blend	Region	Sample flag
202610930	J16232307-2901331	-	-	-	Sco	Y
202876718	J16181616-2802300	A0V	de Bruijne (1999)	-	Sco	Y
203082998	J16244448-2719036	-	-	-	Sco	Y
203083616	J16145253-2718557	-	-	-	Sco	Y
203318214	J16112601-2631558	M2.0	Rizzuto et al. (2015)	-	Sco	Y
203337814	J16164756-2628178	-	-	-	Sco	Y
203343161	J16245587-2627181	M5.5	Ansdell et al. (2016a)	-	Sco	Y
203377650	J16165225-2620387	-	-	-	Sco	Y
203382255	J16144265-2619421	-	-	-	Sco	Y
203385048	J16181618-2619080	M4.5	Luhman & Mamajek (2012)	-	Sco	Y
203410665	J16253849-2613540	K7.0	Ansdell et al. (2016a)	-	Sco	Y
203417549	J16213469-2612269	K5e	Skiff (2014)	-	Sco	Y
203429083	J15570350-2610081	-	-	-	Sco	Y
203440253	J16252883-2607538	M2.5	Rizzuto et al. (2015)	-	Sco	Y
203465909	J16274905-2602437	-	-	-	Sco	Y
203542463	J16180868-2547126	-	-	-	Sco	Y
203559274	J16175432-2543435	-	-	-	Sco	Y
203604427	J16290873-2534240	-	-	-	Sco	Y
203637940	J16262774-2527247	M0	Walter et al. (1994)	-	Sco	Y
203649927	J16240289-2524539	B8II	de Bruijne (1999)	-	Sco	Y
203664569	J16163345-2521505	M0.5	Luhman & Mamajek (2012)	-	Sco	Y
203690414	J16011398-2516281	M4.0	Rizzuto et al. (2015)	-	Sco	Y
203703016	J16145244-2513523	M3.5	Rizzuto et al. (2015)	Y	Sco	Y
203710077	J15554883-2512240	G3	Luhman & Mamajek (2012)	-	Sco	Y
203712588	J16251521-2511540	-	-	-	Sco	Y
203716389	J16251727-2511054	-	-	-	Oph	Y
203725791	J16012902-2509069	M3.5	Rizzuto et al. (2015)	Y	Sco	Y
203726323	J16134880-2509006	M5.0	Lodieu et al. (2006)	-	Sco	F
203749770	J16271273-2504017	M1.0	Rizzuto et al. (2015)	-	Oph	Y
203750883	J16133650-2503473	M3.5	Luhman & Mamajek (2012)	-	Sco	Y
203770366	J16150524-2459351	M5.25	Luhman & Mamajek (2012)	-	Sco	Y
203770559	J16250208-2459323	M4.5	Erickson et al. (2011)	Y	Oph	Y
203770673	J16145928-2459308	M4.25	Luhman & Mamajek (2012)	-	Sco	Y
203774126	J16295459-2458459	A2V	de Bruijne (1999)	-	Sco	Y
203785905	J16281385-2456113	M0	Erickson et al. (2011)	-	Oph	Y
203786695	J16245974-2456008	M3.5	Erickson et al. (2011)	Y	Oph	Y
203789325	J16174768-2455251	-	-	-	Sco	Y
203789507	J15570490-2455227	-	-	-	Sco	Y
203791768	J16271836-2454537	M3.75	Erickson et al. (2011)	-	Oph	Y
203794605	J16302339-2454161	em	Skiff (2014)	-	Sco	Y
203795359	J16282992-2454062	-	-	-	Oph	F
203797163	J16280011-2453427	M5	Erickson et al. (2011)	-	Oph	Y
203801323	J16255893-2452483	M4	Erickson et al. (2011)	Y	Oph	Y
203806628	J16271513-2451388	M2	Reboussin et al. (2015)	-	Oph	Y
203810851	J15575444-2450424	-	-	-	Sco	Y
203822485	J16272297-2448071	M4.25	Erickson et al. (2011)	-	Oph	Y

TABLE 1 — *Continued*

EPIC id	2MASS id	SpT	Reference	Blend	Region	Sample flag
203822946	J16251891-2448006	M3	Erickson et al. (2011)	-	Oph	Y
203824153	J16285407-2447442	M1.5	Erickson et al. (2011)	-	Oph	Y
203826403	J16264441-2447138	M4	Erickson et al. (2011)	-	Oph	Y
203833873	J16265843-2445318	K7	Wahhaj et al. (2010)	Y	Oph	Y
203837701	J16262189-2444397	M6.5	Manara et al. (2015)	-	Oph	Y
203842632	J16271382-2443316	M3.5	Manara et al. (2015)	-	Oph	Y
203843009	J16075567-2443267	M5.5	Slesnick et al. (2008)	-	Sco	Y
203843841	J16273982-2443150	-	-	-	Oph	F
203843911	J16262367-2443138	K5	Reboussin et al. (2015)	-	Oph	Y
203848625	J16202863-2442087	-	-	-	Sco	Y
203848661	J16255754-2442082	K2	Erickson et al. (2011)	-	Oph	Y
203849739	J16262753-2441535	-	-	-	Oph	Y
203850058	J16270659-2441488	M5	Manara et al. (2015)	-	Oph	Y
203850425	J16272146-2441430	-	-	-	Oph	F
203850605	J16271951-2441403	M0IVe	Pecaut & Mamajek (2016)	-	Oph	Y
203851860	J16294427-2441218	M5	Walter et al. (1994)	Y	Sco	Y
203852282	J16273311-2441152	K8	Luhman & Rieke (1999)	-	Oph	Y
203856041	J16273894-2440206	M2.5	Manara et al. (2015)	-	Oph	F
203856109	J16095198-2440197	-	-	-	Sco	Y
203856244	J16264125-2440179	M5	Erickson et al. (2011)	-	Oph	Y
203860070	J16272648-2439230	M1	Reboussin et al. (2015)	-	Oph	F
203860546	J16272943-2439161	-	-	-	Oph	F
203860592	J16273942-2439155	K5	Reboussin et al. (2015)	-	Oph	Y
203862309	J16274270-2438506	M2	Erickson et al. (2011)	-	Oph	Y
203863066	J16273863-2438391	M8	Manara et al. (2015)	-	Oph	Y
203864032	J16264897-2438252	M3.5	Manara et al. (2015)	-	Oph	Y
203867167	J16254767-2437394	M3.5	Erickson et al. (2011)	-	Oph	Y
203867975	J16270233-2437272	-	-	-	Oph	F
203868595	J16270943-2437187	-	-	-	Oph	F
203870022	J16273832-2436585	M0	Reboussin et al. (2015)	-	Oph	Y
203870058	J16281650-2436579	M4	Reboussin et al. (2015)	-	Oph	Y
203874287	J16265904-2435568	M4	Luhman & Rieke (1999)	-	Oph	F
203876897	J16150807-2435184	-	-	-	Sco	Y
203877533	J16243969-2435091	M4.5	Erickson et al. (2011)	-	Oph	Y
203878861	J16271213-2434491	M2	Manara et al. (2015)	-	Oph	F
203878912	J16264419-2434483	-	-	-	Oph	F
203881373	J16260931-2434121	A0	Luhman & Rieke (1999)	-	Oph	Y
203881640	J16270910-2434081	K8	Luhman & Rieke (1999)	-	Oph	Y
203884731	J16273267-2433239	-	-	-	Oph	F
203887087	J16281379-2432494	M4	Erickson et al. (2011)	-	Oph	Y
203888154	J16273285-2432348	-	-	-	Oph	F
203889938	J16072625-2432079	M3.5	Luhman & Mamajek (2012)	-	Sco	Y
203891430	J16275180-2431455	-	-	-	Oph	F
203891751	J16274629-2431411	M7.5	Manara et al. (2015)	-	Oph	Y
203892903	J16224539-2431237	-	-	-	Sco	Y
203893434	J16272738-2431165	M0	Luhman & Rieke (1999)	-	Oph	Y
203893891	J16285694-2431096	M5.5	Erickson et al. (2011)	-	Oph	Y
203894375	J16264214-2431029	-	-	-	Oph	F
203895738	J16273812-2430429	M4	Luhman & Rieke (1999)	-	Oph	Y
203895983	J16041893-2430392	M2.5	Rizzuto et al. (2015)	-	Sco	Y
203896277	J16273718-2430350	A0	Erickson et al. (2011)	-	Oph	Y
203899786	J16252434-2429442	M4.5	Erickson et al. (2011)	-	Oph	Y
203901938	J16271003-2429133	-	-	-	Oph	F
203902450	J16271848-2429059	M1.5	Luhman & Rieke (1999)	-	Oph	F
203903767	J16262295-2428461	-	-	-	Oph	F
203904212	J16262083-2428395	-	-	-	Oph	F
203904213	J16275525-2428395	-	-	-	Oph	Y
203904426	J16270597-2428363	M6.5	Luhman & Rieke (1999)	-	Oph	F
203904870	J16270410-2428299	-	-	-	Oph	F
203905576	J16261886-2428196	M0	Reboussin et al. (2015)	-	Oph	Y
203905625	J16284527-2428190	M3.75	Erickson et al. (2011)	-	Oph	Y
203905980	J16284703-2428138	M4.5	Erickson et al. (2011)	-	Oph	Y
203908052	J16273018-2427433	K8	Luhman & Rieke (1999)	-	Oph	F
203909356	J16260704-2427241	-	-	-	Oph	F
203909577	J16272844-2427210	K6.5	Luhman & Rieke (1999)	-	Oph	F
203909943	J16270457-2427156	-	-	-	Oph	F
203912136	J16110360-2426429	M8	Luhman & Mamajek (2012)	-	Sco	Y
203912674	J16253958-2426349	M2	Erickson et al. (2011)	-	Oph	Y
203913635	J16265444-2426207	M0	Luhman & Rieke (1999)	-	Oph	F
203913804	J16275558-2426179	M2	Erickson et al. (2011)	-	Oph	Y
203914316	J16261882-2426105	M7	Manara et al. (2015)	-	Oph	F
203914960	J16262152-2426009	M7	Manara et al. (2015)	-	Oph	Y
203915424	J16272658-2425543	M8	Erickson et al. (2011)	-	Oph	Y
203916376	J16274987-2425402	A7	Erickson et al. (2011)	-	Oph	Y

TABLE 1 — *Continued*

EPIC id	2MASS id	SpT	Reference	Blend	Region	Sample flag
203917608	J16274978-2425219	-	-	-	Oph	Y
203917711	J16260137-2425203	-	-	-	Oph	F
203919315	J16273084-2424560	M3.25	Erickson et al. (2011)	-	Oph	Y
203920354	J16262357-2424394	K7	Manara et al. (2015)	-	Oph	Y
203922515	J16262226-2424070	M8	Manara et al. (2015)	-	Oph	F
203923185	J16252622-2423566	G7	Erickson et al. (2011)	-	Oph	Y
203924150	J16271168-2423419	-	-	-	Oph	F
203924502	J16260302-2423360	K1	Luhman & Rieke (1999) ^a	-	Oph	Y
203925443	J16281475-2423225	K0:	Erickson et al. (2011)	-	Oph	Y
203926424	J16264502-2423077	M0	Reboussin et al. (2015)	-	Oph	Y
203926667	J16262138-2423040	-	-	-	Oph	F
203926890	J16263778-2423007	K8	Luhman & Rieke (1999)	-	Oph	F
203927902	J16283266-2422449	G7	Erickson et al. (2011)	-	Oph	Y
203928175	J16282333-2422405	K5	Erickson et al. (2011)	-	Oph	Y
203928921	J16265497-2422296	K8	Luhman & Rieke (1999)	-	Oph	F
203929332	J16261684-2422231	K6	Erickson et al. (2011)	-	Oph	Y
203930599	J16274028-242040	K5	Erickson et al. (2011)	-	Oph	Y
203931628	J16221989-2421482	A1III/IV	de Bruijne (1999)	-	Sco	Y
203932787	J16265839-2421299	-	-	-	Oph	F
203933268	J16255965-2421223	M5.5	Erickson et al. (2011)	-	Oph	Y
203934728	J16262335-2420597	G6	Erickson et al. (2011)	-	Oph	Y
203935066	J16261033-2420548	M0	Reboussin et al. (2015)	-	Oph	F
203935537	J16255615-2420481	K5	Reboussin et al. (2015)	-	Oph	Y
203936815	J16264285-2420299	M1	Erickson et al. (2011)	Y	Oph	Y
203937317	J16261706-2420216	K7.5	Ansdell et al. (2016a)	-	Oph	Y
203938167	J16151239-2420091	-	-	-	Sco	Y
203938591	J16264923-2420029	K6	Luhman & Rieke (1999)	-	Oph	Y
203941210	J16272622-2419229	-	-	-	Oph	F
203941868	J16271027-2419127	G3	Reboussin et al. (2015)	-	Oph	Y
203943710	J16250062-2418442	-	-	-	Oph	Y
203944338	J16265863-2418346	M4.5	Manara et al. (2015)	-	Oph	F
203945512	J16271372-2418168	-	-	-	Oph	Y
203946909	J16273742-2417548	M7.5	Manara et al. (2015)	-	Oph	Y
203947119	J16260457-2417514	-	-	-	Oph	F
203947305	J16244104-2417488	M2	Erickson et al. (2011)	-	Oph	Y
203950167	J16230923-2417047	-	-	-	Sco	Y
203953466	J16262407-2416134	K6	Reboussin et al. (2015)	-	Oph	Y
203954898	J16263682-2415518	M0	Erickson et al. (2011)	-	Oph	Y
203955457	J16253673-2415424	K4	Erickson et al. (2011)	-	Oph	Y
203956650	J16283256-2415242	M3.5	Erickson et al. (2011)	-	Oph	Y
203962599	J16265677-2413515	K7	Erickson et al. (2011)	-	Oph	Y
203969672	J16270907-2412007	M2.5	Erickson et al. (2011)	-	Oph	Y
203969721	J16264643-2412000	G3.5	Erickson et al. (2011)	-	Oph	Y
203971352	J16281271-2411355	M6	Manara et al. (2015)	-	Oph	Y
203972079	J16245729-2411240	M3.5	Erickson et al. (2011)	-	Oph	Y
203981774	J16262097-2408518	M2	Erickson et al. (2011)	-	Oph	Y
203982074	J16260289-2408474	F3	Erickson et al. (2011)	-	Oph	Y
203987773	J16261877-2407190	M3.25	Erickson et al. (2011)	-	Oph	Y
203995761	J16281673-2405142	K6	Erickson et al. (2011)	-	Oph	Y
204078097	J16095852-2345186	M6	Luhman & Mamajek (2012)	-	Sco	Y
204094503	J16084836-2341209	M5	Luhman & Mamajek (2012)	-	Sco	Y
204103213	J16142144-2339146	M7	Lodieu et al. (2011)	Y	Sco	F
204107757	J15560104-2338081	M5.5	Luhman & Mamajek (2012)	-	Sco	Y
204108293	J15591135-2338002	M6.5	Luhman & Mamajek (2012)	-	Sco	Y
204120066	J16083048-2335109	M8.25	Luhman & Mamajek (2012)	Y	Sco	F
204130613	J16145026-2332397	-	-	-	Sco	Y
204137184	J16020517-2331070	M4.5	Ansdell et al. (2016a)	-	Sco	Y
204141928	J16002323-2329595	M6.5+M6.5	Luhman & Mamajek (2012)	Y	Sco	F
204142243	J16222497-2329553	em	Skiff (2014)	-	Sco	Y
204147776	J15581270-2328364	G2IV	Pecaut & Mamajek (2016)	-	Sco	Y
204160652	J16224680-2325331	M1	Wahhaj et al. (2010)	Y	Sco	Y
204161056	J16254289-2325260	em	Skiff (2014)	-	Sco	Y
204176565	J16221852-2321480	K/M	Skiff (2014)	-	Sco	Y
204181799	J16135434-2320342	M4.5	Lodieu et al. (2011)	Y	Sco	Y
204182919	J16023587-2320170	M3.5	Rizzuto et al. (2015)	-	Sco	Y
204187094	J16111907-2319202	M5	Lodieu et al. (2011)	-	Sco	Y
204187469	J16251052-2319145	K6-7	Guenther et al. (2007)	-	Sco	Y
204193996	J15575396-2317416	-	-	-	Sco	Y
204206295	J16264741-2314521	-	-	-	Sco	Y
204211116	J16214199-2313432	-	-	-	Sco	Y
204226548	J15582981-2310077	M3	Carpenter et al. (2014)	-	Sco	Y
204231861	J16145131-2308515	-	-	-	Sco	Y
204233955	J16072955-2308221	-	-	-	Sco	Y
204239132	J16225177-2307070	A1III/IV	de Bruijne (1999)	-	Sco	Y

TABLE 1 — *Continued*

EPIC id	2MASS id	SpT	Reference	Blend	Region	Sample flag
204245509	J16141107-2305362	K2	Carpenter et al. (2014)	-	Sco	Y
204248645	J16024575-2304509	M5	Luhman & Mamajek (2012)	-	Sco	Y
204250417	J16151361-2304261	M6.5	Slesnick et al. (2008)	-	Sco	Y
204256494	J16243654-2303000	-	-	-	Sco	Y
204262368	J16012652-2301343	-	-	-	Sco	Y
204268916	J16243520-2300022	-	-	-	Sco	Y
204274536	J16233283-2258468	-	-	-	Sco	Y
204274743	J15572986-2258438	M4	Carpenter et al. (2014)	-	Sco	Y
204277211	J16014086-2258103	M4	Luhman & Mamajek (2012)	Y	Sco	Y
204278916	J16020757-2257467	M2.5	Luhman & Mamajek (2012)	-	Sco	Y
204281210	J15583692-2257153	G5IVe	Pecaut & Mamajek (2016)	-	Sco	Y
204290918	J16211848-2254578	-	-	-	Sco	Y
204317053	J16024142-2248419	M5.5	Slesnick et al. (2008)	-	Sco	Y
204329690	J16220194-2245410	-	-	-	Sco	Y
204342099	J16153456-2242421	M1	Preibisch et al. (1998)	Y	Sco	Y
204344180	J16143287-2242133	M6.5	Lodieu et al. (2011)	-	Sco	Y
204347422	J16195140-2241266	-	-	-	Sco	Y
204347824	J16243182-2241207	-	-	Y	Sco	Y
204360645	J16032277-2238206	-	-	-	Sco	Y
204360807	J16215741-2238180	-	-	-	Sco	Y
204365840	J16320136-2237081	M5.5	Luhman & Mamajek (2012)	Y	Sco	Y
204372172	J16205022-2235387	A9V	de Bruijne (1999)	-	Sco	Y
204388640	J16020429-2231468	-	-	-	Sco	Y
204395393	J16001844-2230114	M4.5	Luhman & Mamajek (2012)	-	Sco	Y
204397408	J16081081-2229428	M5.75	Lodieu et al. (2011)	-	Sco	Y
204397879	J16093229-2229360	-	-	-	Sco	Y
204398857	J16093164-2229224	M2.0	Rizzuto et al. (2015)	-	Sco	Y
204399980	J16131158-2229066	A8III/IV	de Bruijne (1999)	-	Sco	Y
204401119	J16110737-2228501	M5.75	Lodieu et al. (2011)	-	Sco	Y
204408707	J16202291-2227041	-	-	-	Sco	Y
204409463	J16125528-2226542	M5.5	Lodieu et al. (2011)	-	Sco	Y
204413641	J15562477-2225552	M4	Carpenter et al. (2014)	-	Sco	Y
204419255	J16095804-2224348	-	-	-	Sco	B
204428864	J16081566-2222199	M3.25	Lodieu et al. (2011)	-	Sco	Y
204434363	J16075039-2221021	M5.75	Lodieu et al. (2011)	-	Sco	Y
204435866	J16192393-2220412	-	-	-	Sco	Y
204440603	J16142312-2219338	M5.75	Lodieu et al. (2011)	-	Sco	Y
204447221	J16094098-2217594	M0	Preibisch et al. (1998)	-	Sco	Y
204449274	J16222160-2217307	M5	Slesnick et al. (2008)	-	Sco	Y
204449389	J16082733-2217292	-	-	-	Sco	Y
204467371	J16154914-2213117	-	-	-	Sco	Y
204467584	J16111705-2213085	M5	Lodieu et al. (2011)	-	Sco	Y
204469637	J16200616-2212385	M3.5	Rizzuto et al. (2015)	-	Sco	Y
204472612	J16083455-2211559	-	-	-	Sco	Y
204487447	J16103069-2208229	-	-	-	Sco	Y
204489514	J16030161-2207523	M4.75	Luhman & Mamajek (2012)	-	Sco	Y
204495624	J16104259-2206212	-	-	-	Sco	Y
204496657	J15570641-2206060	M4	Carpenter et al. (2014)	-	Sco	Y
204501712	J16105691-2204515	-	-	-	Sco	Y
204508462	J16194711-2203112	M5.0	Rizzuto et al. (2015)	-	Sco	Y
204512343	J15572109-2202130	-	-	-	Sco	Y
204514546	J15564002-2201400	A8	Houk & Smith-Moore (1988)	-	Sco	Y
204517888	J16023227-2200486	M5:	Luhman & Mamajek (2012)	-	Sco	F
204530046	J16105011-2157481	-	-	-	Sco	Y
204538777	J16032625-2155378	M5	Luhman & Mamajek (2012)	-	Sco	Y
204565982	J16270942-2148457	M4.5	Slesnick et al. (2008)	-	Sco	Y
204578601	J16193976-2145349	M6	Luhman & Mamajek (2012)	-	Sco	Y
204581550	J16123414-2144500	-	-	-	Sco	Y
204584778	J16152516-2144013	-	-	-	Sco	Y
204602441	J16092136-2139342	M5	Luhman & Mamajek (2012)	-	Sco	Y
204607034	J16024152-2138245	M4.75	Luhman & Mamajek (2012)	-	Sco	Y
204611292	J16082870-2137198	M5:	Luhman & Mamajek (2012)	-	Sco	Y
204615647	J16132190-2136136	M1.5	Rizzuto et al. (2015)	-	Sco	Y
204630363	J16100501-2132318	M0.0	Rizzuto et al. (2015)	-	Sco	Y
204637622	J16042097-2130415	M3.5	Luhman & Mamajek (2012)	-	Sco	Y
204638512	J16042165-2130284	K2	Luhman & Mamajek (2012)	-	Sco	Y
204649301	J16100608-2127440	M8	Luhman & Mamajek (2012)	Y	Sco	F
204651122	J16122289-2127158	-	-	-	Sco	Y
204662993	J16192923-2124132	F2/3 V	de Bruijne (1999)	-	Sco	Y
204757338	J16072747-2059442	M4.75	Luhman & Mamajek (2012)	-	Sco	Y
204769599	J16002669-2056316	M5	Luhman & Mamajek (2012)	-	Sco	Y
204776782	J16152083-2054372	-	-	-	Sco	Y
204807722	J15570146-2046184	-	-	-	Sco	Y
204810161	J16221481-2045398	-	-	-	Sco	Y

TABLE 1 — *Continued*

EPIC id	2MASS id	SpT	Reference	Blend	Region	Sample flag
204811478	J15555600-2045187	M5	Luhman & Mamajek (2012)	-	Sco	Y
204817605	J16120505-2043404	M1.0	Rizzuto et al. (2015)	-	Sco	Y
204830786	J16075796-2040087	em	Skiff (2014)	-	Sco	Y
204832936	J15564244-2039339	M3.5	Rizzuto et al. (2015)	-	Sco	Y
204856535	J16070014-2033092	M2.75	Luhman & Mamajek (2012)	-	Sco	Y
204860656	J16104391-2032025	-		Y	Sco	Y
204864076	J16035767-2031055	K5	Luhman & Mamajek (2012)	-	Sco	Y
204870258	J15594426-2029232	M5.0	Rizzuto et al. (2015)	-	Sco	Y
204871202	J16090071-2029086	M5	Luhman & Mamajek (2012)	-	Sco	Y
204871862	J16070169-2028579	M5.25	Luhman & Mamajek (2012)	-	Sco	Y
204874314	J16353913-2028195	-	-	-	Sco	Y
204894208	J16002945-2022536	-	-	-	Sco	Y
204906020	J16070211-2019387	M5	Carpenter et al. (2014)	Y	Sco	Y
204908189	J16111330-2019029	M3	Luhman & Mamajek (2012)	-	Sco	Y
204932990	J16115091-2012098	M3.5	Luhman & Mamajek (2012)	-	Sco	Y
204933717	J16072240-2011581	M5.5	Slesnick et al. (2008)	-	Sco	Y
204939243	J16153220-2010236	M1.5	Rizzuto et al. (2015)	-	Sco	Y
204940701	J16122737-2009596	M4.5	Luhman & Mamajek (2012)	Y	Sco	Y
204951022	J16203026-2007037	-	-	-	Sco	Y
204951731	J16203056-2006518	B9.5Va	Skiff (2014)	-	Sco	B
204964091	J16200549-2003228	B9II/III	de Bruijne (1999)	-	Sco	Y
204966512	J16200397-2002413	A0V	de Bruijne (1999)	-	Sco	B
204982702	J16095206-1958065	-	-	-	Sco	Y
205000676	J16220961-1953005	-	-	-	Sco	Y
205002311	J16474733-1952319	F3V	Pecaut et al. (2012)	-	Sco	B
205008727	J16193570-1950426	-	-	-	Sco	Y
205024407	J15583620-1946135	M4.0	Rizzuto et al. (2015)	-	Sco	Y
205037578	J16041740-1942287	M3.5	Luhman & Mamajek (2012)	Y	Sco	Y
205038557	J16035793-1942108	M2	Preibisch et al. (2002)	-	Sco	Y
205051240	J16140792-1938292	-	-	-	Sco	Y
205061092	J16145178-1935402	-	-	-	Sco	Y
205063210	J16073915-1935041	-	-	-	Sco	Y
205064383	J16122183-1934445	B9V	de Bruijne (1999)	-	Sco	Y
205068630	J16111095-1933320	M5	Preibisch et al. (2002)	Y	Sco	Y
205080089	J16124410-1930102	B9V	de Bruijne (1999)	-	Sco	B
205080616	J16082324-1930009	K9	Carpenter et al. (2014)	-	Sco	Y
205086621	J16114534-1928132	M5Ve	Skiff (2014)	-	Sco	Y
205088645	J16111237-1927374	M5	Preibisch et al. (2002)	-	Sco	Y
205089268	J16092089-1927259	A0V	de Bruijne (1999)	-	Sco	B
205091879	J16115763-1926389	-	-	-	Sco	Y
205092303	J16092054-1926318	M5.5	Luhman & Mamajek (2012)	-	Sco	Y
205092842	J16120239-1926218	-	-	-	Sco	F
205110000	J16154416-1921171	K5.Ve	Torres et al. (2006)	-	Sco	Y
205115701	J16100541-1919362	M5.75	Luhman & Mamajek (2012)	-	Sco	Y
205145188	J16102819-1910444	M4	Preibisch et al. (2002)	-	Sco	Y
205151387	J16090075-1908526	M1.0	Ansdell et al. (2016a)	-	Sco	Y
205152244	J16090002-1908368	M5	Carpenter et al. (2014)	-	Sco	Y
205154017	J16064385-1908056	M0.0	Rizzuto et al. (2015)	-	Sco	Y
205156547	J16121242-1907191	-	-	-	Sco	Y
205158239	J16142029-1906481	K5	Carpenter et al. (2014)	-	Sco	Y
205160565	J16142091-1906051	-	-	-	Sco	Y
205164892	J16102857-1904469	M3	Preibisch et al. (1998)	-	Sco	Y
205164999	J16130235-1904450	M6	Luhman & Mamajek (2012)	-	Sco	Y
205165965	J16130996-1904269	-	-	-	Sco	Y
205179845	J16143367-1900133	M2	Preibisch et al. (2002)	-	Sco	Y
205182200	J16123916-1859284	K2.5IV	Pecaut & Mamajek (2016)	-	Sco	Y
205198363	J16153341-1854249	-	-	-	Sco	Y
205208701	J16064266-1851140	M8	Luhman & Mamajek (2012)	-	Sco	Y
205218826	J16093653-1848009	M3	Preibisch et al. (2002)	-	Sco	Y
205238942	J16064794-1841437	M0.0	Rizzuto et al. (2015)	-	Sco	Y
205241182	J16104636-1840598	M4.5	Slesnick et al. (2008)	-	Sco	Y
205249328	J16113134-1838259	K5	Reboussin et al. (2015)	-	Sco	Y
205327575	J16382865-1813136	B9.5IV	de Bruijne (1999)	-	Sco	B
205345560	J16062383-1807183	-	-	-	Sco	Y
205364526	J16124893-1800525	M3	Preibisch et al. (2002)	-	Sco	Y
205366676	J16095933-1800090	M4	Carpenter et al. (2014)	-	Sco	Y
205375290	J16111534-1757214	M1	Preibisch et al. (1998)	-	Sco	Y
205383125	J16095361-1754474	M3	Preibisch et al. (2002)	-	Sco	Y
205519771	J16071403-1702425	M3.5	Rizzuto et al. (2015)	-	Sco	Y
205684783	J16340916-1548168	G5	Reboussin et al. (2015)	-	Sco	Y
210282528	J16333496-1832540	M3.5	Rizzuto et al. (2015)	-	Sco	Y
210282534	J16265850-2445368	K2	Reboussin et al. (2015)	Y	Oph	Y

TABLE 1 — *Continued*

EPIC id	2MASS id	SpT	Reference	Blend	Region	Sample flag

NOTE. — Stars with inner disks observed in K2 Campaign 2, in order of EPIC id. In column 5, a 'Y' appears for blends— cases in which ground-based photometry indicates another star or stars contaminating the K2 aperture. In column 7, 'Y' denotes objects that are included in our ultimate sample of disk-bearing stars. Objects with 'F' were too faint for K2 photometry, whereas objects with 'B' were too bright; none of these were retained in the ultimate sample of 288.

^a For EPIC 203924502 we disregard the spectral type of B2V given by Wahhaj et al. 2010 for this source, as it is inconsistent with all previously reported spectral types, as well as our own examination of independent spectra. Comments in the paper suggest that a nearby HII region contaminates Spitzer photometry, which implies possible contamination in the optical spectrum as well if sky subtraction was not handled properly.

3. K2 PHOTOMETRY AND LIGHT CURVES

With our 288 disk-bearing stars with good quality K_2 photometry, we now proceed to examine the light curve variability properties. We created our own light curves starting with the target pixel files. As is well known, unstable pointing of the Kepler telescope during the K_2 phase has a significant (but surmountable) effect on the mission's light curve quality, and we tested several mitigation methods during light curve extraction.

All tests were conducted on a set of non-variable Campaign 2 stars encompassing the full range of Kepler magnitudes. For each of these targets, we produced aperture photometry with radii of 1, 2, 3, and 4 pixels. In one experiment, we allowed the apertures to move along with the object centroid (as determined by a flux-weighted moment), and in another experiment, we fixed the aperture location on the detector and allowed the centroid to wobble within it. The latter method produces light curves with stronger systematic effects, but these are often just as easily removed with a detrending algorithm. For bright saturated stars, we additionally produced photometry based on a summation of the background-subtracted flux across the entire pixel stamp. The resulting light curve was satisfactory (i.e., free of strong systematics) in all but seven cases that we eliminated from the sample, as discussed in Section 2.3 and listed with 'B' flags in Table 1.

Before comparing the precision of the raw the light curves, we cleaned them of pointing related systematics using the approach and code described in Aigrain et al. (2016). In brief, this uses Gaussian process regression to separately model the position and time-dependent systematics in K_2 light curves. In general, we find that the photometric performance depends on both object magnitude and detector position.

We have estimated our own K_p magnitudes directly from spacecraft-measured stellar flux, as opposed to adopting the values from the Ecliptic Plane Input Catalog (EPIC) which are interpolated and sometimes extrapolated from magnitudes measured at other wavelengths. The latter can be systematically too bright for young stars with disks, since many of these only have near-infrared photometry and the disk contributes emission at these wavelengths. We recalibrated stellar magni-

tudes for the entire ρ Oph/Upper Sco sample by deriving the median relation between K_p and (log) measured flux from the target pixel files of quiet field stars.

The best RMS photometric precisions achieved are approximately 0.13 millimagnitudes for a star with $K_p=10.0$ and 1.8 mmag for a star with $K_p=16.0$. These values are measured over the *entire* light curve *after* detrending for pointing systematics and time-dependent drift in the light curve values. We have also measured the so-called CDPP ("combined differential photometric precision"), which is an assessment of the detectability of signals on six-hour timescales, and a standard metric of the *Kepler* Mission (Christensen et al.). CDPP values ranged from 39 for a 10th magnitude star to 417 for a 16th magnitude star. Some targets had better precision with moving apertures, while others had better precision for fixed apertures. For each target, we selected the light curve with the best performance by selecting the one with the lowest CDPP value after detrending both position- and time-dependent effects. After making this choice, we reverted to the version that was position detrended only, so as to preserve intrinsic stellar variability.

We display the full set of disk bearing light curves in Figure 14.

4. VARIABILITY SELECTION

Most young accreting stars are variable, though at K_2 photometric precision, most stars of any age are measurably variable. In order to detect generic aperiodic as well as periodic variability, we require a photometrically quiet control sample. Since we did not process the entire K_2 Campaign 2 set, we used the set of stars rejected as young cluster members (as described in §3) as a potential benchmark for typical field star variability.

We initially attempted to assess variability by examining the standard deviations of cluster stars in comparison to the "field" sample, as a function of magnitude. This is a standard method for picking out outliers with excess variability. Unfortunately, some of the unlikely cluster members turned out to be variable as well at K_2 precision, and furthermore, there was no clear boundary between variables and non-variables as a function of magnitude. Even the true noise floor was difficult to discern, perhaps because of systematic effects remaining in the data.

We thus identified a better metric for discerning true variables, both aperiodic and periodic. The detrending code provided by Aigrain et al. (2016) provides not only a method to remove pointing systematics, but also an additional option to flatten out all variability via Gaussian process modeling. For most of our light curve assessments, we did not use this option, as it destroys the intrinsic variability by design. However, we found that a comparison of the noise levels before and after flattening provided a measure of how variable a given light curve is. To quantify the noise levels, we used an estimate of the CDPP on 6-hour timescales, as described in Aigrain et al. (2016). Our final variability metric was

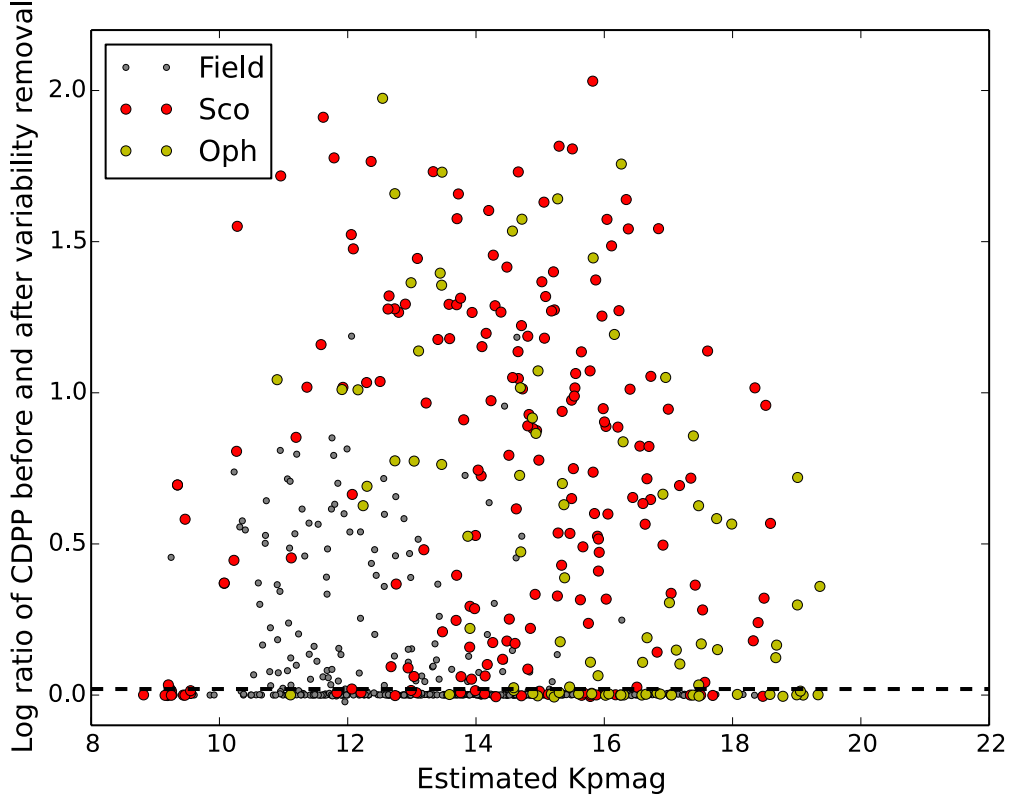


FIG. 4.— We plot the ratio of the CDPP (a measure of statistical spread in flux on 6-hour timescales) before and after variability detrending, against estimated Kepler magnitudes for both our 288 member disk-bearing young star sample, along with a control sample of field stars that were rejected as Upper Sco/ρ Ophiuchus members (see §2.1). The samples depicted here bifurcate into a group with similar CDPP before and after detrending (i.e., zero in the ordinate), and a group with much lower CDPP after detrending (positive values along the ordinate). Variable stars were selected based on a cut-off value of 0.02, plotted as the horizontal dashed line.

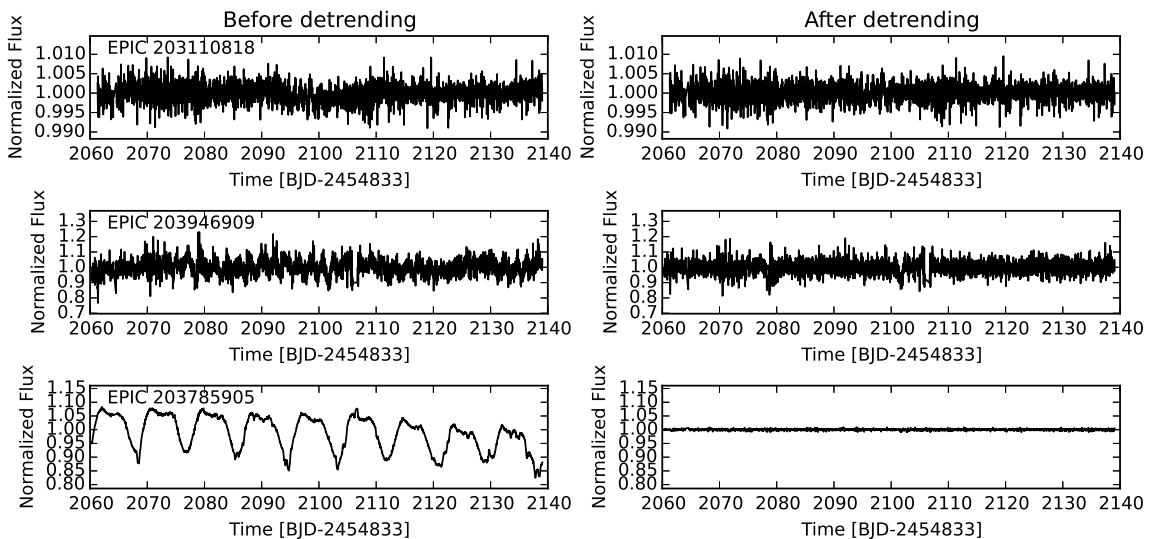


FIG. 5.— Illustrative lightcurves at various CDPP ratios, for three example stars having similar brightness, $K_p=14.5-15.5$. The left side illustrates the light curve before variability removal, and the right after this detrending, for log CDPP ratios of 0.0 (top), 0.02 (middle), and 0.2 (bottom).

the logarithm of the ratio of the CDPP before flattening to the CDPP after flattening. We plot this statistic against source brightness, expressed as K_p magnitude, in Figure 4.

Many disk-bearing stars clearly stand out in Figure 4 as having high amplitude variations, with CDPP ratios in excess of 100. To quantitatively gauge variability, we created a histogram of log CDPP ratios for the field star sample. Most of these are non-variable, and hence have log CDPP ratios near zero. But there is a population of presumably variable objects at higher ratios. We note a sharp cut-off between the variable and non-variable populations around $\log \text{CDPP} \sim 0.015$. To be conservative, we select as variable any object with a log ratio larger than 0.02; this cut-off is drawn as a horizontal dashed line in Figure 4. Examples of light curves at different log CDPP ratio values are shown before and after detrending in Figure 5.

The only drawback to using the CDPP ratio to select variables is that variability appearing only on long timescales goes undetected. This is because the algorithm we have employed to measure CDPP (Aigrain et al. 2016) initially removes trends on timescales of more than a few days. We therefore added to the variability sample targets for which the overall photometric amplitude was more than a factor of 10 times the standard deviation of the trend-removed light curve.

After these assessments, We find 268 variables (77 in ρ Oph and 191 in Upper Sco) among the disk-bearing sample. The field stars (gray) with high CDPP ratio are

objects that display variations on the $<1\%$ level that are inconsistent with white noise. Some of these may be real variables, and others may have light curves contaminated by systematics.

There is a handful of additional young cluster members that fall below the CDPP ratio cut-off, but are (quasi-)periodically variable, as revealed in a periodogram and/or autocorrelation analysis. These were likely missed because of flukes in the detrending regimen. We identified such objects during the variability classification process, as described below and in citecody2014. We identify a total of 9 periodic or quasi-periodic young disk-bearing stars not selected by the CDPP ratio method. This includes 3 in ρ Oph and 6 in Upper Sco that were below the generic variability cut-off but are included in our final variable tally.

The overall variability fraction of inner disk-bearing stars is thus 96%. Broken down into the two clusters, we find $94^{+2}_{-4}\%$ (80/85) of ρ Oph disk-bearing targets and $97^{+1}_{-2}\%$ (197/203) of Upper Sco disk-bearing targets are variable at the precision of K_2 photometry. While the variability fractions are not particularly distinguishable, there are small differences between the two regions in terms of the *type* of variability exhibited (see Table 3 presented below).

We list the variability status of all disk-bearing stars (illustrated in Figure 14) in Table 2, including the variability type, amplitude, timescale, and metrics regarding the degree of periodicity and flux asymmetry about the mean value. The derivation of these values is discussed below.

TABLE 2
VARIABILITY PROPERTIES OF YOUNG DISK-BEARING STARS IN K_2 CAMPAIGN 2

EPIC id	2MASS id	Variability type	Amplitude (Norm. Flux)	Timescale (d)	Q	M
202610930	J16232307-2901331	B	0.18	11.91	1.0	-0.35
202876718	J16181616-2802300	QPS	0.002	1.95	0.58	0.09
203082998	J16244448-2719036	N	0.06	13.16	0.85	-0.01
203083616	J16145253-2718557	QPD	0.33	1.35	0.75	0.53
203318214	J16112601-2631558	P	0.13	4.17	0.03	0.19
203337814	J16164756-2628178	P	0.06	0.78	0.06	-0.21
203343161	J16245587-2627181	APD	0.09	2.23	0.77	0.62
203377650	J16165225-2620387	QPS	0.08	61.46	0.83	-0.14
203382255	J16144265-2619421	B	0.10	78.66	1.0	-1.14
203385048	J16181618-2619080	MP	0.03	1.08	0.16	0.13
203410665	J16253849-2613540	APD	0.24	7.36	0.91	0.88
203417549	J16213469-2612269	S	0.45	18.7	0.83	0.37
203429083	J15570350-2610081	APD	0.17	25.36	0.82	0.64
203440253	J16252883-2607538	QPS	0.05	6.76	0.32	0.29
203465909	J16274905-2602437	QPS	0.79	3.79	0.37	0.2
203542463	J16180868-2547126	QPD	0.09	1.56	0.72	0.44
203559274	J16175432-2543435	QPD	0.10	1.84	0.5	0.56
203604427	J16290873-2534240	U	0.04	95.25	1.0	-0.36
203637940	J16262774-2527247	QPS	0.49	3.29	0.78	-0.13
203649927	J16240289-2524539	QPS	0.003	2.63	0.48	-0.39
203664569	J16163345-2521505	APD	0.08	47.57	1.0	1.04
203690414	J16011398-2516281	MP	0.02	1.81	0.55	0.11
203703016	J16145244-2513523	QPS	0.09	4.9	0.24	0.01
203710077	J15554883-2512240	MP	0.03	3.73	0.38	-0.11
203712588	J16251521-2511540	QPD	0.13	3.29	0.53	0.52
203716389	J16251727-2511054	B	0.46	31.08	0.83	-0.42
203725791	J16012902-2509069	B	0.26	10.95	0.87	-0.28
203749770	J16271273-2504017	APD	0.18	11.16	0.91	0.72
203750883	J16133650-2503473	APD	0.29	4.94	0.9	0.37
203770366	J16150524-2459351	QPD	0.08	1.81	0.42	0.47
203770559	J16250208-2459323	QPS	0.19	12.5	0.34	0.32
203770673	J16145928-2459308	P	0.07	2.29	0.07	0.1
203774126	J16295459-2458459	QPS	0.002	1.95	0.29	-0.39

TABLE 2 — *Continued*

EPIC id	2MASS id	Variability type	Amplitude (Norm. Flux)	Timescale (d)	<i>Q</i>	<i>M</i>
203785905	J16281385-2456113	QPD	0.18	8.93	0.17	0.49
203786695	J16245974-2456008	B	0.11	35.65	1.0	-0.59
203789325	J16174768-2455251	QPS	0.09	1.28	0.43	0.06
203789507	J15570490-2455227	B	0.14	29.89	0.97	-0.41
203791768	J16271836-2454537	APD	0.72	4.0	0.84	0.37
203794605	J16302339-2454161	B	0.47	4.46	0.55	-0.25
203797163	J16280011-2453427	QPS	0.10	14.71	0.3	-0.06
203801323	J16255893-2452483	MP	0.07	1.26	0.55	0.12
203806628	J16271513-2451388	APD	0.20	7.31	0.97	1.1
203810851	J15575444-2450424	QPD	0.56	4.24	0.56	0.08
203822485	J16272297-2448071	B	0.31	20.33	0.84	-0.29
203822946	J16251891-2448006	MP	0.17	0.68	0.56	-0.12
203824153	J16285407-2447442	QPD	0.28	11.9	0.59	0.32
203826403	J16264441-2447138	P	0.09	3.97	0.07	0.03
203833873	J16265843-2445318	S	0.38	14.55	0.83	-0.18
203837701	J16262189-2444397	QPS	0.17	2.63	0.3	-0.06
203842632	J16271382-2443316	S	0.22	50.36	0.87	-0.13
203843009	J16075567-2443267	QPD	0.14	1.35	0.53	0.69
203843911	J16262367-2443138	QPD	0.35	8.93	0.31	0.1
203848625	J16202863-2442087	QPS	0.05	8.06	0.17	-0.13
203848661	J16255754-2442082	L	0.07	78.76	1.0	0.03
203849739	J16262753-2441535	QPS	0.23	39.64	0.84	0.14
203850058	J16270659-2441488	QPD	0.22	2.87	0.66	0.03
203850605	J16271951-2441403	MP	0.18	3.91	0.38	-0.14
203851860	J16294427-2441218	MP	0.04	3.52	0.42	0.07
203852282	J16273311-2441152	B	0.12	79.48	1.0	-0.3
203856109	J16095198-2440197	B	0.10	55.84	0.92	-1.0
203856244	J16264125-2440179	QPD	0.08	4.03	0.7	0.29
203860592	J16273942-2439155	QPD	0.20	6.25	0.08	0.4
203862309	J16274270-2438506	QPD	0.16	4.31	0.67	0.38
203863066	J16273863-2438391	QPS	0.14	4.1	0.75	-0.14
203864032	J16264897-2438252	B	0.56	13.22	0.93	-0.25
203867167	J16254767-2437394	P	0.09	3.16	0.13	-0.12
203870022	J16273832-2436585	QPS	0.18	12.5	0.57	-0.24
203870058	J16281650-2436579	S	0.24	10.24	0.96	-0.19
203876897	J16150807-2435184	N	0.004	7.4	1.0	-0.03
203877533	J16243969-2435091	P	0.13	1.62	0.08	-0.09
203881373	J16260931-2434121	MP	0.02	0.28	0.66	0.13
203881640	J16270910-2434081	QPS	0.52	2.4	0.6	0.05
203887087	J16281379-2432494	QPD	0.21	6.76	0.38	0.96
203889938	J16072625-2432079	S	0.05	8.19	0.94	-0.13
203891751	J16274629-2431411	U	0.21	77.8	1.0	-0.14
203892903	J16224539-2431237	APD	0.31	24.38	1.0	0.6
203893434	J16272738-2431165	APD	0.14	8.34	1.0	0.26
203893891	J16285694-2431096	QPS	0.19	3.97	0.56	-0.43
203895738	J16273812-2430429	QPS	0.12	1.36	0.71	-0.16
203895983	J16041893-2430392	QPS	0.11	2.45	0.74	0.08
203896277	J16273718-2430350	L	0.08	21.68	1.0	0.19
203899786	J16252434-2429442	B	0.48	5.95	0.61	-0.83
203904213	J16275525-2428395	N	0.08	23.54	0.95	-0.04
203905576	J16261886-2428196	B	2.11	23.82	1.0	-0.66
203905625	J16284527-2428190	B	0.18	24.07	1.0	-0.31
203905980	J16284703-2428138	QPS	1.13	1.89	0.36	-0.29
203912136	J16110360-2426429	QPS	0.16	1.41	0.77	-0.0
203912674	J16253958-2426349	S	0.44	28.05	0.82	-0.11
203913804	J16275558-2426179	S	0.26	13.53	1.0	-0.37
203914960	J16262152-2426009	U	0.08	37.86	1.0	0.04
203915424	J16272658-2425543	QPS	0.36	2.87	0.42	-0.06
203916376	J16274987-2425402	L	0.03	6.93	1.0	0.1
203917608	J16274978-2425219	QPS	0.38	2.58	0.71	0.09
203919315	J16273084-2424560	APD	0.2	64.67	0.94	0.86
203920354	J16262357-2424394	N	0.69	12.77	1.0	-0.04
203923185	J16252622-2423566	N	0.09	40.29	1.0	0.02
203924502	J16260302-2423360	P	0.07	3.47	0.18	0.27
203925443	J16281475-2423225	L	0.36	37.51	1.0	0.09
203926424	J16264502-2423077	S	0.46	9.3	0.88	-0.12
203927902	J16283266-2422449	APD	0.17	0.69	0.5	0.58
203928175	J16282333-2422405	B	2.41	4.39	0.54	-0.66
203929332	J16261684-2422231	QPS	0.12	3.57	0.2	-0.07
203930599	J16274028-2422040	S	0.11	21.02	0.88	-0.11
203931628	J16221989-2421482	N	0.002	41.25	0.97	0.1
203933268	J16255965-2421223	QPD	0.08	2.38	0.49	0.35
203934728	J16262335-2420597	QPS	0.03	5.81	0.74	-0.15
203935537	J16255615-2420481	B	0.13	19.78	1.0	-0.31
203936815	J16264285-2420299	QPD	0.55	8.93	0.66	0.79

TABLE 2 — *Continued*

EPIC id	2MASS id	Variability type	Amplitude (Norm. Flux)	Timescale (d)	Q	M
203937317	J16261706-2420216	APD	0.07	7.8	0.85	0.81
203938167	J16151239-2420091	QPS	0.07	1.61	0.31	-0.06
203938591	J16264923-2420029	QP	0.11	2.55	0.8	-0.05
203941868	J16271027-2419127	MP	0.02	2.05	0.59	-0.06
203943710	J16250062-2418442	N	0.04	69.22	1.0	-0.09
203945512	J16271372-2418168	N	0.14	31.85	1.0	-0.22
203946909	J16273742-2417548	S	0.16	28.69	0.84	0.0
203947305	J16244104-2417488	L	0.06	45.89	1.0	-0.18
203950167	J16230923-2417047	APD	0.13	8.09	0.94	0.8
203953466	J16262407-2416134	B	0.17	34.45	1.0	-0.83
203954898	J16263682-2415518	B	2.17	20.83	0.61	-1.35
203955457	J16253673-2415424	L	0.07	34.78	1.0	0.19
203956650	J16283256-2415242	MP	0.09	0.68	0.53	0.24
203962599	J16265677-2413515	APD	0.41	15.94	0.88	0.51
203969672	J16270907-2412007	QPD	0.44	4.9	0.74	0.68
203969721	J16264643-2412000	QPS	0.04	3.38	0.45	0.07
203971352	J16281271-2411355	S	0.31	3.68	0.84	0.14
203972079	J16245729-2411240	QPS	0.04	6.41	0.23	0.12
203981774	J16262097-2408518	P	0.11	0.82	0.09	-0.07
203982074	J16260289-2408474	L	0.08	78.76	1.0	0.07
203987773	J16261877-2407190	QPS	0.04	6.41	0.57	0.09
203995761	J16281673-2405142	QPD	0.41	5.1	0.53	0.67
204078097	J16095852-2345186	QPS	0.06	1.41	0.69	-0.31
204094503	J16084836-2341209	QPS	0.05	1.66	0.6	-0.21
204107757	J15560104-2338081	APD	0.13	3.23	0.88	0.55
204108293	J15591135-2338002	QPS	0.11	1.21	0.61	0.06
204130613	J16145026-2332397	B	0.98	10.67	0.85	-0.35
204137184	J16020517-2331070	QPD	0.21	2.63	0.58	1.24
204142243	J16222497-2329553	QPD	0.42	6.94	0.58	0.3
204147776	J15581270-2328364	QPS	0.05	1.72	0.42	0.11
204160652	J16224680-2325331	QPS	0.13	2.81	0.46	-0.2
204161056	J16254289-2325260	B	0.12	28.18	1.0	-0.55
204176565	J16221852-2321480	APD	0.54	7.93	0.91	0.63
204181799	J16135434-2320342	QPS	0.4	2.21	0.72	-0.19
204182919	J16023587-2320170	P	0.14	6.76	0.04	-0.04
204187094	J16111907-2319202	S	1.62	17.2	1.0	-0.14
204187469	J16251052-2319145	B	0.07	5.95	0.75	-0.22
204193996	J15575396-2317416	QPS	0.07	15.62	0.19	-0.31
204206295	J16264741-2314521	QPD	0.23	14.71	0.45	0.35
204211116	J16214199-2313432	QPD	0.16	16.57	0.88	0.52
204226548	J15582981-2310077	B	0.27	20.17	1.0	-0.53
204231861	J16145131-2308515	B	0.05	10.3	0.95	-0.37
204233955	J16072955-2308221	B	0.59	39.29	0.85	-0.82
204239132	J16225177-2307070	QPS	0.01	4.24	0.47	-0.03
204245509	J16141107-2305362	APD	0.11	30.61	0.95	0.75
204248645	J16024575-2304509	APD	0.03	30.44	0.9	0.4
204250417	J16151361-2304261	QPS	0.15	1.34	0.7	-0.19
204256494	J16243654-2303000	QPD	0.14	3.29	0.54	0.5
204262368	J16012652-2301343	QPS	0.02	1.87	0.32	-0.09
204268916	J16243520-2300022	QPS	0.08	1.75	0.42	-0.48
204274536	J16233283-2258468	QPD	0.49	5.1	0.24	0.57
204274743	J15572986-2258438	QPD	0.18	1.77	0.57	0.46
204277211	J16014086-2258103	QPS	0.67	2.55	0.52	-0.14
204278916	J16020757-2257467	APD	0.10	39.68	0.86	0.78
204281210	J15583692-2257153	APD	0.04	18.51	0.94	0.4
204290918	J16211848-2254578	QPD	0.18	2.52	0.74	0.4
204317053	J16024142-2248419	QPS	0.16	1.59	0.74	-0.22
204329690	J16220194-2245410	QPD	0.08	2.15	0.61	0.3
204342099	J16153456-2242421	B	0.36	11.2	0.91	-0.72
204344180	J16143287-2242133	QPD	0.17	1.82	0.73	0.29
204347422	J16195140-2241266	B	0.24	6.94	0.75	-1.1
204347824	J16243182-2241207	QPS	0.08	1.58	0.66	0.2
204360645	J16032277-2238206	QPS	0.03	1.89	0.62	-0.07
204360807	J16215741-2238180	B	0.24	26.4	0.87	-0.49
204365840	J16320136-2237081	QPS	0.07	1.94	0.62	0.07
204372172	J16205022-2235387	MP	0.002	1.97	0.68	-0.14
204388640	J16020429-2231468	S	0.91	5.76	0.95	0.12
204395393	J16001844-2230114	B	0.15	27.48	0.89	-0.28
204397408	J16081081-2229428	B	0.07	1.64	0.59	-0.68
204397879	J16093229-2229360	QPD	0.10	3.68	0.39	0.32
204398857	J16093164-2229224	QPS	0.07	13.16	0.21	0.04
204399980	J16131158-2229066	APD	0.17	14.87	0.98	1.1
204401119	J16110737-2228501	QPS	0.10	1.79	0.78	-0.12
204408707	J16202291-2227041	QPD	0.13	3.29	0.68	0.36
204409463	J16125528-2226542	QPS	0.05	1.76	0.47	0.11

TABLE 2 — *Continued*

EPIC id	2MASS id	Variability type	Amplitude (Norm. Flux)	Timescale (d)	<i>Q</i>	<i>M</i>
204413641	J15562477-2225552	QPS	0.02	1.97	0.46	-0.03
204428864	J16081566-2222199	S	0.02	5.19	0.89	0.0
204434363	J16075039-2221021	QPS	0.05	1.59	0.41	-0.26
204435866	J16192393-2220412	QPS	0.07	1.4	0.65	-0.2
204440603	J16142312-2219338	B	0.22	8.3	1.0	-0.93
204447221	J16094098-2217594	QPS	0.07	9.62	0.2	-0.33
204449274	J16222160-2217307	QPD	0.10	70.57	0.83	-0.22
204449389	J16082733-2217292	QPD	0.04	1.87	0.55	0.32
204467371	J16154914-2213117	P	0.10	1.81	0.12	0.11
204467584	J16111705-2213085	QPD	0.09	2.07	0.61	0.62
204469637	J16200616-2212385	APD	0.14	4.54	0.9	0.5
204472612	J16083455-2211559	APD	0.06	11.91	0.94	0.26
204487447	J16103069-2208229	APD	0.18	8.95	0.93	0.37
204489514	J16030161-2207523	APD	0.16	3.35	0.83	0.74
204495624	J16104259-2206212	QPS	0.05	1.97	0.2	0.02
204496657	J15570641-2206060	QPD	0.36	1.8	0.75	0.36
204501712	J16105691-2204515	P	0.05	2.03	0.12	-0.02
204508462	J16194711-2203112	QPS	0.05	12.18	0.84	-0.16
204512343	J15572109-2202130	APD	0.66	7.52	0.88	0.98
204514546	J15564002-2201400	APD	0.41	7.33	0.89	0.52
204530046	J16105011-2157481	APD	0.09	55.66	0.86	0.89
204538777	J16032625-2155378	QPD	0.11	61.21	0.82	0.26
204565982	J16270942-2148457	QPS	0.46	1.55	0.78	-0.06
204578601	J16193976-2145349	MP	0.05	1.71	0.68	-0.0
204581550	J16123414-2144500	QPD	0.03	1.91	0.78	0.24
204584778	J16152516-2144013	QPS	0.06	1.74	0.46	-0.14
204602441	J16092136-2139342	B	0.10	15.08	0.96	-0.39
204607034	J16024152-2138245	B	0.13	24.62	0.9	-0.41
204611292	J16082870-2137198	P	0.05	1.77	0.18	0.03
204615647	J16132190-2136136	APD	0.05	7.81	0.77	0.3
204630363	J16100501-2132318	QPS	0.09	6.58	0.47	-0.07
204637622	J16042097-2130415	MP	0.12	1.05	0.46	0.03
204638512	J16042165-2130284	APD	0.45	15.08	0.9	0.89
204651122	J16122289-2127158	QPS	0.09	4.92	0.8	-0.24
204662993	J16192923-2124132	N	0.003	41.35	1.01	-0.08
204757338	J16072747-2059442	APD	0.04	3.6	0.86	0.2
204769599	J16002669-2056316	QPS	0.05	1.64	0.42	-0.03
204776782	J16152083-2054372	QPS	0.07	1.92	0.53	0.02
204807722	J15570146-2046184	QPD	0.37	2.17	0.65	0.64
204810161	J16221481-2045398	QPS	0.02	1.66	0.74	-0.02
204811478	J15555600-2045187	QPD	0.16	1.7	0.73	0.58
204817605	J16120505-2043404	P	0.18	9.26	0.02	0.02
204830786	J16075796-2040087	B	1.14	34.57	1.0	-0.67
204832936	J15564244-2039339	QPS	0.04	4.24	0.31	0.22
204856535	J16070014-2033092	APD	0.14	58.15	1.0	0.42
204860656	J16104391-2032025	MP	0.04	1.91	0.35	0.02
204864076	J16035767-2031055	APD	0.19	8.36	0.84	0.21
204870258	J15594426-2029232	N	0.01	74.86	1.0	-0.05
204871202	J16090071-2029086	APD	0.11	12.57	0.9	0.15
204871862	J16070169-2028579	APD	0.16	5.93	0.91	0.54
204874314	J16353913-2028195	L	0.90	72.94	1.0	0.0
204894208	J16002945-2022536	QPD	0.08	1.7	0.79	0.47
204906020	J16070211-2019387	B	0.16	8.38	0.93	-0.47
204908189	J16111330-2019029	B	0.35	19.23	0.76	-0.59
204932990	J16115091-2012098	QPD	0.09	2.32	0.75	0.52
204933717	J16072240-2011581	QPS	0.05	1.55	0.76	-0.17
204939243	J16153220-2010236	QPD	0.46	8.3	0.85	0.45
204940701	J16122737-2009596	QPS	0.01	8.7	0.86	-0.26
204951022	J16203026-2007037	S	0.001	37.08	0.84	-0.29
204964091	J16200549-2003228	P	0.03	3.91	0.19	0.32
204982702	J16095206-1958065	QPD	0.96	2.4	0.61	0.34
205000676	J16220961-1953005	QPS	0.05	3.2	0.24	0.06
205008727	J16193570-1950426	B	0.39	39.11	1.0	-0.68
205024407	J15583620-1946135	P	0.04	3.01	0.15	-0.08
205037578	J16041740-1942287	APD	0.03	22.9	0.87	0.26
205038557	J16035793-1942108	P	0.06	3.85	0.09	0.02
205051240	J16140792-1938292	QPD	0.06	5.32	0.33	0.32
205061092	J16145178-1935402	B	0.14	72.25	1.0	-0.51
205063210	J16073915-1935041	QPS	0.08	2.43	0.3	-0.04
205064383	J16122183-1934445	N	0.001	34.69	0.96	-0.14
205068630	J16111095-1933320	APD	0.07	17.37	0.93	0.45
205080616	J16082324-1930009	APD	0.25	5.32	0.68	0.21
205086621	J16114534-1928132	QPD	0.15	1.75	0.73	0.71
205088645	J16111237-1927374	B	0.19	16.96	1.0	-0.57
205091879	J16115763-1926389	MP	0.10	0.36	0.58	-0.12

TABLE 2 — *Continued*

EPIC id	2MASS id	Variability type	Amplitude (Norm. Flux)	Timescale (d)	<i>Q</i>	<i>M</i>
205092303	J16092054-1926318	QPD	0.11	1.72	0.68	0.3
205110000	J16154416-1921171	S	1.13	18.02	0.9	-0.1
205115701	J16100541-1919362	APD	0.38	28.56	0.88	0.13
205145188	J16102819-1910444	QPS	0.04	1.76	0.76	0.14
205151387	J16090075-1908526	APD	0.24	10.0	0.59	0.87
205152244	J16090002-1908368	P	0.05	1.81	0.21	-0.1
205154017	J16064385-1908056	P	0.20	6.94	0.07	-0.63
205156547	J16121242-1907191	B	0.05	7.03	1.0	-1.01
205158239	J16142029-1906481	S	1.47	13.18	0.87	-0.11
205160565	J16142091-1906051	S	0.74	24.4	1.0	0.18
205164892	J16102857-1904469	P	0.15	6.58	0.14	-0.06
205164999	J16130235-1904450	APD	0.20	17.55	0.98	0.61
205165965	J16130996-1904269	S	0.13	1.8	0.73	-0.49
205179845	J16143367-1900133	QPS	0.05	2.6	0.74	0.02
205182200	J16123916-1859284	S	0.16	68.85	0.82	0.05
205198363	J16153341-1854249	QPS	0.12	1.91	0.79	-0.02
205208701	J16064266-1851140	QPS	0.13	0.91	0.71	-0.03
205218826	J16093653-1848009	APD	0.16	7.89	0.87	0.47
205238942	J16064794-1841437	QPD	0.23	9.26	0.57	0.23
205241182	J16104636-1840598	QPD	0.28	7.07	0.82	0.86
205249328	J16113134-1838259	S	0.85	51.77	1.0	-0.05
205345560	J16062383-1807183	APD	0.04	21.04	1.0	0.33
205364526	J16124893-1800525	QPS	0.02	2.91	0.22	-0.31
205366676	J16095933-1800090	QPS	0.04	3.68	0.2	0.06
205375290	J16111534-1757214	QPS	0.05	6.1	0.21	-0.06
205383125	J16095361-1754474	QPD	0.45	2.03	0.69	0.47
205519771	J16071403-1702425	APD	0.04	19.27	0.94	0.74
205684783	J16340916-1548168	QPS	1.18	3.29	0.7	0.17
210282528	J16333496-1832540	QPS	0.16	2.21	0.28	-0.02
210282534	J16265850-2445368	S	0.4	14.55	0.83	-0.2

NOTE. — Variability properties for stars with inner disks observed in K2 Campaign 2. Variability types are determined by eye and supported by statistical measures. The types consist of the following: "P" is for strictly periodic behavior, "MP" is reserved for stars with multiple distinct periods, "QPD" is for quasi-periodic dippers, "QPS" means quasi-periodic symmetric (i.e., quasi-periodic stars that neither burst nor dip), "APD" are aperiodic dippers, "B" is for bursters, "S" is for stochastic stars, "L" is the label for long-timescale behavior that doesn't fall into the other categories, "U" is reserved for objects we were unable to classify, and "N" denotes non-variable objects.

5. VARIABILITY CLASSES

With the full set of disk-bearing variables in hand, we can ask what sort of time domain behavior comprises this sample. In Cody et al. (2014), we devised a set of statistical metrics that could separate YSO light curve shapes into different categories. We define them fully in that work and briefly summarize them here. The first of these metrics is the flux asymmetry, "*M*", which is a measure of the tendency of a light curve to display fading events (positive *M*) or brightening events (negative *M*), or a more symmetric, non-skewed light curve that is perhaps a mixture of the two (*M* ~ 0). The value of *M* is determined by calculating a "mean" flux value (by averaging the bottom and top 95th percentile points), subtracting off the *median* flux value, and then dividing by the estimated white noise level.

The second metric is the quasi-periodicity, "*Q*," which measures on a scale of 0 to 1 how periodic (0) or stochastic (1) the light curve is. It is determined by identifying peaks in the autocorrelation, refining their periods with the Fourier transform periodogram, phasing the light curve to the associated period(s), and then measuring the residual noise after the phased light curve pattern is subtracted out. *Q* represents the ratio of the residual

variance to the original light curve variance. Light curves with low residual noise after removal of the phased pattern are then highly periodic (*Q* ~ 0), whereas those that have larger residuals are quasi-periodic or aperiodic. We computed these *M* and *Q* statistics for all disk-bearing light curves. A difference from the Cody et al. (2014) implementation is that, instead of using magnitude values, we use normalized flux. The resulting *Q* – *M* diagram is displayed in Figure 6, with the variability types assigned by our trained eye also indicated. The values span the space from *Q*=0 to 1 and *M*=-1.4 to 1.4.

To classify observed variability into different categories based on the *Q* and *M* metrics, we have defined boundaries that demarcate different *Q* and *M* ranges. Along the flux asymmetry axis, *M* < -0.25 indicates "bursters" (preference for brightening events) and *M* > 0.25 indicates "dippers" (preference for fading events). These are same *M* boundaries promoted in Cody et al. (2014). The quasi-periodicity boundaries are *Q* < 0.11 for purely periodic behavior, and *Q* > 0.85 for purely stochastic behavior. The upper bound is different than that promoted in Cody et al. (2014) which was *Q* > 0.61 for purely stochastic behavior. It is unclear why this value is so different, although it may be related to different quantification of photometric uncertainty in the *K2* light curves, as compared to *CoRoT*. The dependence of *Q* on data precision and time sampling will be the subject of future work. We plot the modified boundaries on top of all *Q* and *M* values for disk-bearing stars in Figure 6.

We thus divide the disk-bearing variables of Upper Sco and ρ Oph into eight different categories (plus two additional groups for non-variable or unclassifiable sources), as defined in Cody et al. (2014) and shown in Figure 7.

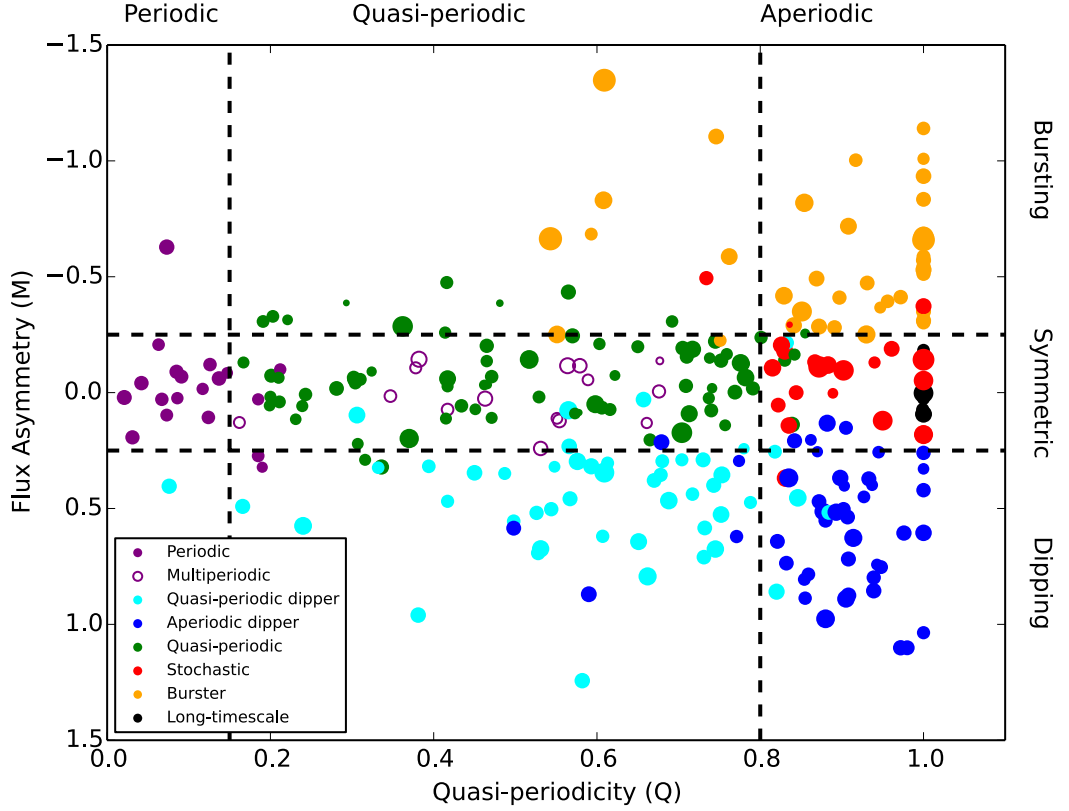


FIG. 6.— Q and M statistics for our sample of disk-bearing stars in Upper Scorpius and ρ Ophiuchus. Non-variable objects are excluded. Colors in this and subsequent plots denote different types of variables, as identified by eye; see text. Point areas in this and subsequent plots are scaled according to variability amplitude to the one-third power.

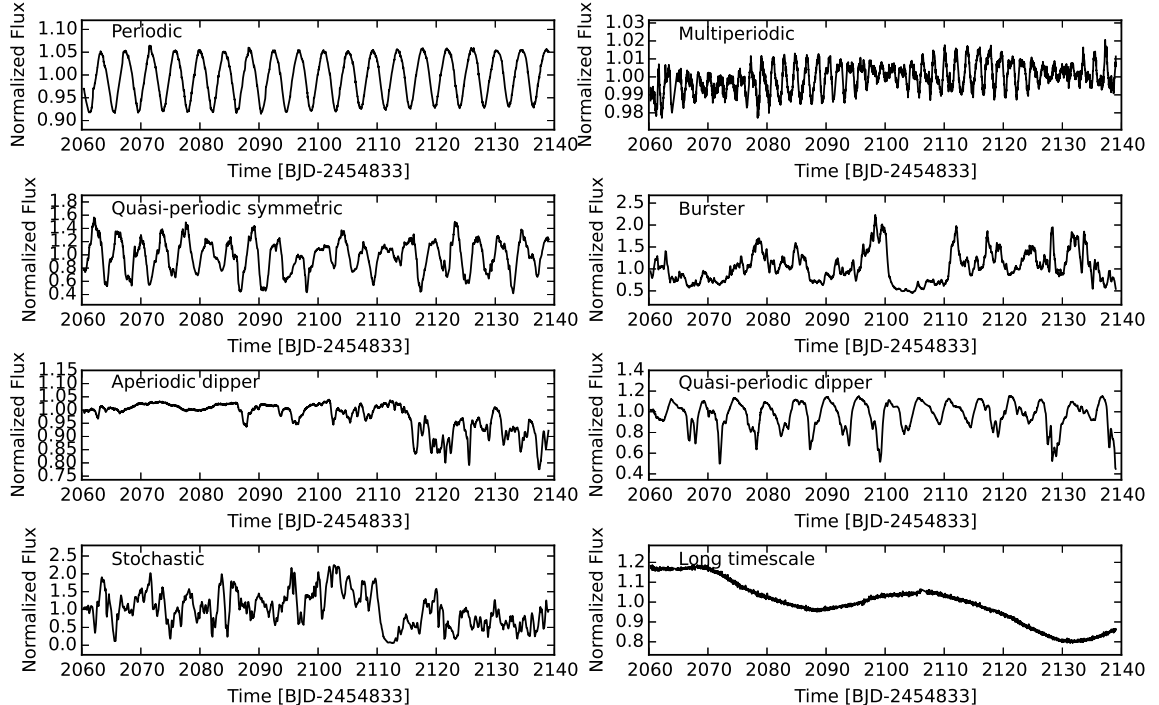


FIG. 7.— Examples of different light curve morphologies seen among disk-bearing stars in $K2$'s Campaign 2 observations of ρ Ophiuchus and Upper Scorpius. These examples also appear in Figure 14 where their EPIC identifiers and their Q and M values are given.

The categories (with denotation elsewhere in this paper given in parentheses) and their Q and M ranges are:

- burster (B)
 $M < -0.25$
- purely periodic symmetric (P)
 $Q < 0.15$ and $-0.25 < M < 0.25$
- quasi-periodic symmetric (QPS)
 $0.15 < Q < 0.85$ and $-0.25 < M < 0.25$
- purely stochastic (S)
 $Q > 0.85$ and $-0.25 < M < 0.25$
- quasi-periodic dipper (QPD)
 $0.15 < Q < 0.85$ and $M > 0.25$
- aperiodic dipper (APD)
 $Q > 0.85$ and $M > 0.25$
- long timescale (L)
- unclassifiable (U)
- non-variable (N).

Relative to Cody et al. (2014), there are no eclipsing binaries identified in the disk-bearing sample studied here. An additional category is dedicated to “long-term” variables that showed a trend on > 30 day timescales. Two stars were labeled “unclassifiable” since their CDPPs indicated variability, but a single brightness bump superimposed on noise or a gradual trend made it impossible

to label them as long-term variables or to assign any of the other categories.

As seen from examination of Figure 14, the Q and M statistics reflect the visual variability categorization quite well. Problematic borderline cases can occur, however, I would for example in which a light curve falls into one class by eye but has a systematic brightness trend that pushes it into another class based on M . Likewise, there are cases for which an object is periodically variable for part of the time series, but aperiodic for the rest; a viewer may classify this behavior as quasi-periodic or aperiodic, but the Q statistic may report otherwise. We therefore continue to rely on the human eye for the final determination of each star’s variability class, but use the statistics for guidance. All light curves and their classifications are provided in the Appendix, along with a discussion of stars that displayed multiple types of variability over the duration of observations.

The percentage of disk-bearing stars in each lightcurve group are listed in Table 3. Uncertainties are generally asymmetric and determined by assuming a binomial probability distribution for the number stars observed each group. Notably, there is a somewhat higher number of bursters than reported by Cody et al. (2017) due to our increased reliance on statistical measurements to identify them in the current work. The sample contains young stars in different environments and potentially at a variety of ages; thus we also report the variability category percentages separately for ρ Oph and Upper Sco members. The tallies for the equivalent categories as measured in NGC 2264 are also provided, and comparisons discussed in §7.2.

TABLE 3
VARIABILITY TYPES AMONG YOUNG DISK-BEARING STARS

Morphology class	Oph	Sco	Sco/Oph composite	NGC 2264
	%	%	%	%
Categories based on periodicity and stochasticity				
All Bursters	14^{+5}_{-3}	13^{+3}_{-2}	14^{+2}_{-2}	13^{+3}_{-2}
Aperiodic symmetric (Stochastic)	12^{+4}_{-3}	6^{+2}_{-1}	8^{+2}_{-2}	13^{+3}_{-2}
Quasi-periodic symmetric	20^{+5}_{-4}	29^{+3}_{-3}	26^{+3}_{-2}	17 ± 3
Aperiodic dippers	9^{+5}_{-2}	18^{+3}_{-2}	16^{+2}_{-2}	11^{+3}_{-2}
Quasi-periodic dippers	14^{+5}_{-3}	18^{+3}_{-2}	17^{+2}_{-2}	10.5^{+3}_{-2}
Periodic symmetric	6^{+4}_{-2}	7^{+2}_{-2}	7^{+1}_{-2}	3^{+2}_{-1}
Other Categories				
Multiperiodic	7^{+4}_{-2}	4^{+2}_{-1}	5^{+2}_{-1}	1^{+2}_{-1}
Long timescale	8^{+4}_{-2}	0^{+2}_{-0}	3^{+1}_{-1}	1^{+2}_{-1}
Unclassifiable	2^{+3}_{-0}	0^{+2}_{-0}	1^{+1}_{-1}	11^{+3}_{-2}
Non-variable	6^{+4}_{-2}	3^{+2}_{-1}	4^{+1}_{-1}	19 ± 3

NOTE. — Fraction of young stars in each light curve morphology group, as defined by eye but generally supported by the statistical measures Q and M (§5). There are eight variability categories, plus two more for non-variable or unclassifiable sources.

The variability timescale given in Table 2 is defined as the period from periodogram analysis, if $Q < 0.8$ (i.e., the light curve is [quasi]-periodic). For stars with $Q > 0.8$, a timescale is derived in the same manner as described in Cody et al. (2014, ;see §6.5). Amplitudes

are measured by determining the normalized flux difference between the 95th and 5th percentile points in the light curve; this is similar to a peak-to-peak amplitude, but is less sensitive to outliers and other errant points.

Figure 8 illustrates the light curve amplitudes as a function of the variability timescale. The bursting (B) and stochastic (S) sources, taken in aggregate, have the longest timescales (along with the identified long timescale (L) but generally smooth sources). Over-

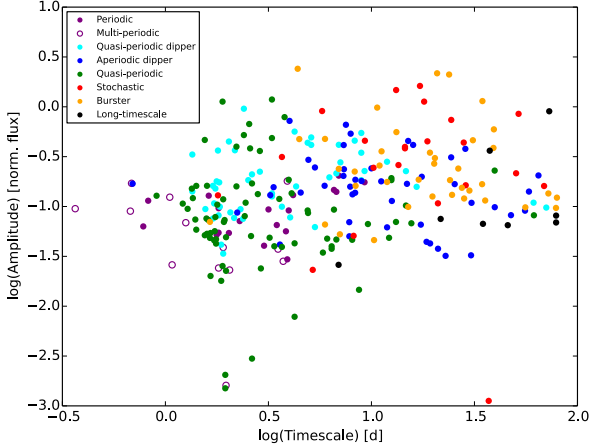


FIG. 8.— Log of the amplitude in normalized flux units versus measured timescale for all disk-bearing light curves. No point size scaling with amplitude is applied in this Figure, since one of the axes is amplitude. Although there is significant overlap within the phase-space, some clumping of variability types is apparent.

lapping the burster and stochastic sources in timescale are the aperiodic dippers (APDs), which have longer timescales than the quasi-periodic dippers (QPDs). Quasi-periodic symmetric (QPS) sources occupy the same range in timescale as the quasi-periodic dippers (QPDs), though have a broader range of amplitudes. Periodic/multi-periodic (P/MP) sources have the shortest timescales. The amplitude ranges of the various light curve categories are fairly similar, with periodic and multi-periodic sources spanning the narrowest amplitude range. Burster and stochastic sources perhaps extend to slightly higher amplitudes than other categories, and quasi-periodic symmetric sources extend to lower amplitudes than other categories.

6. CONNECTION BETWEEN VARIABILITY AND STELLAR/CIRCUMSTELLAR PROPERTIES

In this section, we explore relationships between variability type and stellar / circumstellar properties. Our sample is selected to have disks. Thus, we are more likely to detect the disk-related variability, and less likely to detect processes associated with normal stellar rotation and activity, that generally underlay the disk effects, but occur at lower amplitude.

6.1. Variability and Circumstellar Disks

Figure 6, introduced earlier, illustrates that larger amplitude variables are predominantly found among objects with both $Q > 0.35$ – in the quasi-periodic and aperiodic categories – and $M < 0.25$ – in the symmetric and bursting categories. Figure 8 just above also shows this segregation of bursting and quasi-periodic symmetric lightcurve types towards higher amplitudes.

As we now demonstrate, these larger-amplitude sources also tend to have stronger $H\alpha$ emission and redder infrared colors - especially for the bursters. These findings directly link the presence of accreting gas and the strength of the inner disk, with photometric variability categories that are attributed to accretion.

Figure 9 reproduces Figure 1 but now colored by the variability type. At bluer $J - K$ color, moving from

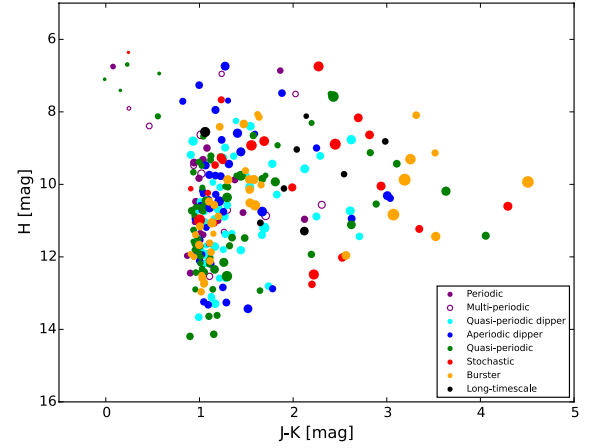


FIG. 9.— The near-infrared color-magnitude diagram of Figure 1, now colored for the variables of different types. Non-variable objects are excluded. Location of any individual source in this diagram is influenced by its: mass, age, inner disk properties, and the line-of-sight extinction.

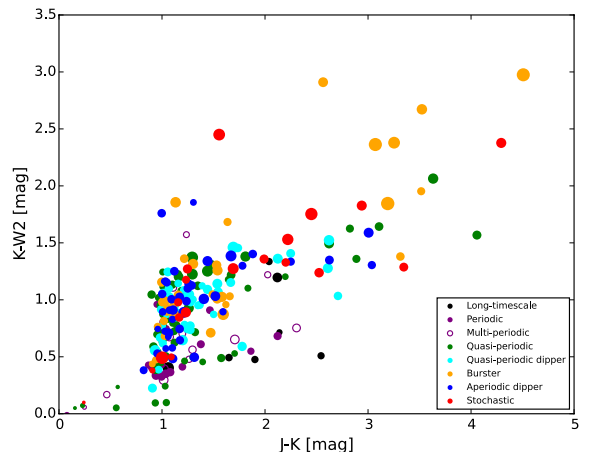
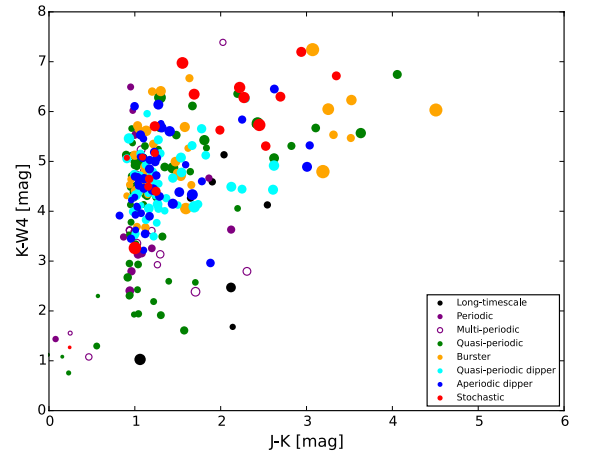


FIG. 10.— For variables of different types, top panel shows K-W4 (sensitive to disk emission) vs $J - K$ (measuring photospheric color plus inner disk color excess plus reddening effects), while bottom shows the same plot with K-W2 along the ordinate. Non-variable objects are excluded.

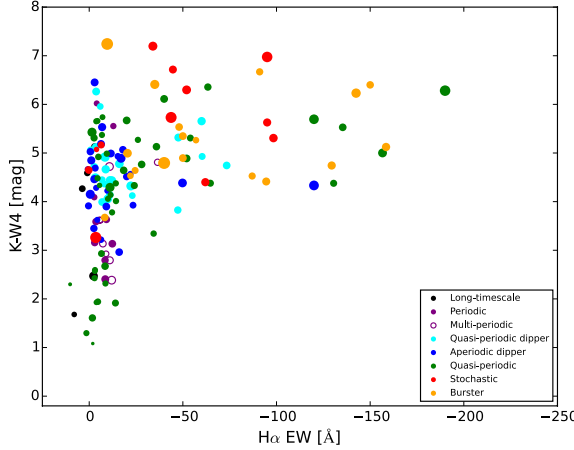


FIG. 11.— $K - W4$ color versus $H\alpha$ equivalent width for disk variables of different types.

brighter to fainter H magnitudes is equivalent to moving from higher to lower mass stars. There is no apparent systematic relationship between variability type and stellar mass (see also §6.2). Assuming low foreground extinction, redder $J - K$ color indicates objects with stronger inner disk contributions. Larger amplitude variability appears to occur for redder objects, and the sources are predominantly bursters, stochastic, and quasi-periodic dippers.

Figure 10 highlights the variability types versus dust excess. For stars with disks, $K - W4$ color probes the disk region associated with few hundred Kelvin dust (the terrestrial planet zone for solar-type stars), $K - W2$ color hotter dust (roughly the inner 1 AU for solar type stars), and $J - K$ the region containing the hottest, up to 1400 K near the inner disk edge (in the range 0.03–0.1 AU for solar type stars). For the M-type stars that dominate our sample, the wavelengths probe smaller physical radii than the numbers given above for G-type stars. Quasi-periodic dippers are relatively clustered in $K - W4$ color, with redder colors than the periodic sources, as well as bluer colors than the bursters and stochastic objects. The same segregation is not as apparent in $K - W2$ colors, suggesting that accretion-related burster and stochastic variability is driven by strong mid-infrared excess arising around 1 AU (for solar type stars), rather than being purely inner-disk phenomena.

Figure 11 highlights the variability versus accretion strength. Strong $H\alpha$ emission is seen only among the redder $K - W4$ colors, solidifying the connection between mid-infrared disks, accretion-related emission lines, and photometric variability. Long-timescale variables, periodic sources, and quasi-periodic dippers are weak accretors. Quasi-periodic sources have the broadest distribution across the empirical parameter space.

Beyond the presence and strength of disks, a critical parameter that determines the observables from star/disk systems is the orientation of the disks. In Figure 12, we present the variability types in the context of the disk sizes and inclinations to our line-of-sight, as derived by Barenfeld et al. (2017) from spatially resolved dust and gas images from ALMA. Although the formal

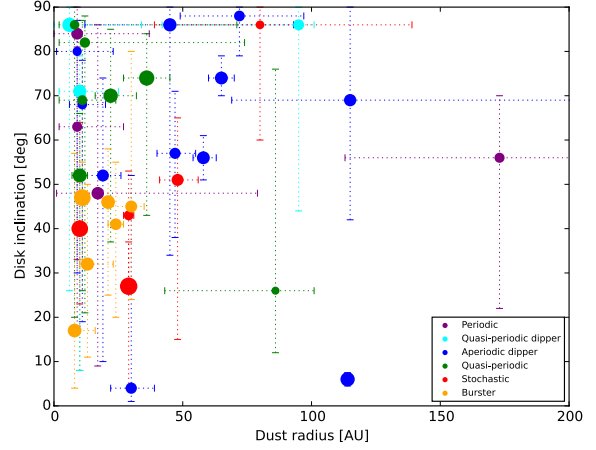


FIG. 12.— Dust continuum (top panel) and CO gas (bottom panel) disk radius, versus disk inclination, based on ALMA observations where they are available for our sample. Point sizes are scaled proportional to light curve amplitude. Although the measurements are noisy, there is clear segregation of some variability types in inclination.

errors in the inclinations are quite large⁵, some intriguing trends emerge with respect to the variability categories that we have defined – without regard to the disk characteristics beyond a sample selected based on mid-infrared excess. Dippers of both aperiodic and quasi-periodic flavors tend to have more highly inclined disks ($i > 50$ deg), though several such variables are found at $i < 10$ deg (EPIC 204245509 and EPIC 204638512). The quasi-periodic symmetric sources that are neither dipping nor bursting, also tend to have larger inclinations. Burster sources, by contrast, have ($i < 50$ deg), and are clustered at small dust radii. Stochastic sources also tend to have smaller inclinations, but have larger disks by about a factor of two. For both the burster and the stochastic categories, the gas radii are larger than the dust radii.

Considering the locations of the different variability categories in the above diagrams, our observations include:

⁵ Where disk parameters are derived from both dust and gas, the inclinations agree to within about $\pm 15^\circ$ for most, but not all, sources. Radii can be discrepant at the factor-of-two level, in both directions, again with larger outliers present.

- The bursters (B) and the stochastic (S) variables have the reddest disk colors, even redder than the dippers (APD). This is consistent with overall stronger disks for the variables that are dominated by their accretion behavior. Dippers may have relatively weaker disks, or different inner-disk geometry.
- The quasi-periodic dippers (QPD) and aperiodic dippers (APD) have somewhat smaller infrared colors, with only a narrow range of $K - W4$ and $K - W3$ disk color that is spanned relative to other lightcurve categories. The colors may be telling us about disk flaring, which could be low (thus confining the color range to only that spanned by inclination effects rather than the broader color range allowed by considering vertical disk geometry effects) compared to, e.g., bursters and stochastics with typically larger $K - W4$ and $K - W3$ colors (which require some amount of flaring to produce, especially given the tendency towards lower inclinations illustrated in Figure 12).
- The quasi-periodic symmetric (QPS) stars exhibit among the largest $H\alpha$ equivalent widths. The widths are higher than those of many sources in the burster category, for which Cody et al. (2017) established a correlation between burst activity and $H\alpha$ strength.
- There may be multiple different sub-categories within the quasi-periodic symmetric (QPS) category, with the higher amplitude sources dominated by large, hot accretion spots on top of underlying accretion variations. The lower amplitude sources, on the other hand, may be dominated by cool spot modulation, with inter-cycle variations due to a low-level accretion contribution. Venuti et al. (2015) found that quasi-periodic objects with larger amplitudes had u and r -band variations more consistent with hot spots than with cool spots (see their Figure 9). We note that the QPS sources also tend to cluster at the shorter timescales (Figure 8), similar to both the QPD and P/MP categories. In addition, both the higher and the lower amplitude QPS sources cluster at the higher disk inclinations (Figure 12). These findings are consistent with the hypothesis of spot-related variability for QPS sources, as a low inclination view of the star would result in little light modulation, due to the spots always being visible.
- The periodic (P) symmetric sources all have relatively low infrared color, bluer than the disk-related categories. This is consistent with the periodic sources lacking strong accretion that would introduce additional variability effects that swamp the periodic signal.
- The multi-periodics (MP) seem redder in $J - K$ but not other infrared colors. This could imply binarity (as opposed to disk effects) as the dominant cause of the variability.
- Disk inclination is an important parameter in the observed variability type. Dipper-type sources

(both QPD and APD) tend towards higher inclinations, $i > 50^\circ$, as originally envisioned by, e.g. Bouvier et al. (1999), Cody & Hillenbrand (2010), Morales-Calderón et al. (2011), and Stauffer et al. (2015), who invoke dust in the co-rotating inner-disk or stellar magnetosphere to explain the flux dips. The QPS sources, as mentioned above, also occupy the high-inclination half of the distribution. Burster-type and stochastic sources are not seen among higher inclination sources, but have $i < 50 - 60^\circ$, consistent with our viewing of the accretion zone more directly, unobscured by the disk.

- There are a few objects that fall in a very different part of the diagrams compared to objects of similar variability class and amplitude. We highlight the example of EPIC 204187094/2MASS J16111907-2319202, a brown dwarf in Upper Scorpius. Its light curve shows a high level of erratic variability, suggestive of strong accretion and a significant disk. But surprisingly, its reported $H\alpha$ width and infrared colors are low (see the red dot at $H\alpha < 10$ in Figure 11). We speculate that both variability type and accretion properties change intermittently, and the discrepancy here is due to the non-simultaneous nature of spectroscopic versus photometric data taking.

6.2. Variability and Stellar Properties

We can also compare the variability properties in ρ Oph and Upper Sco, across stellar masses, using spectral type as a proxy. Figure 13 shows variability with spectroscopically determined spectral type. Variability amplitudes decrease significantly at spectral types earlier than mid-G, with a range of variability types seen. Several early type stars display very clear but low amplitude (<1%) quasi-periodic variability. We also encounter the dipper phenomenon with clear aperiodic fading events in the light curves of the late A stars EPIC 204399980 and EPIC 204514546.

While the sample of early-type stars is too small to conduct a full statistical evaluation of the prevalence of each variability type, we can speculate on the reasons for the drop-off in amplitude. If the quasi-periodic behavior is due to the rotational modulation of accretion hotspots, then one would expect the smaller spot-photosphere contrast to produce lower amplitude light curves. If it is instead due to obscuration effects by the inner disk, then the lower amplitudes could point to a decrease in size and/or larger radial distance of occulting structures.

In terms of stellar rotation, while we found that 96% of our disk-selected sample of stars is variable, only 12% among these are periodic (P), with 40% of these multi-periodic (MP), in a manner consistent with rotating starspot behavior. However, another 25% of the sample is quasi-periodic with symmetric light curves (QPS), and an additional 17% is quasi-periodic with dipper type light curves (QPD). The quasi-periodic and disk-related variability could also be related to a rotation-regulated mechanism – either accretion at the stellar surface, or dipping associated with material entrained in magnetic fields that are co-rotating with the star, or with dust located in asymmetric structures at or near the inner disk edge.

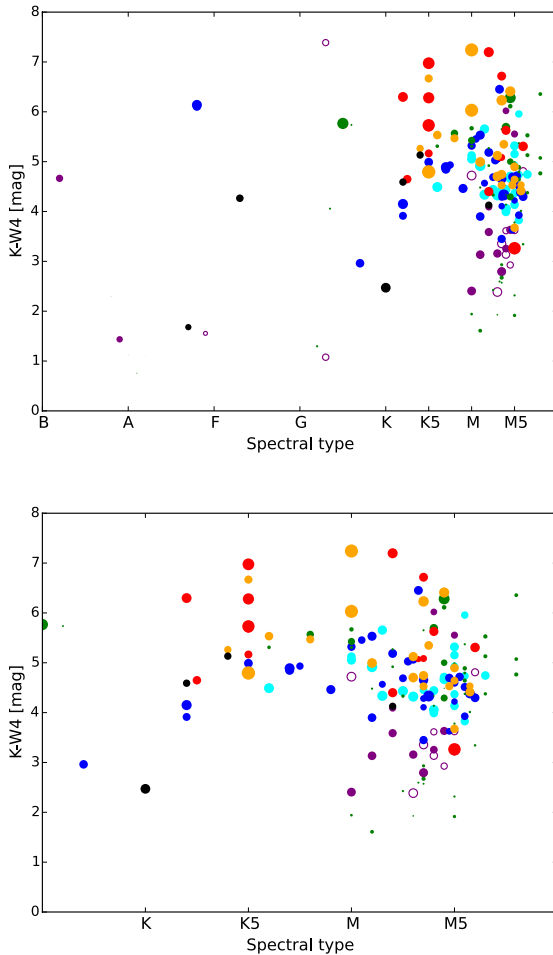


FIG. 13.— K -W4 disk excess versus spectral type ; colors are as in Figs. 8–10. We show another version (bottom) zoomed in on types K through M. We note that the points for the two A8 stars EPIC 20439980 and EPIC 204514546 (both aperiodic dippers) fall exactly on top of each other.

7. COMPARISONS

7.1. Comparison with *CoRoT* study of young disked star light curves in NGC 2264

The variability demographics established here can be compared with results from Cody et al. (2014) on the ~ 3 Myr NGC 2264 cluster, which are also given in Table 3.

We find that towards the ρ Oph core, which is perhaps 1–3 Myr old, that the fractions in each of the variability categories defined from Q and M statistics are approximately the same. We do note that a somewhat lower mass population is probed in ρ Oph, due to its closer distance (though higher extinction), as discussed in §2.4.

Towards the somewhat older 5–10 Myr, and more populous Upper Sco region, however, there are notable differences in the population of the light curve categories. The burster fraction is in fact identical across the groups, at $\approx 13\%$. However, relative to the younger NGC 2264 and ρ Oph, there is a higher fraction among the Upper Sco light curves that are symmetric (approximately equal upward and downward flux excursions) for periodic and multi-periodic sources, and fractionally fewer aperi-

odic (also known as stochastic) sources, perhaps because the disk activity is lower. There are also more dippers overall among Upper Sco stars, including each of the periodic, quasi-periodic, and aperiodic sub-categories. This could be evidence of the dipper behavior being related to evolving disks, perhaps as accretion activity declines and inner disk cleared regions grow and present more surface area for photons originating at the stellar surface and accretion zone to be absorbed.

7.2. Comparison with *K2* study of periodic sources in Upper Sco

Rebull et al. (2018) undertook an investigation of periodic behavior among a much larger sample of Upper Sco and ρ Oph members than considered here. Their sample was selected based on proper motions and color-magnitude diagrams and includes both non-disk and disked (likely) members. They concluded that more than 85% of cluster members overall are periodic, with 20% of these multi-periodic.

We found a much lower fraction of periodic stars among the disk-bearing sample, only 7%. Even attributing all of the quasi-periodic variability to some rotation-regulated mechanism (e.g. accretion or dipping associated with structures that are co-rotating with the star), the fraction of periodic sources in the disk-selected sample is only about half of that among the broader Upper Sco and ρ Oph sample of Rebull et al. (2018).

7.3. Comparison with other analyses of *K2* Campaign 2 young star lightcurves

Independent analyses of the variability types exhibited by members of the young Upper Sco and ρ Oph regions in *K2* data have been conducted by Ansdell et al. (2016a) and Hedges et al. (2018); the latter study appeared just as we were finalizing the present work for submission.

Comparing our dipper and burster classifications with these groups, we find that our sample includes 26 dippers and 14 bursters that do not appear in previous lists (excluding Cody et al. 2017). We also find that we do not agree with some of the dipper or burster classifications by these groups. Although guided by our M and Q statistics, our light curve categorization is ultimately determined by-eye.

Ansdell et al. (2016a) applied a high-pass filter and used measured depth and significance of repeated dips to identify 25 dipper sources. We agree with all but EPIC 203895983 and EPIC 204630363, which we have classified as quasi-periodic-symmetric (QPS) rather than as dippers (APD or QPD). However, we do have disagreements for about half of the remaining cases between quasi-periodic ($Q < 0.8$ in our scheme) vs aperiodic ($Q < 0.8$ in our scheme) dipper categorization.

Hedges et al. (2018) use a machine-learning method to identify 95 dippers, based on distinguishing them from other non-young-star periodic variable classes consisting of various pulsators and binaries. Given the richness of young star variability behavior, especially the quasi-periodicity and aperiodicity, it is not surprising that our results differ substantially from those of Hedges et al. (2018). We agree with 69 of their 95 dippers being in either the APD or QPD categories. Of the remaining 26, we find that 5 are not in our final sample due to lack of membership, disk, or good-quality

lightcurve. The rest we categorize as symmetric, either QPS (quasi-periodic-symmetric) or S (stochastic, also called aperiodic-symmetric). Hedges et al. (2018) also identify 30 bursters, seemingly because they stood out as dippers in their random forest classifier, but which upon examination brightened rather than faded. We agree that 25 are bursters, while four (EPIC 203833873, 203870058, 203889938, and 203912674) are labeled by us as stochastic, and the remaining one (EPIC 203668987; Haro1-5) was not in our disk sample.

Among our *disk-selected sample*, we find that $32 \pm 3\%$ of the sources exhibit “dipper” behavior, including both our quasi-periodic dipper (QPD) and aperiodic dipper (APD) categories. We found a higher fraction of dippers in the older Upper Sco compared to the young ρ Oph. Hedges et al. (2018), by contrast, reports $6 \pm 1\%$ and $11 \pm 2.5\%$ as the dipper fractions in Upper Sco and ρ Oph, respectively, but among a sample that includes both disked and non-disk stars, given that the sample is simply a compilation of candidate members from the literature. They claim that among stars with disks, the fractions are higher, $21 \pm 5.5\%$ for the combined regions – but this is still lower than our derived $32 \pm 3\%$ (Table 3).

Also among our *disk-selected sample*, we find $13 \pm 2\%$ of the sources to exhibit “burster” behavior, with no difference between Upper Sco and ρ Oph. As for the dippers, Hedges et al. (2018) report lower numbers of $1 \pm 0.5\%$ and $7.5 \pm 2\%$ for the burster fractions in Upper Sco and ρ Oph, respectively, again considering a disk-plus-non-disk sample. They claim that among stars with disks, the fractions are indeed higher, $4.5 \pm 1.5\%$ and $14.5 \pm 4\%$ – but these are still lower than our combined $13 \pm 2\%$ (Table 3).

In addition to the *K2* studies mentioned above, Ansdell et al. (2018) classified light curves for Upper Sco and ρ Oph members based on ground-based data at lower precision and cadence than the *K2* data, though over longer duration. Among their four identified dippers, we concur with the classification based on our *K2* data analysis of shorter time series for three of the cases, but a fourth (J15554883-2512240 = EPIC 203710077) we have placed in our multi-periodic category. None of their three identified “long period” systems are in our disk-selected sample. And among their six “long-timescale variations”, four are not in our disk-selected sample, one is classified by us as a dipper, and the last is a quasi-periodic symmetric (QPS) system. We would not be sensitive to the noted long timescale behavior.

8. SUMMARY AND DISCUSSION

In this paper, we extend our previous work on time series photometric analysis of NGC 2264 to young members of the ρ Oph and Upper Sco regions. Analysis of the dataset from *K2*’s Campaign 2 reveals that nearly 100% of disk-bearing members of Upper Sco and ρ Oph are photometrically variable, with amplitudes ranging from $\sim 0.1\%$ to a factor of three. We have provided a framework for categorizing young star light curves that is most effective for high precision and high cadence data from space-based photometric monitoring missions. The statistical metrics Q and M originally developed for the NGC 2264 dataset from *CoRoT* allow us to place individual sources into variability categories. A range in light curve repeatability (Q) from periodic, to quasi-periodic,

to stochastic, and a range in light curve flux symmetry (M) from primarily dipping, to symmetric, to primarily bursting, is seen. These metrics may form the basis for feature definition in future machine-learning approaches to lightcurve classification for young stars. Thus far, young stars have stymied unsupervised machine-learning approaches that use general feature sets designed around periodic variable classification (e.g. Richards et al. 2011) due to the admixture of periodic and aperiodic phenomena contributing to the lightcurves.

Upon assigning categories to all young stars in our *K2* dataset, we have explored correlations between variability type and circumstellar properties. We find that bursters, stochastic sources, and quasi-periodic sources tend to have larger infrared colors, which can indicate more rapidly accreting circumstellar disks once geometric effects are accounted for. However, these groups appear to separate in their inclination distributions, with bursters and stochastic sources found exclusively at $i < 50 - 60^\circ$, while quasi-periodic sources tend to have $i > 50^\circ$. On the other hand, dippers, both quasi-periodic and aperiodic, also tend to have $i > 50^\circ$.

While the burster fraction is the same, we find a higher fraction of dippers in the older Upper Sco region than towards sources in the ρ Oph molecular cloud region and towards NGC 2264, consistent with a scenario in which somewhat evolved inner disks give rise to a dipper lightcurve morphology. Furthermore, the dippers appear to be distinguished from the quasi-periodic sources by having lower H α equivalent widths (indicating lower accretion rates on average).

The clustering of particular light curve morphologies in the parameter space of inclination, disk size, and accretion rate lends support to previous suggestions that variability mechanisms include obscuration by inner disk dust (dippers), rapid accretion rate changes (bursters; stochastic stars), and flux modulation by accretion hot spots at the stellar surface (large amplitude quasi-periodic class). The periodic, multiperiodic, and low-amplitude quasi-periodic sources are consistent with cool spots on the stellar surface, seen due to a relative lack of obscuring material and/or accretion. The remaining unclassifiable and long-timescale variables remain to be elucidated and may be contaminants such as asymptotic giant stars.

Dippers have frequently been explained as the manifestation of a warped or otherwise clumpy inner disk occulting parts of the central star (e.g., Bouvier et al. 1999), as seen from a nearly edge-on viewpoint. Bodman et al. (2017) argued that either a disk warp or dust in the accretion stream could be responsible for dipping behavior at moderately high view angle. The appearance of most dipping behavior in systems with disk inclinations between 50° and 90° strongly supports these ideas. There are two notable exceptions with $i < 10^\circ$, EPIC 204245509 and EPIC 204638512, the latter of which was highlighted by Ansdell et al. (2016b). These may represent rare cases in which the inner disk is not aligned with the resolved outer disk.

With approximately equal proportions of periodic and aperiodic dippers, it is as yet unclear as to what determines the repeatability (or lack thereof) of fading events. McGinnis et al. (2015) suggested that the behavior is determined according to whether accretion is

Rayleigh-Taylor unstable, as predicted by Blinova et al. (2016) based on the accretion rate and magnetic dipole tilt relative to the stellar rotation axis. In contrast, we do not detect any correlation between periodicity status and H α equivalent width in this dataset. However, non-simultaneity of the spectroscopic and photometric observations may obscure such an effect. We do find that most dippers have relatively low H α values, consistent with the requirement that the magnetospheric radius (determined in part by accretion rate) must lie far enough out from the star such that dust does not sublime at that location.

The highest amplitude quasi-periodic stars are interesting in that they have very large reported H α equivalent widths. The semi-regular behavior of their light curves implies a stable accretion hot spot configuration. Stability is expected for fairly *low* accretion rates (Romanova et al. 2003, 2004). However, Blinova et al. (2016) have recently shown that there is an additional “unstable ordered” regime in which one or two tongues of accreting gas penetrate the magnetosphere to reach the stellar photosphere. We believe that the quasi-periodic stars with amplitudes from 0.3 to 1.3 (in normalized flux units) may be examples of this effect. They may be seen only at inclinations greater than 50° if the resulting hot spots are situated away from the stellar pole.

Turning finally to the bursters and stochastic stars, we have seen that these have moderately high H α equivalent widths as well, but inclinations typically between 15° and 50°. The chaotic nature of the light curves is suggestive of an unstable accretion regime, while the strong near-

infrared excesses imply dust fairly close to the central star (particularly for the bursters). What distinguishes the bursters and stochastic stars? Stauffer et al. (2016) hypothesized that they are both due to variable mass accretion, with flow for the latter including many more low-amplitude events. The similar ranges of H α and [near]-infrared colors for these two classes lends support to the idea that they are both manifestations of unstable accretion flow, seen at low inclination.

K2's Campaign 2 young star dataset has offered a unique opportunity to correlate detailed variability properties with a large collection of stellar and circumstellar parameters, some of which include resolved measurements. Further *K2* observations, e.g., of the young cluster NGC 6530 and the Taurus association will provide further tests for our framework of variability classification and corresponding suggestions for physical mechanisms.

We extend our appreciation to the referee for helpful comments. We thank Trevor David for help collecting and categorizing *K2* light curves. We acknowledge John Carpenter for early conversations about *ALMA* samples in Upper Sco, as well as Luisa Rebull and John Stauffer for general discussions about young star variability, membership, and disk properties. This paper includes data collected by the *K2* mission. Funding for the *K2* mission is provided by the NASA Science Mission Directorate.

REFERENCES

- Aigrain, S., Parviainen, H., & Pope, B. J. S. 2016, MNRAS, 459, 2408
 Andrews, S. M., & Williams, J. P. 2007, ApJ, 671, 1800
 Ansdell, M., Gaidos, E., Rappaport, S. A., Jacobs, T. L., LaCourse, D. M., Jek, K. J., Mann, A. W., Wyatt, M. C., Kennedy, G., Williams, J. P., & Boyajian, T. S. 2016a, ApJ, 816, 69
 Ansdell, M., Gaidos, E., Williams, J. P., Kennedy, G., Wyatt, M. C., LaCourse, D. M., Jacobs, T. L., & Mann, A. W. 2016b, MNRAS, 462, L101
 Ansdell, M., Oelkers, R. J., Rodriguez, J. E., Gaidos, E., Somers, G., Mamajek, E., Cargile, P. A., Stassun, K. G., Pepper, J., Stevens, D. J., Beatty, T. G., Siverd, R. J., Lund, M. B., Kuhn, R. B., James, D., & Gaudi, B. S. 2018, MNRAS, 473, 1231
 Ardila, D., Martín, E., & Basri, G. 2000, AJ, 120, 479
 Baglin, A., Auvergne, M., Barge, P., Deleuil, M., Catala, C., Michel, E., Weiss, W., & COROT Team. 2006, in ESA Special Publication, Vol. 1306, The CoRoT Mission Pre-Launch Status - Stellar Seismology and Planet Finding, ed. M. Fridlund, A. Baglin, J. Lochard, & L. Conroy, 33
 Barenfeld, S. A., Carpenter, J. M., Sargent, A. I., Isella, A., & Ricci, L. 2017, ApJ, 851, 85
 Blinova, A. A., Romanova, M. M., & Lovelace, R. V. E. 2016, MNRAS, 459, 2354
 Bodman, E. H. L., Quillen, A. C., Ansdell, M., Hippke, M., Boyajian, T. S., Mamajek, E. E., Blackman, E. G., Rizzuto, A., & Kastner, J. H. 2017, MNRAS, 470, 202
 Bouvier, J., Chelli, A., Allain, S., Carrasco, L., Costero, R., Cruz-Gonzalez, I., Dougados, C., Fernández, M., Martín, E. L., Ménard, F., Mennessier, C., Mujica, R., Recillas, E., Salas, L., Schmidt, G., & Wichmann, R. 1999, A&A, 349, 619
 Carpenter, J. M., Ricci, L., & Isella, A. 2014, ApJ, 787, 42
 Cody, A. M., & Hillenbrand, L. A. 2010, ApJS, 191, 389 —. 2011, ApJ, 741, 9
 Cody, A. M., Hillenbrand, L. A., David, T. J., Carpenter, J. M., Everett, M. E., & Howell, S. B. 2017, ApJ, 836, 41
 Cody, A. M., Stauffer, J., Baglin, A., Micela, G., Rebull, L. M., Flaccomio, E., Morales-Calderón, M., Aigrain, S., Bouvier, J., Hillenbrand, L. A., Gutermuth, R., Song, I., Turner, N., Alencar, S. H. P., Zwintz, K., Plavchan, P., Carpenter, J., Findeisen, K., Carey, S., Terebey, S., Hartmann, L., Calvet, N., Teixeira, P., Vrba, F. J., Wolk, S., Covey, K., Poppenhaeger, K., Günther, H. M., Forbrich, J., Whitney, B., Affer, L., Herbst, W., Hora, J., Barrado, D., Holtzman, J., Marchis, F., Wood, K., Medeiros Guimarães, M., Lillo Box, J., Gillen, E., McQuillan, A., Espaillat, C., Allen, L., D'Alessio, P., & Favata, F. 2014, AJ, 147, 82
 David, T. J., Petigura, E. A., Hillenbrand, L. A., Cody, A. M., Collier Cameron, A., Stauffer, J. R., Fulton, B. J., Isaacson, H. T., Howard, A. W., Howell, S. B., Everett, M. E., Wang, J., Benneke, B., Hellier, C., West, R. G., Pollacco, D., & Anderson, D. R. 2017, ApJ, 835, 168
 Dawson, P., Scholz, A., Ray, T. P., Marsh, K. A., Wood, K., Natta, A., Padgett, D., & Ressler, M. E. 2013, MNRAS, 429, 903
 de Bruijne, J. H. J. 1999, MNRAS, 310, 585
 Erickson, K. L., Wilking, B. A., Meyer, M. R., Robinson, J. G., & Stephenson, L. N. 2011, AJ, 142, 140
 Fang, Q., Herczeg, G. J., & Rizzuto, A. 2017, ApJ, 842, 123
 Findeisen, K., Cody, A. M., & Hillenbrand, L. 2015, ApJ, 798, 89
 Guenther, E. W., Esposito, M., Mundt, R., Covino, E., Alcalá, J. M., Cusano, F., & Stecklum, B. 2007, A&A, 467, 1147
 Gutermuth, R. A., Megeath, S. T., Myers, P. C., Allen, L. E., Pipher, J. L., & Fazio, G. G. 2009, ApJS, 184, 18
 Hedges, C., Hodgkin, S., & Kennedy, G. 2018, ArXiv e-prints
 Herbig, G. H. 1954, ApJ, 119, 483
 Honda, M., Maaskant, K., Okamoto, Y. K., Kataza, H., Yamashita, T., Miyata, T., Sako, S., Fujiyoshi, T., Sakon, I., Fujiwara, H., Kamizuka, T., Mulders, G. D., Lopez-Rodriguez, E., Packham, C., & Onaka, T. 2015, ApJ, 804, 143

- Houk, N., & Smith-Moore, M. 1988, Michigan Catalogue of Two-dimensional Spectral Types for the HD Stars. Volume 4, Declinations -26deg.0 to -12deg.0.
- Howell, S. B., Sobeck, C., Haas, M., Still, M., Barclay, T., Mullally, F., Troeltzsch, J., Aigrain, S., Bryson, S. T., Caldwell, D., Chaplin, W. J., Cochran, W. D., Huber, D., Marcy, G. W., Miglio, A., Najita, J. R., Smith, M., Twicken, J. D., & Fortney, J. J. . 2014, PASP, 126, 398
- Isella, A., Carpenter, J. M., & Sargent, A. I. 2009, ApJ, 701, 260
- Joy, A. H. 1945, ApJ, 102, 168
- Köhler, R., Kunkel, M., Leinert, C., & Zinnecker, H. 2000, A&A, 356, 541
- Lodie, N. 2013, MNRAS, 431, 3222
- Lodie, N., Dobbie, P. D., & Hambly, N. C. 2011, A&A, 527, A24
- Lodie, N., Hambly, N. C., & Jameson, R. F. 2006, MNRAS, 373, 95
- Luhman, K. L., & Mamajek, E. E. 2012, ApJ, 758, 31
- Luhman, K. L., & Rieke, G. H. 1999, ApJ, 525, 440
- Manara, C. F., Testi, L., Natta, A., & Alcalá, J. M. 2015, A&A, 579, A66
- McGinnis, P. T., Alencar, S. H. P., Guimaraes, M. M., Sousa, A. P., Stauffer, J., Bouvier, J., Rebull, L., Fonseca, N. N. J., Venuti, L., Hillenbrand, L., Cody, A. M., Teixeira, P. S., Aigrain, S., Favata, F., Füreß, G., Vrba, F. J., Flaccomio, E., Turner, N. J., Gameiro, J. F., Dougados, C., Herbst, W., Morales-Calderón, M., & Micela, G. 2015, A&A, 577, A11
- Morales-Calderón, M., Stauffer, J. R., Hillenbrand, L. A., Gutermuth, R., Song, I., Rebull, L. M., Plavchan, P., Carpenter, J. M., Whitney, B. A., Covey, K., Alves de Oliveira, C., Winston, E., McCaughrean, M. J., Bouvier, J., Guieu, S., Vrba, F. J., Holtzman, J., Marchis, F., Hora, J. L., Wasserman, L. H., Terebey, S., Megeath, T., Guinan, E., Forbrich, J., Huéamo, N., Riviere-Marichalar, P., Barrado, D., Stapelfeldt, K., Hernández, J., Allen, L. E., Ardila, D. R., Bayo, A., Favata, F., James, D., Werner, M., & Wood, K. 2011, ApJ, 733, 50
- Najita, J. R., Andrews, S. M., & Muzerolle, J. 2015, MNRAS, 450, 3559
- Parks, J. R., Plavchan, P., White, R. J., & Gee, A. H. 2014, ApJS, 211, 3
- Pecaut, M. J., & Mamajek, E. E. 2016, MNRAS, 461, 794
- Pecaut, M. J., Mamajek, E. E., & Bubar, E. J. 2012, ApJ, 746, 154
- Preibisch, T., Brown, A. G. A., Bridges, T., Guenther, E., & Zinnecker, H. 2002, AJ, 124, 404
- Preibisch, T., Guenther, E., Zinnecker, H., Sterzik, M., Frink, S., & Roeser, S. 1998, A&A, 333, 619
- Preibisch, T., & Mamajek, E. 2008, The Nearest OB Association: Scorpius-Centaurus (Sco OB2), ed. B. Reipurth, 235
- Rebollido, I., Merín, B., Ribas, Á., Bustamante, I., Bouy, H., Riviere-Marichalar, P., Prusti, T., Pilbratt, G. L., André, P., & Ábrahám, P. 2015, A&A, 581, A30
- Reboussin, L., Guilloteau, S., Simon, M., Gross, N., Wakelam, V., Di Folco, E., Dutrey, A., & Piétu, V. 2015, A&A, 578, A31
- Rebull, L. M., Stauffer, J. R., Cody, A. M., Hillenbrand, L. A., David, T. J., & Pinsonneault, M. 2018, ApJ
- Rice, T. S., Wolk, S. J., & Aspin, C. 2012, ApJ, 755, 65
- Richards, J. W., Starr, D. L., Butler, N. R., Bloom, J. S., Brewer, J. M., Crellin-Quick, A., Higgins, J., Kennedy, R., & Rischard, M. 2011, ApJ, 733, 10
- Rizzuto, A. C., Ireland, M. J., & Kraus, A. L. 2015, MNRAS, 448, 2737
- Rizzuto, A. C., Ireland, M. J., & Robertson, J. G. 2011, MNRAS, 416, 3108
- Romanova, M. M., Ustyugova, G. V., Koldoba, A. V., & Lovelace, R. V. E. 2004, ApJ, 610, 920
- Romanova, M. M., Ustyugova, G. V., Koldoba, A. V., Wick, J. V., & Lovelace, R. V. E. 2003, ApJ, 595, 1009
- Scaringi, S., Manara, C. F., Barenfeld, S. A., Groot, P. J., Isella, A., Kenworthy, M. A., Knigge, C., Maccarone, T. J., Ricci, L., & Ansdell, M. 2016, MNRAS, 463, 2265
- Skiff, B. A. 2014, VizieR Online Data Catalog, 1
- Slesnick, C. L., Carpenter, J. M., & Hillenbrand, L. A. a nd Mamajek, E. E. 2006, AJ, 132, 2665
- Slesnick, C. L., Hillenbrand, L. A., & Carpenter, J. M. 2008, ApJ, 688, 377
- Stauffer, J., Cody, A. M., McGinnis, P., Rebull, L., Hillenbrand, L. A., Turner, N. J., Carpenter, J., Plavchan, P., Carey, S., Terebey, S., Morales-Calderón, M., Alencar, S. H. P., Bouvier, J., Venuti, L., Hartmann, L., Calvet, N., Micela, G., Flaccomio, E., Song, I., Gutermuth, R., Barrado, D., Vrba, F. J., Covey, K., Padgett, D., Herbst, W., Gillen, E., Lyra, W., Medeiros Guimaraes, M., Bouy, H., & Favata, F. 2015, AJ, 149, 130
- Stauffer, J., Cody, A. M., Rebull, L., Hillenbrand, L. A., Turner, N. J., Carpenter, J., Carey, S., Terebey, S., Morales-Calderón, M., Alencar, S. H. P., McGinnis, P., Sousa, A., Bouvier, J., Venuti, L., Hartmann, L., Calvet, N., Micela, G., Flaccomio, E., Song, I., Gutermuth, R., Barrado, D., Vrba, F. J., Covey, K., Herbst, W., Gillen, E., Medeiros Guimaraes, M., Bouy, H., & Favata, F. 2016, AJ, 151, 60
- Stauffer, J., Collier Cameron, A., Jardine, M., David, T. J., Rebull, L., Cody, A. M., Hillenbrand, L. A., Barrado, D., Wolk, S., Davenport, J., & Pinsonneault, M. 2017, AJ, 153, 152
- Torres, C. A. O., Quast, G. R., da Silva, L., de La Reza, R., Melo, C. H. F., & Sterzik, M. 2006, A&A, 460, 695
- Wahhaj, Z., Cieza, L., Koerner, D. W., Stapelfeldt, K. R., Padgett, D. L., Case, A., Keller, J. R., Merín, B., Evans, II, N. J., Harvey, P., Sargent, A., van Dishoeck, E. F., Allen, L., Blake, G., Brooke, T., Chapman, N., Mundy, L., & Myers, P. C. 2010, ApJ, 724, 835
- Walker, M. F. 1954, AJ, 59, 333
- Walter, F. M., Vrba, F. J., Mathieu, R. D., Brown, A., & Myers, P. C. 1994, AJ, 107, 692
- Wilking, B. A., Gagné, M., & Allen, L. E. 2008, Star Formation in the ρ Ophiuchi Molecular Cloud, ed. B. Reipurth, 351

APPENDIX

HYBRID VARIABILITY CLASSES

While we have assigned a single morphology to each light curve in Table 2 and Figure 14, in some cases the behavior appears to fall into more than one category. We describe the various combinations of variability types and hybrid behaviors, below.

- Around 10 stars in our disk sample display both dips and spot signatures. Rebull et al. (2018) identified these from the perspective of examining periodic stars in the Upper Sco and ρ Oph *K2* data, and presented evidence that the dip events have nearly the same period as the spot pattern. They argued this was evidence of disk locking, with the stellar photosphere and material at the inner disk radius co-rotating due to linkage by the magnetosphere. Specific objects include EPIC 203542463, EPIC 203770366 (periodic behavior for many weeks, after which narrow dips suddenly appear during the last 25 days), EPIC 204274536, EPIC 204489514, EPIC 204344180 (narrow dips in the first third of the light curve, at the spot period), EPIC 204449389 (evolving spot plus occasional narrow dips), and EPIC 205051240 (occasional narrow dips on top of spot pattern). EPIC 203927902 is a special case in which periodic behavior dominates for most of the light curve, apart from a large (20% depth) double dip that lasts approximately 10 days. EPIC 204278916 similarly exhibits gradually diminishing aperiodic dips over the first 30 days, yielding to a spot pattern; this source is also discussed by Scaringi et al. (2016).

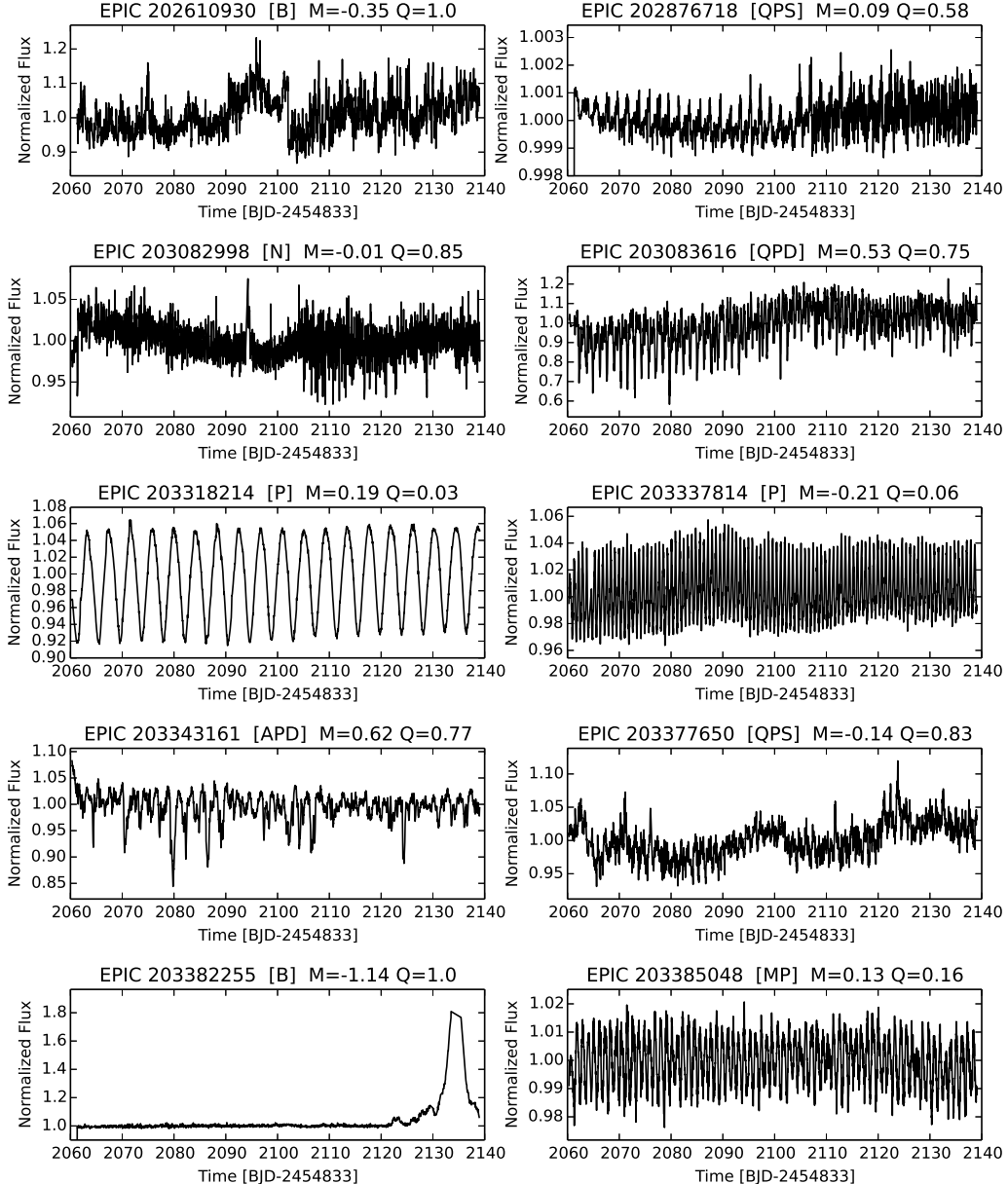


FIG. 14.— Light curves of disk-bearing stars over the 80-day duration of *K2* Campaign 2, in order of EPIC identifier. Figure labels include the variability type from Table 2, namely "P" = strictly periodic behavior, "MP" = multiple distinct periods, "QPD" = quasi-periodic dippers, "QPS" = quasi-periodic symmetric, "APD" = aperiodic dippers, "B" = bursters, "S" = stochastic stars, "L" = long-timescale behavior that doesn't fall into the other categories. Values of flux symmetry metric M and the quasi-periodicity metric Q from Table 2 are also provided.

- In some objects, there is stochastic or otherwise noisy behavior on timescales of several weeks, after which dipping suddenly appears to turn on. An example is EPIC 204538777.
- A small set of stars shows both bursts and spots; these include EPIC 204397408, EPIC 203856109 and EPIC 205156547. One unique star, EPIC 204449274, displays all three behaviors.
- There are stars with a long-term trend on top of the dominant variability type that we list in Table 2. It is difficult to discern whether these trends are real or simply uncorrected systematics.
- Finally, a significant fraction ($\sim 5\%$) of periodic stars show more than one period, as indicated by the variability type "MP" in Table 2.

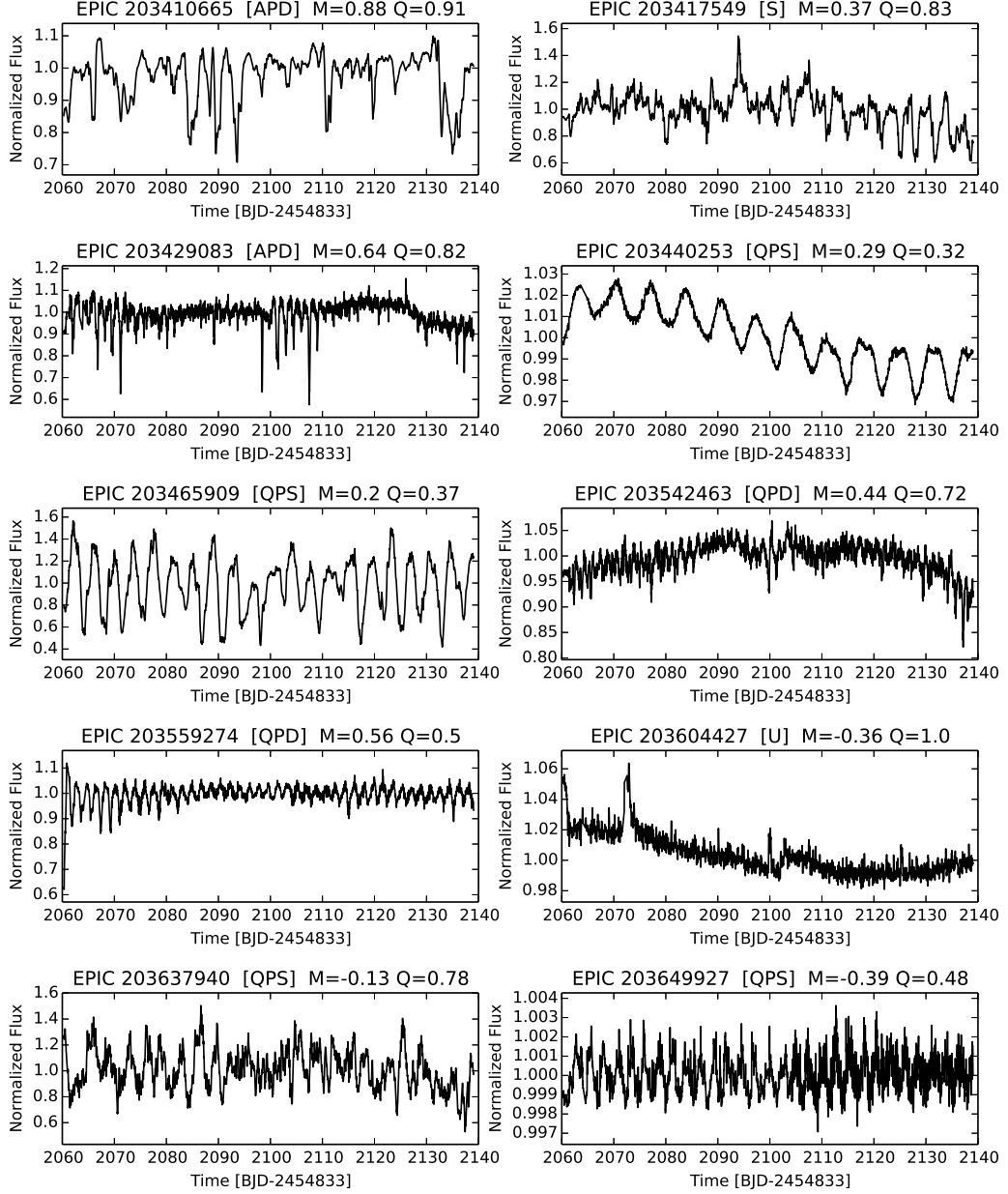


FIG. 14.— Cont.

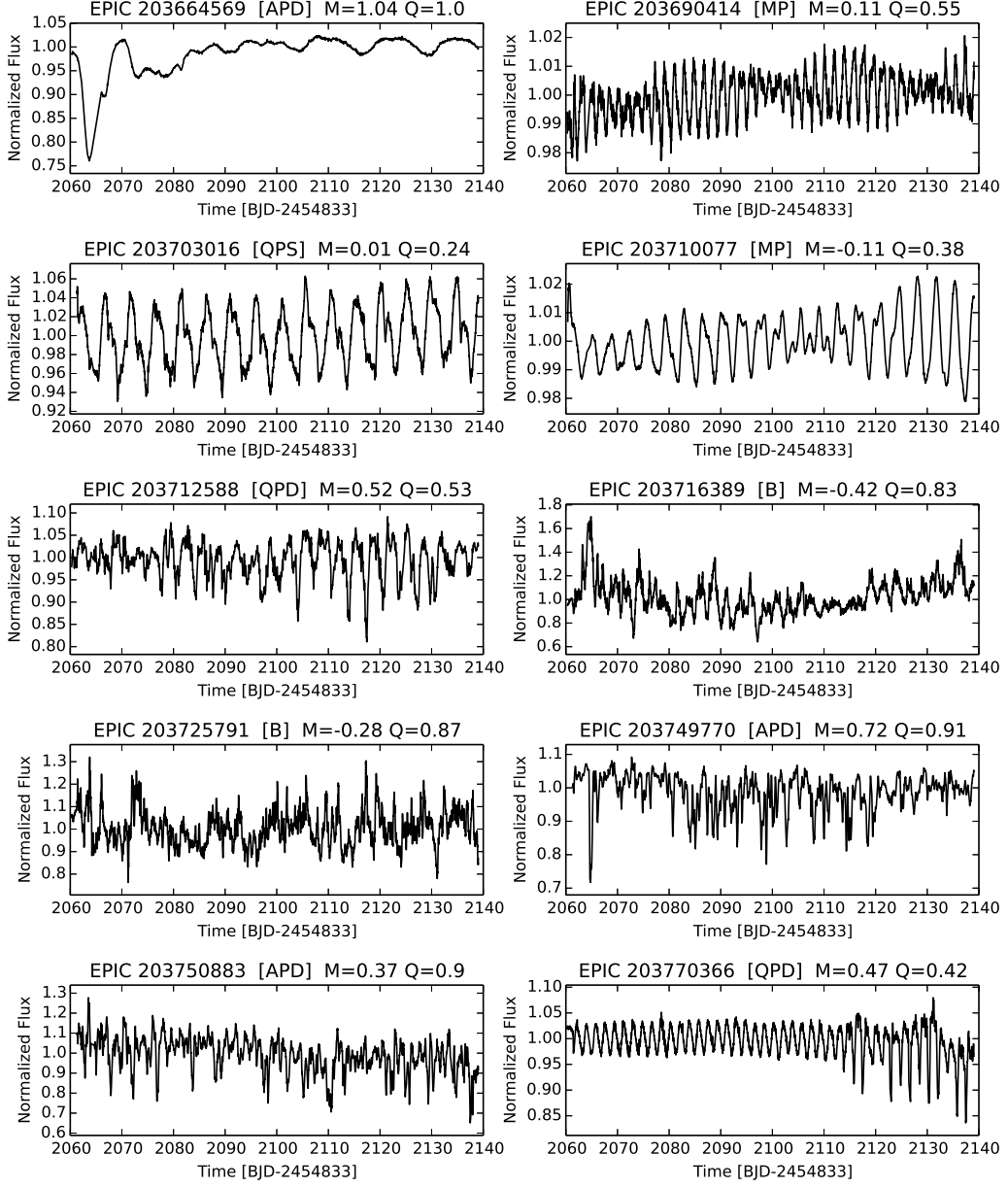


FIG. 14.— Cont.

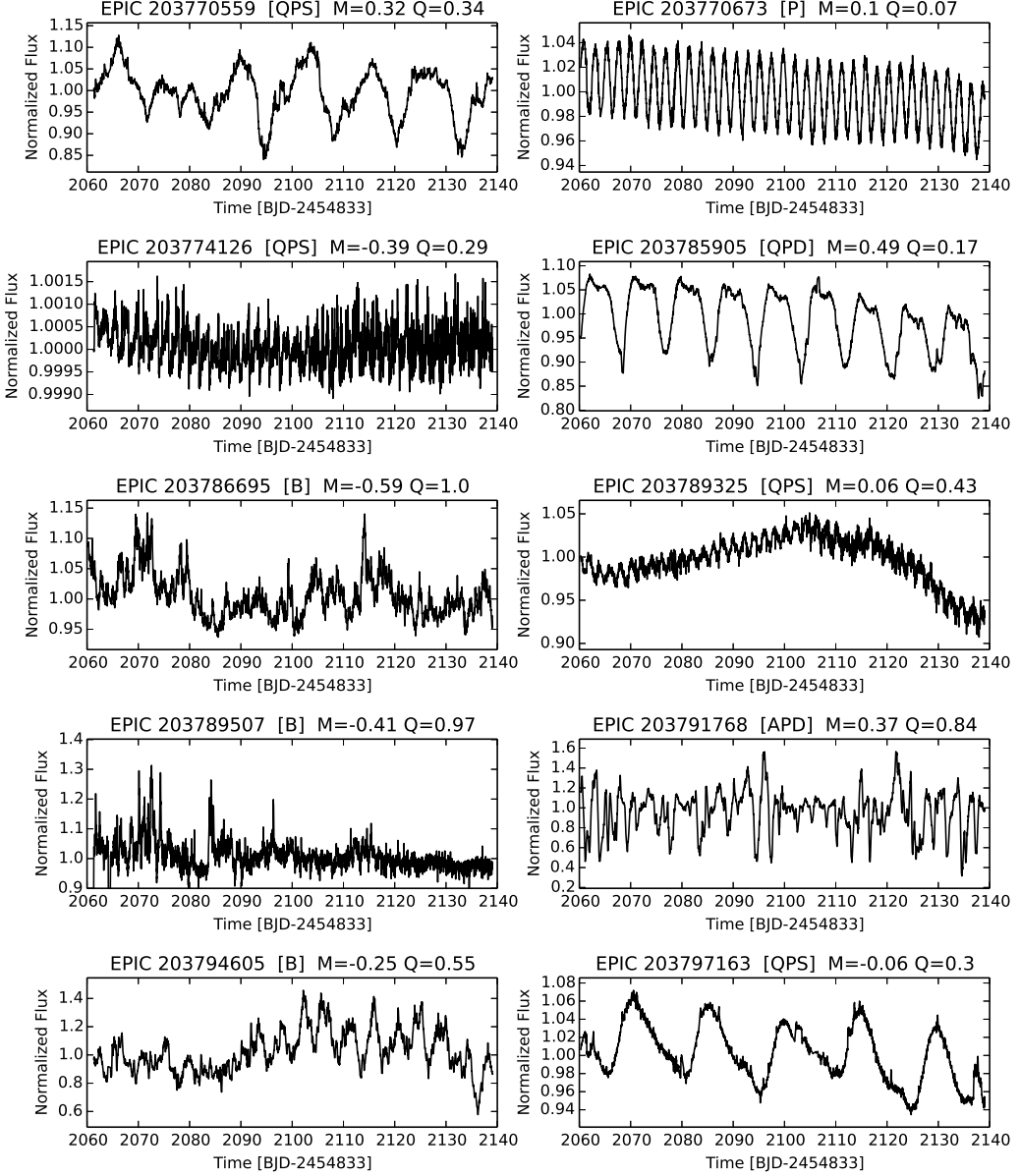


FIG. 14.— Cont.

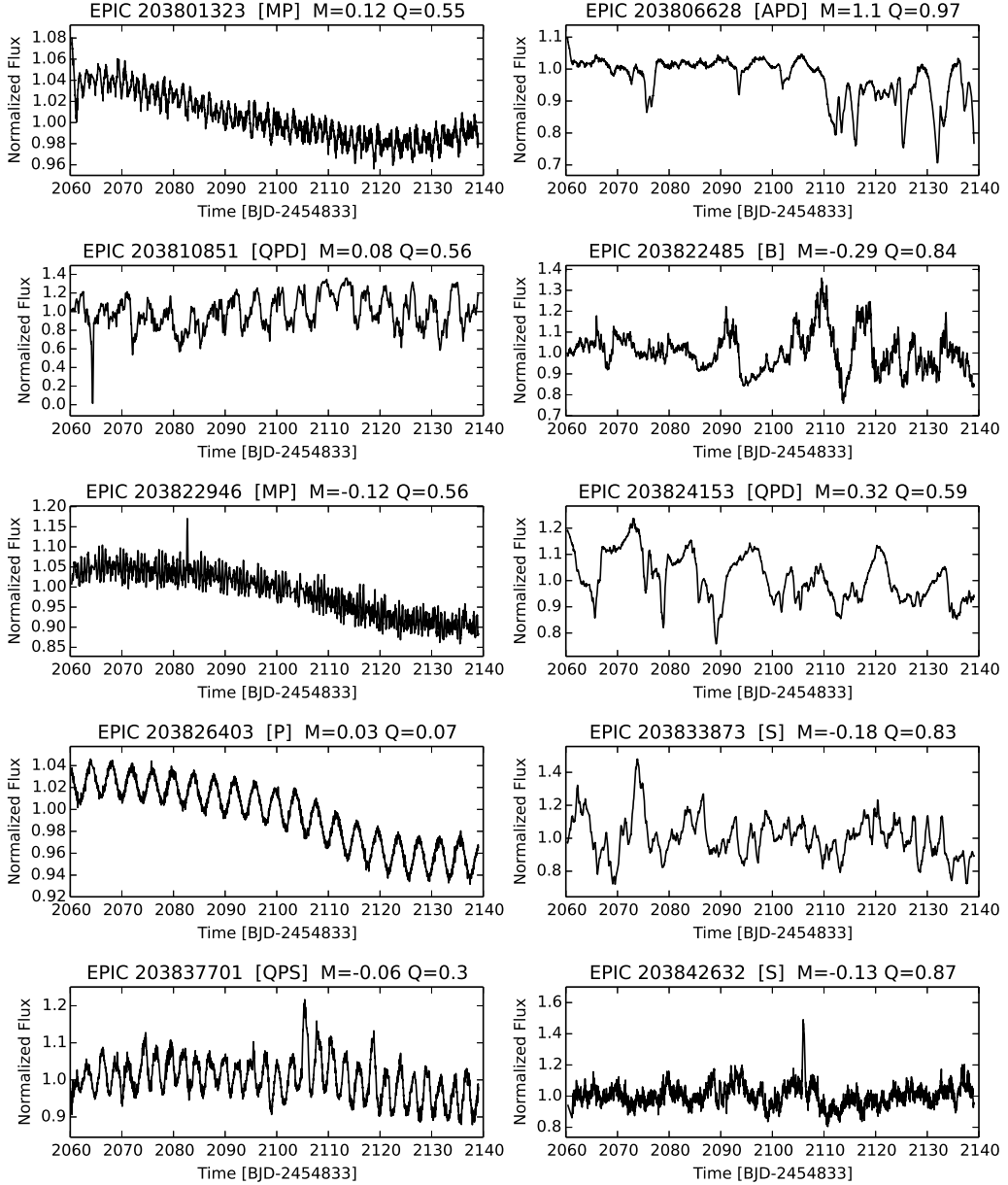


FIG. 14.— Cont.

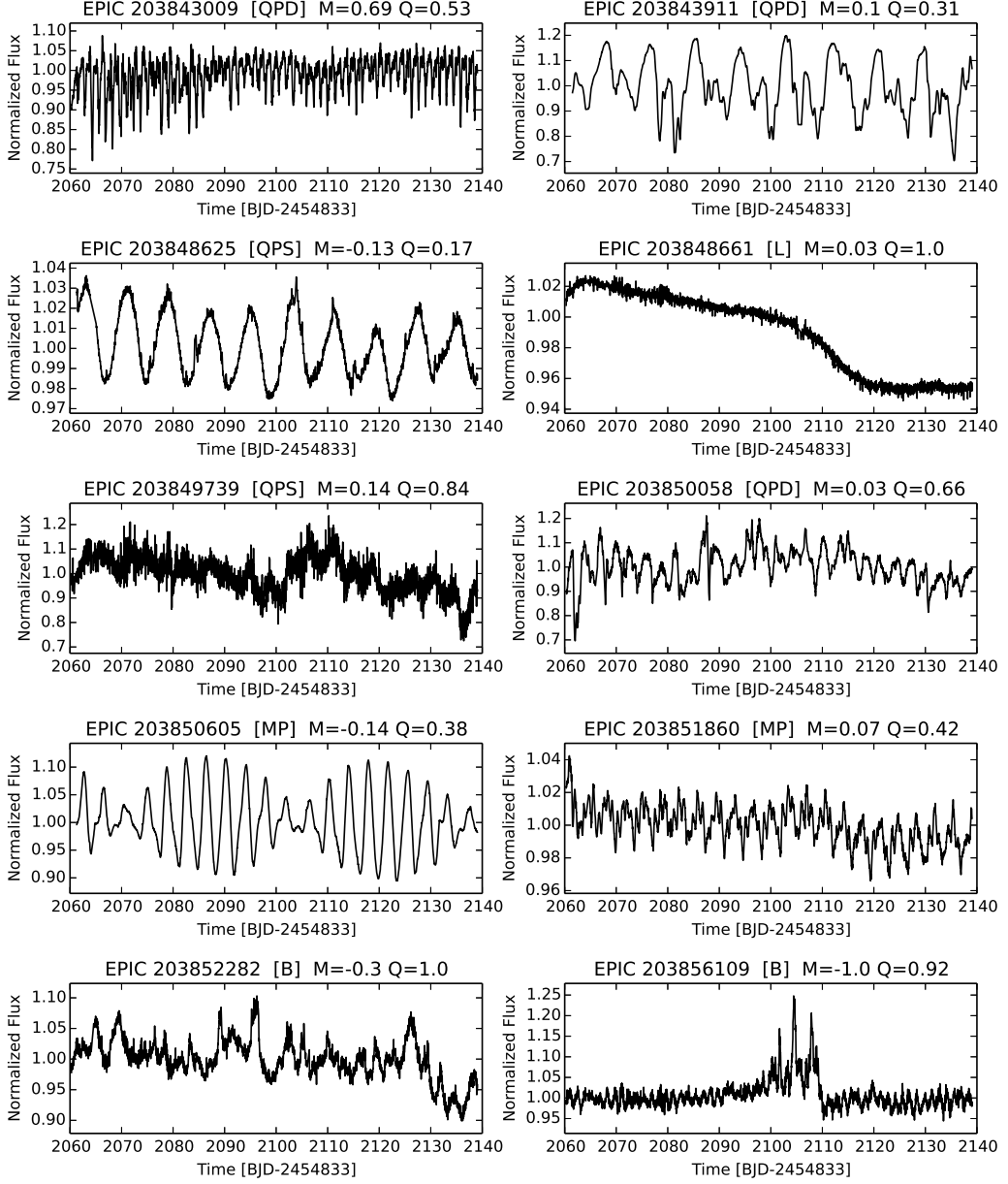


FIG. 14.— Cont.

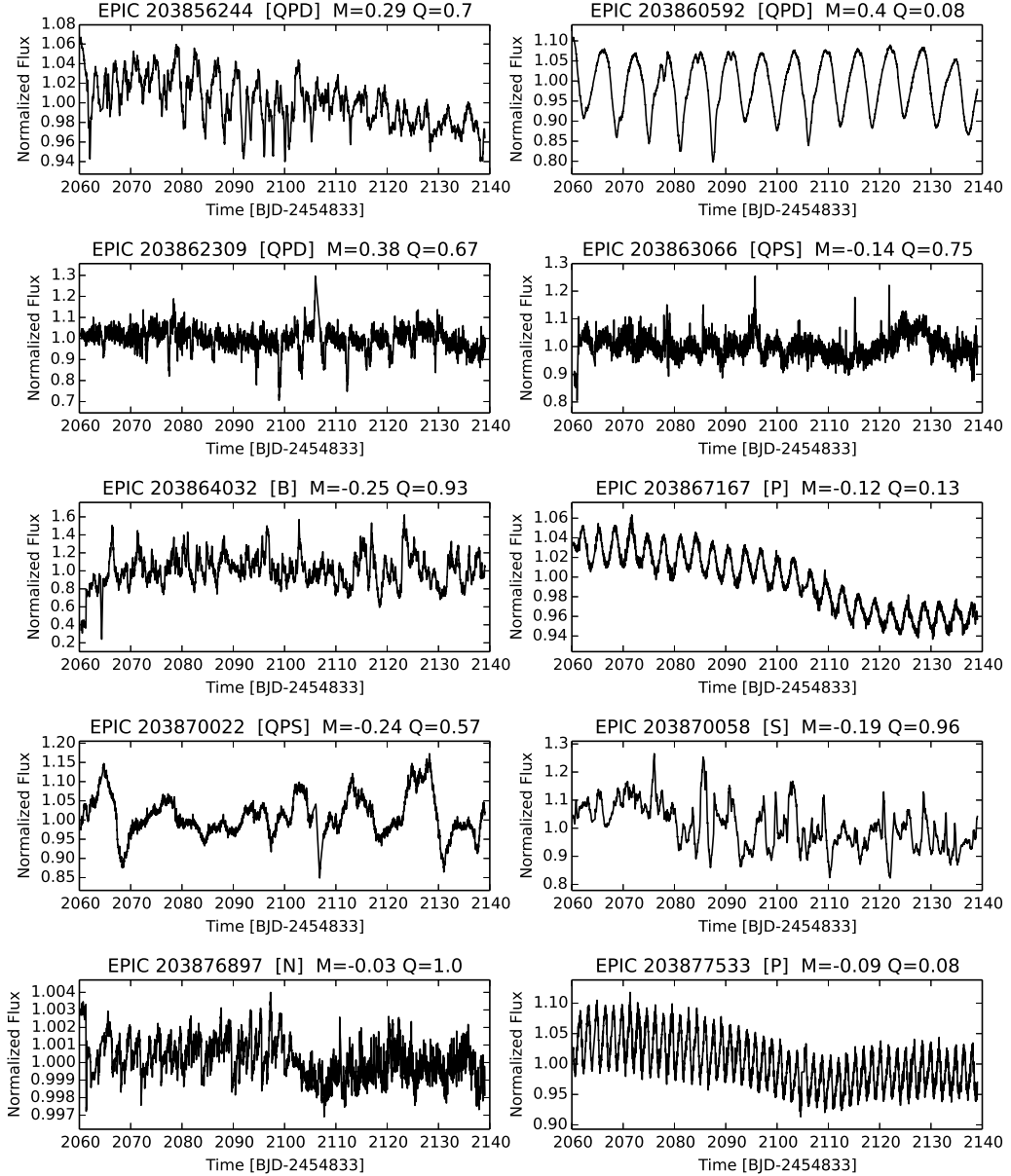


FIG. 14.— Cont.

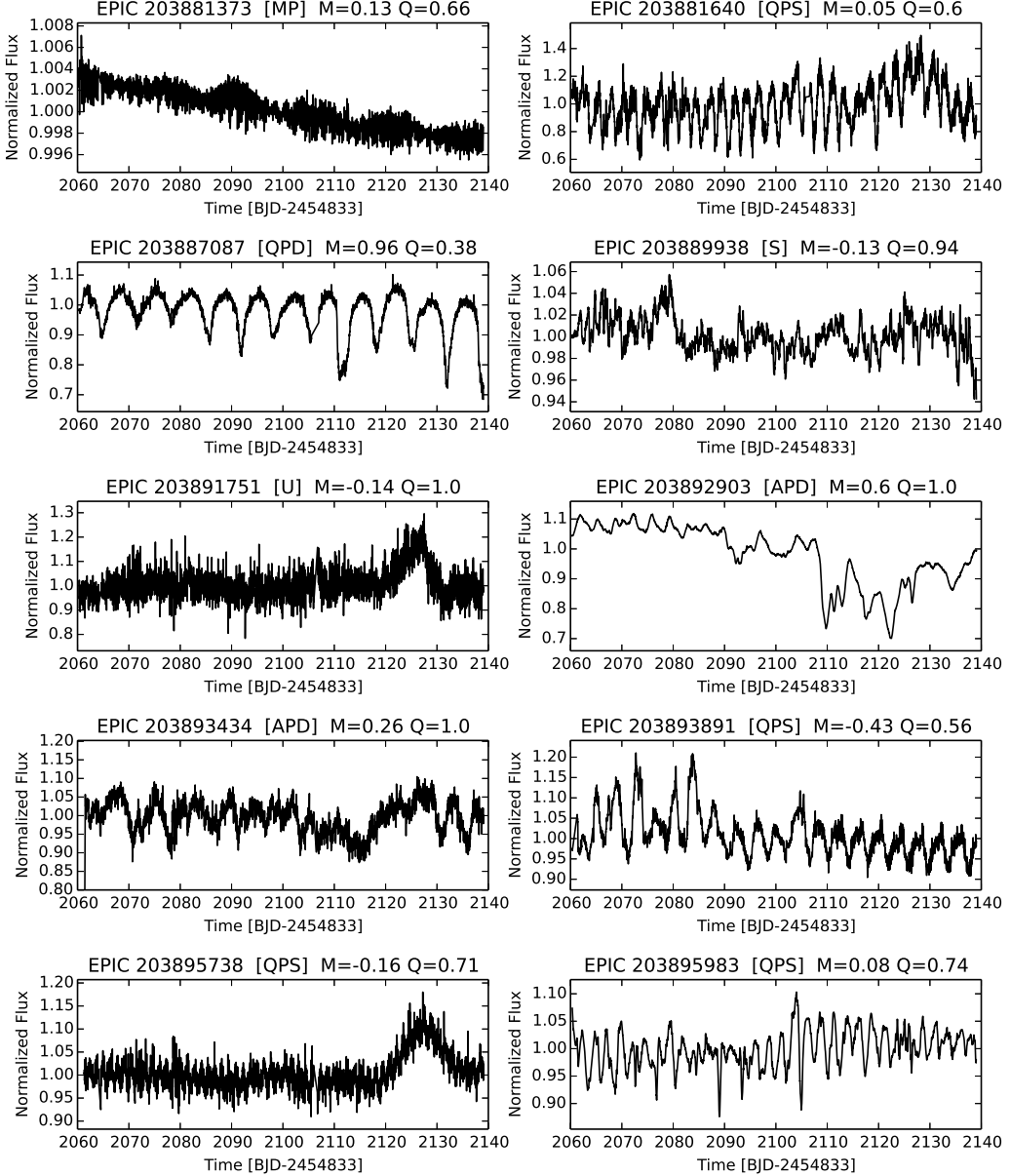


FIG. 14.— Cont.

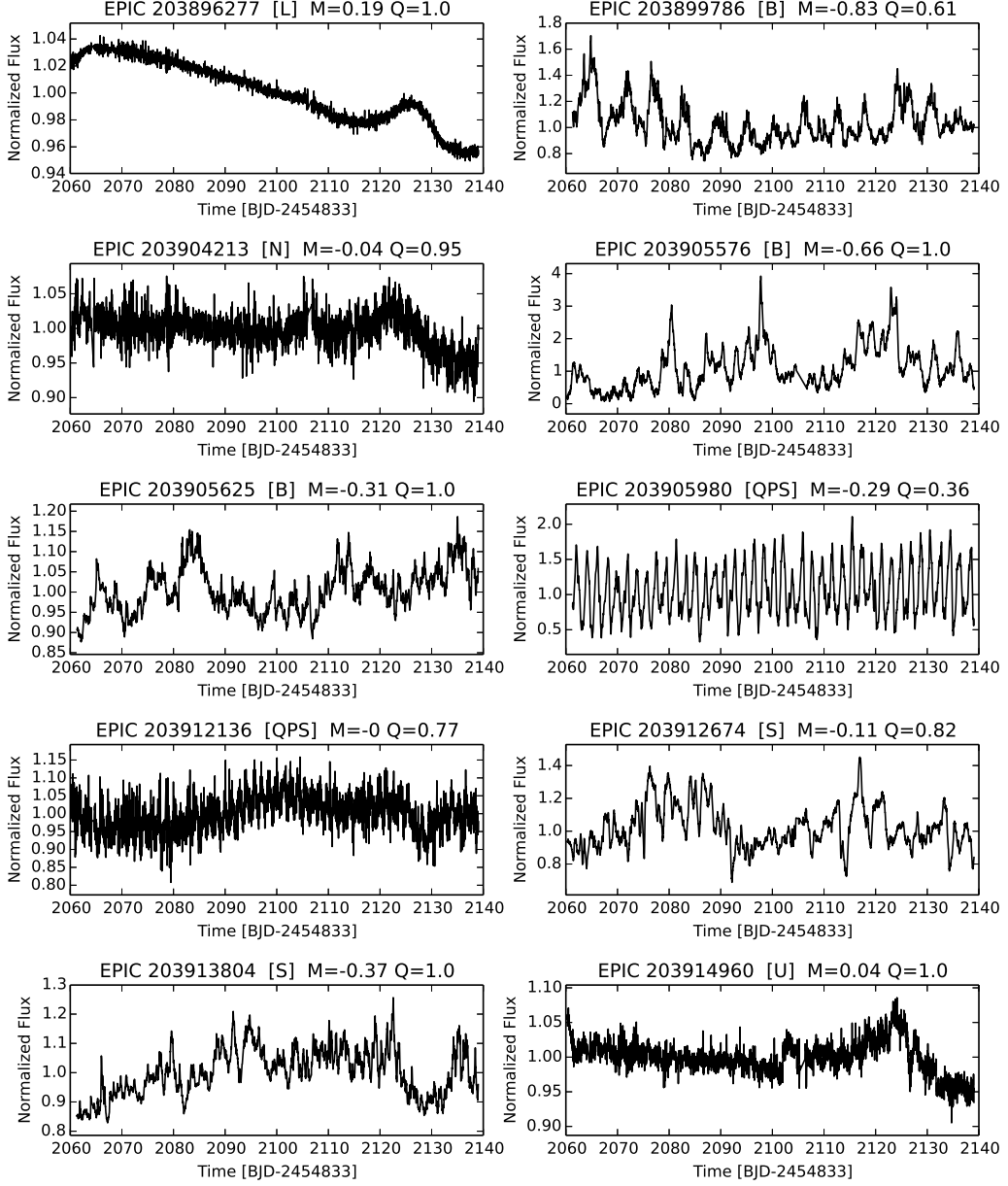


FIG. 14.— Cont.

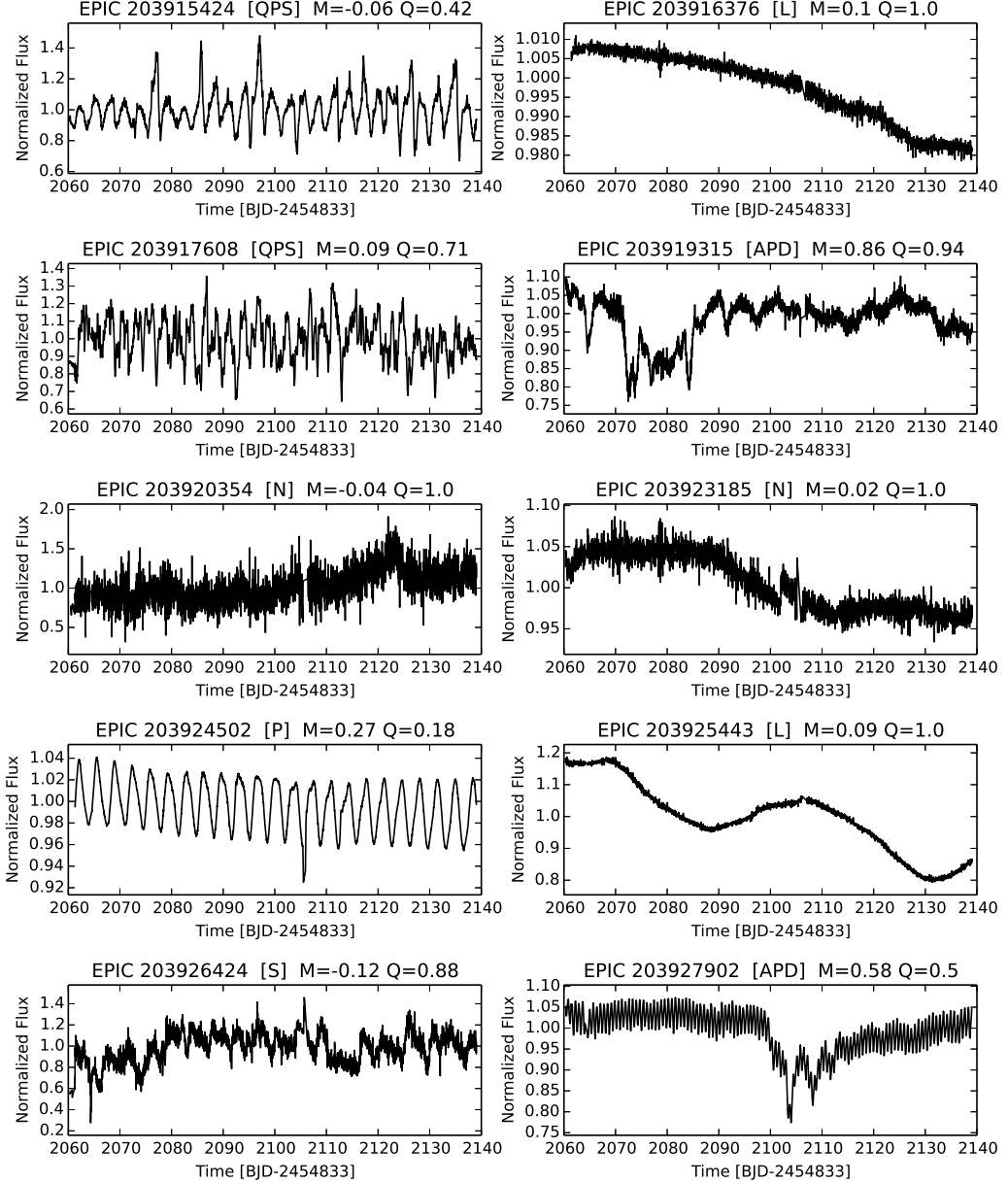


FIG. 14.— Cont.

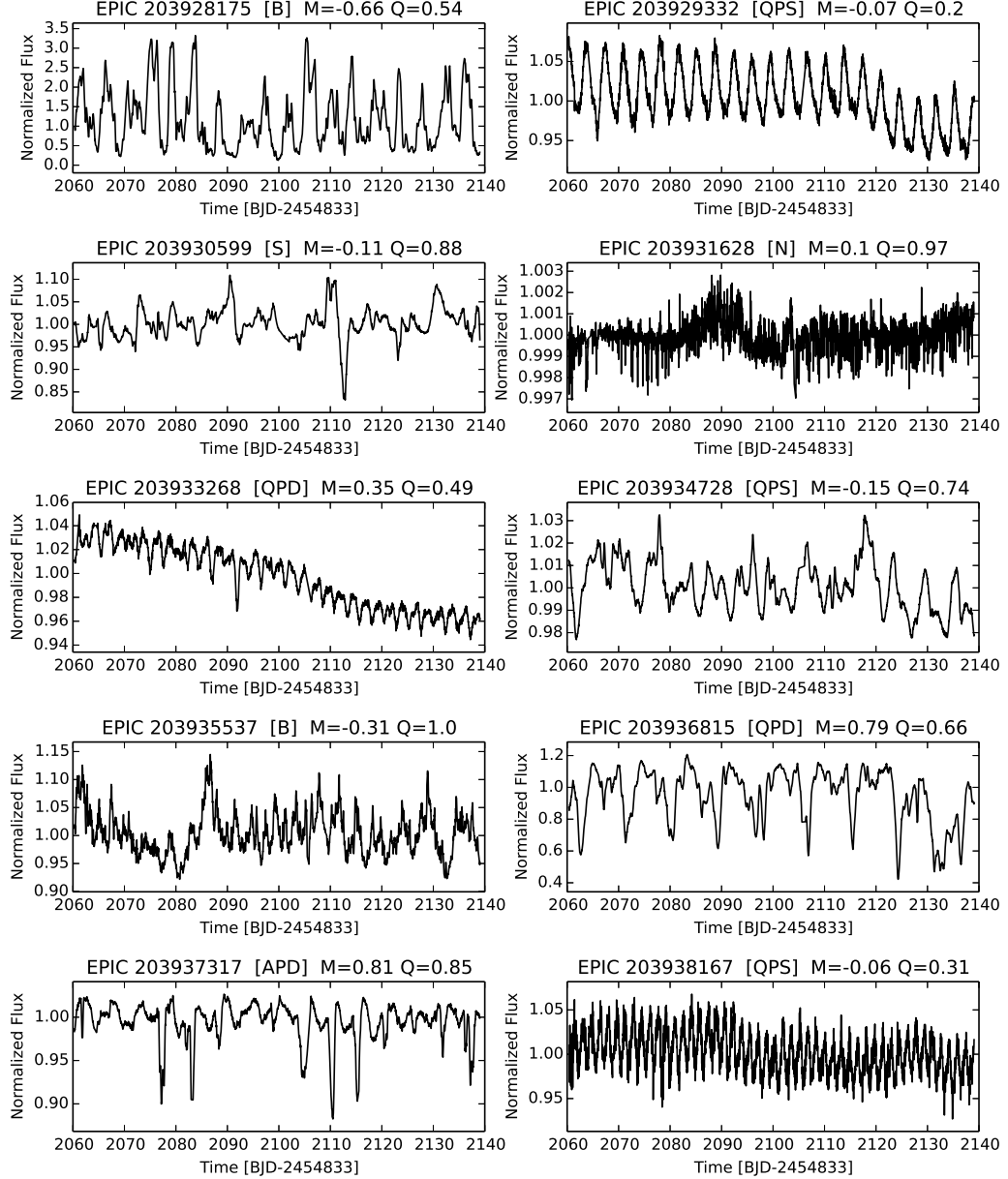


FIG. 14.— Cont.

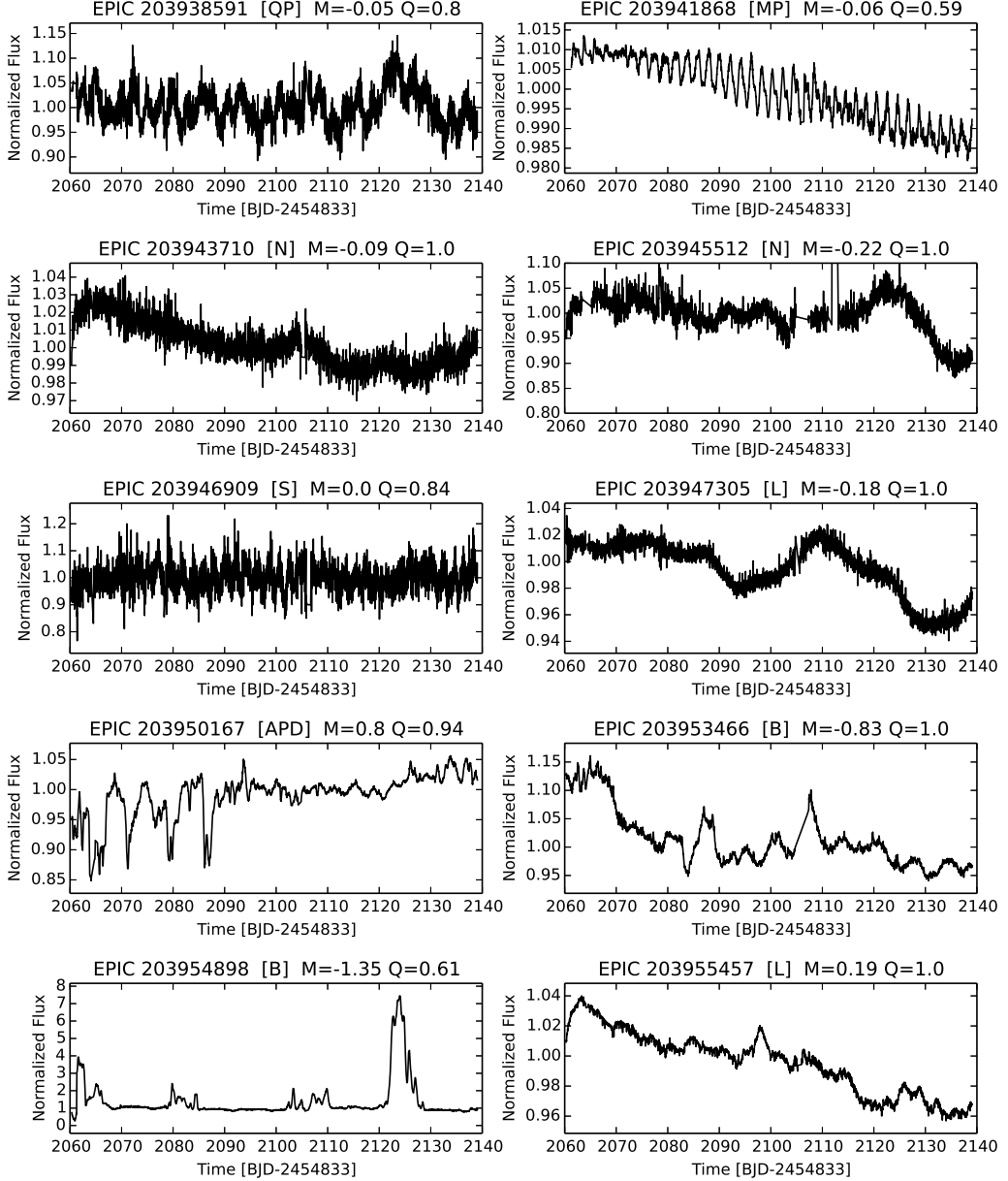


FIG. 14.— Cont.

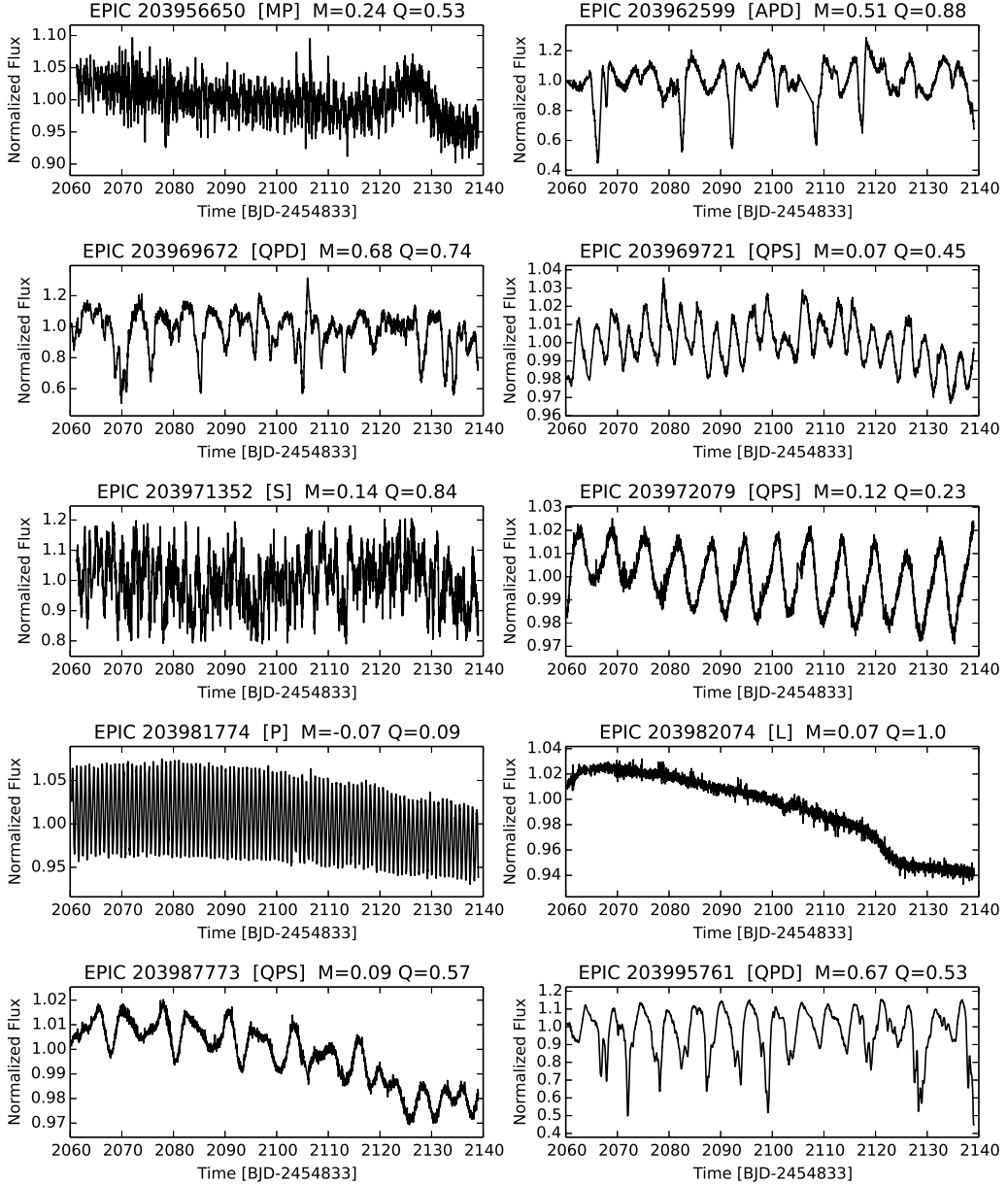


FIG. 14.— Cont.

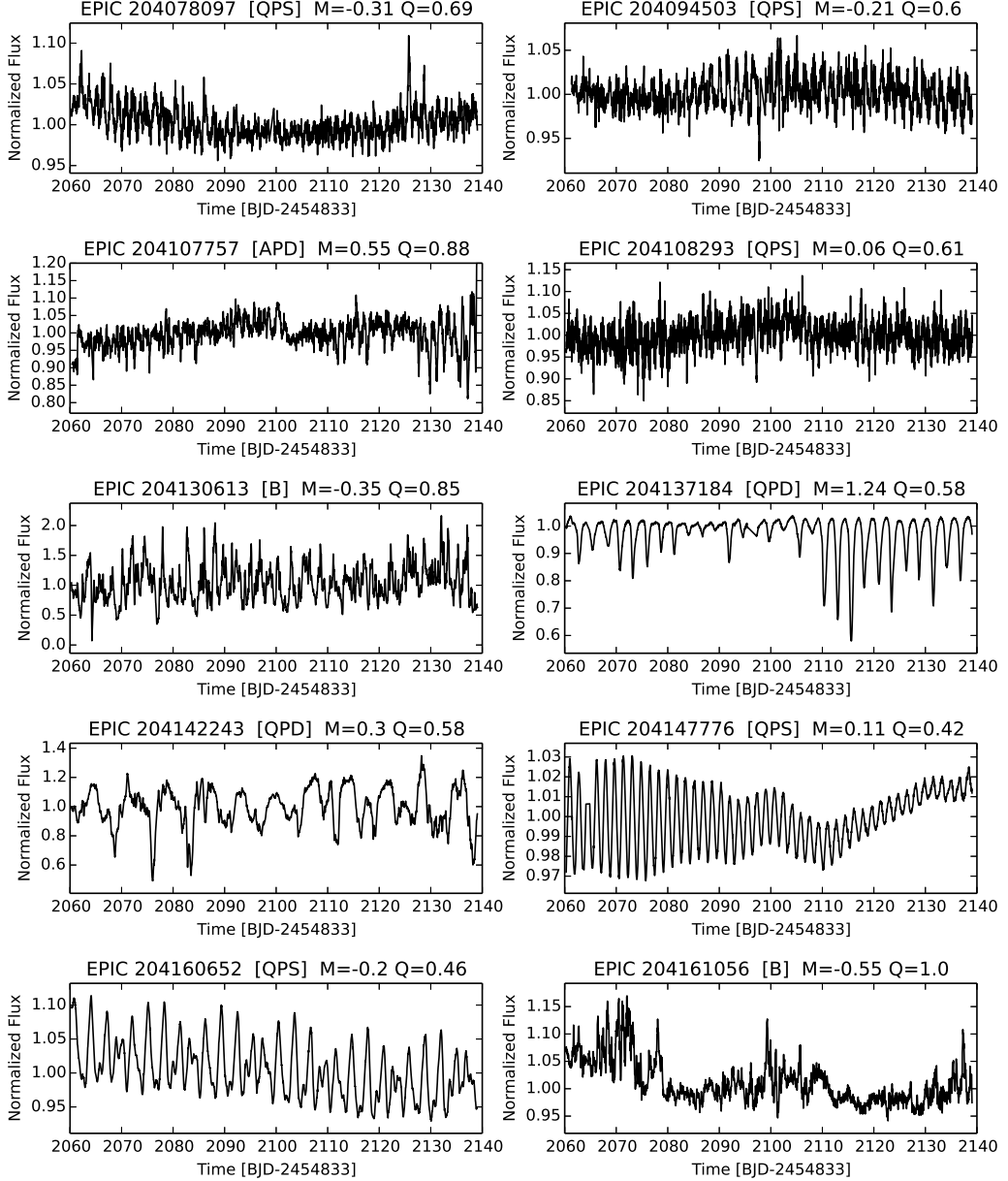


FIG. 14.— Cont.

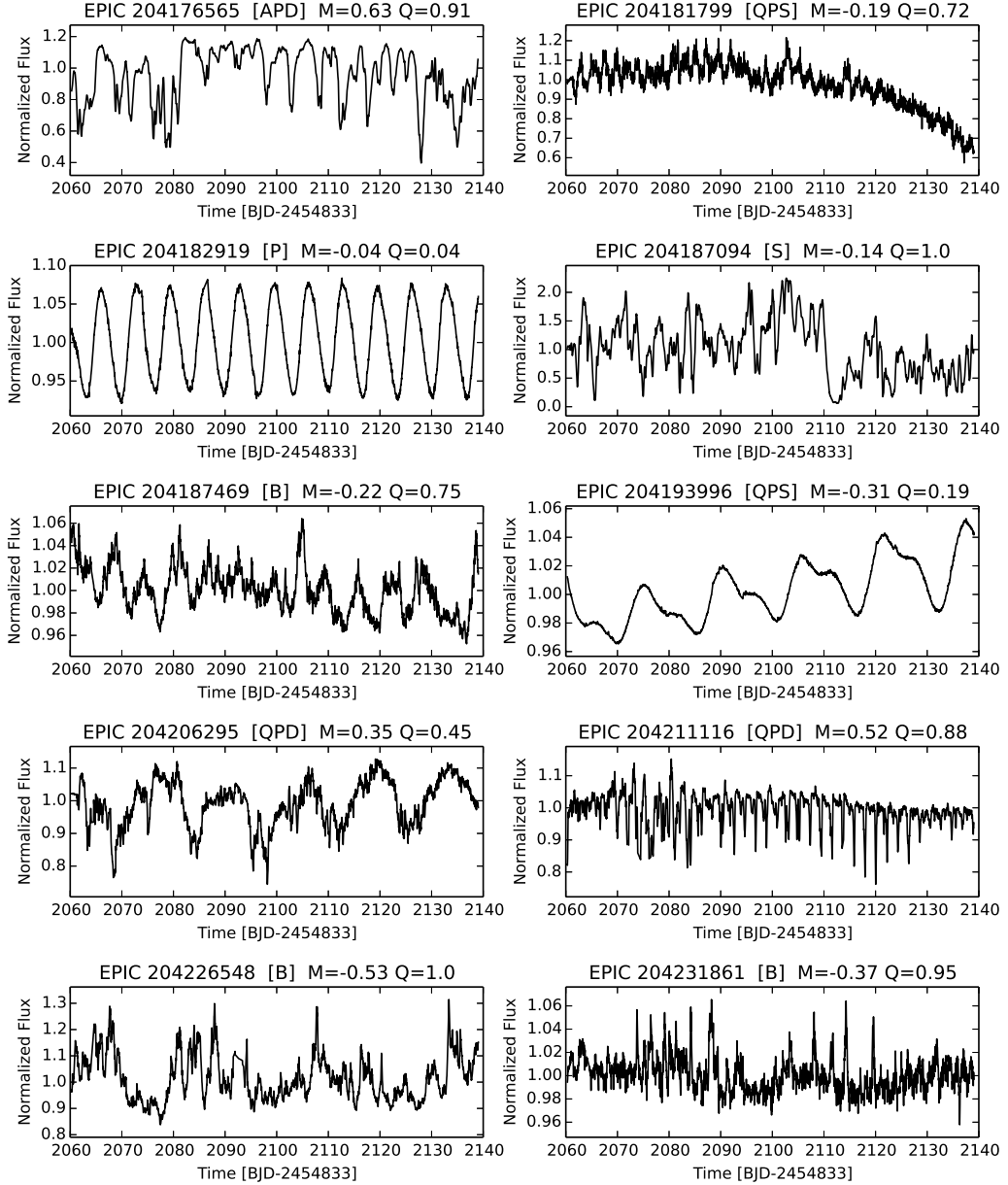


FIG. 14.— Cont.

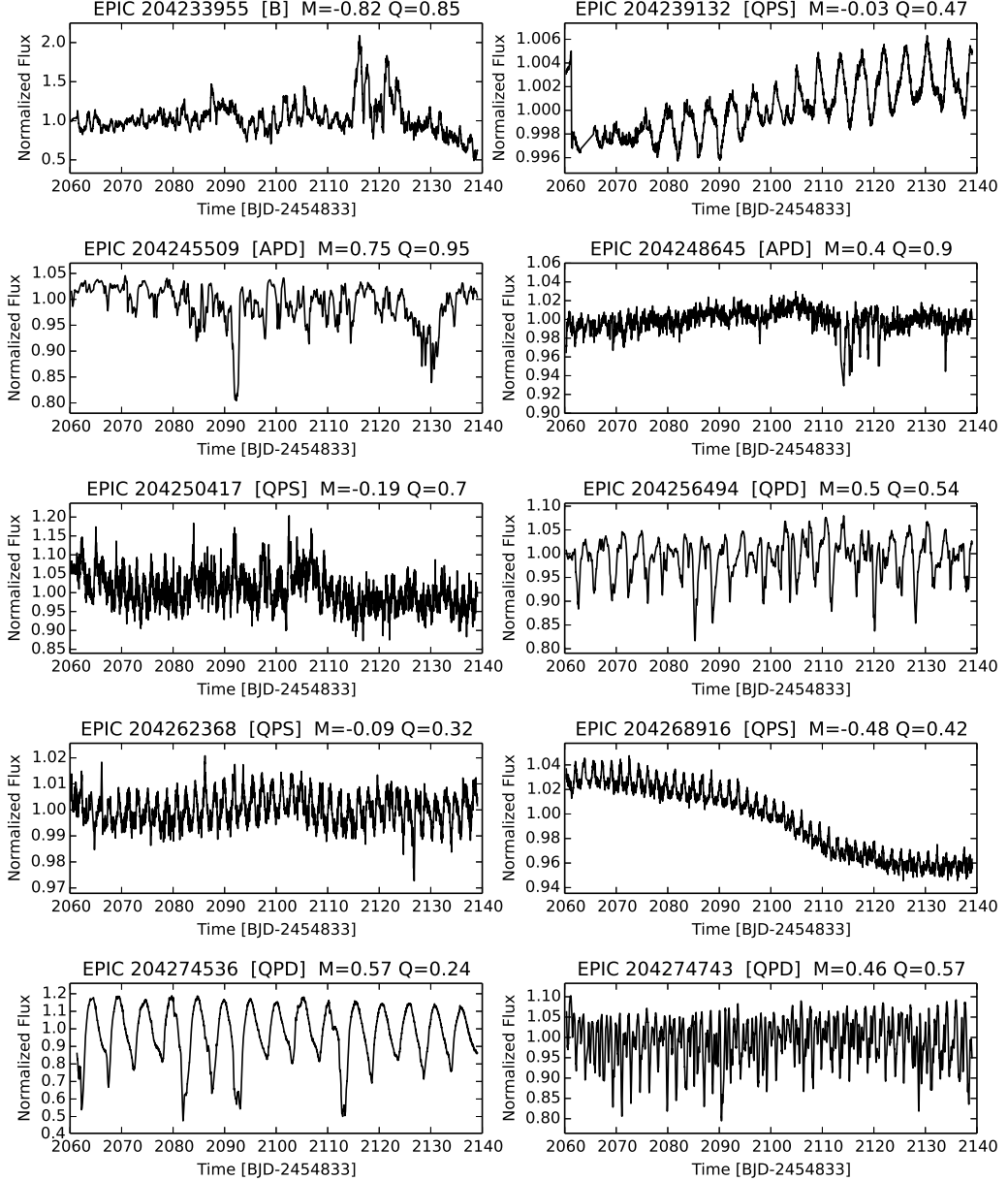


FIG. 14.— Cont.

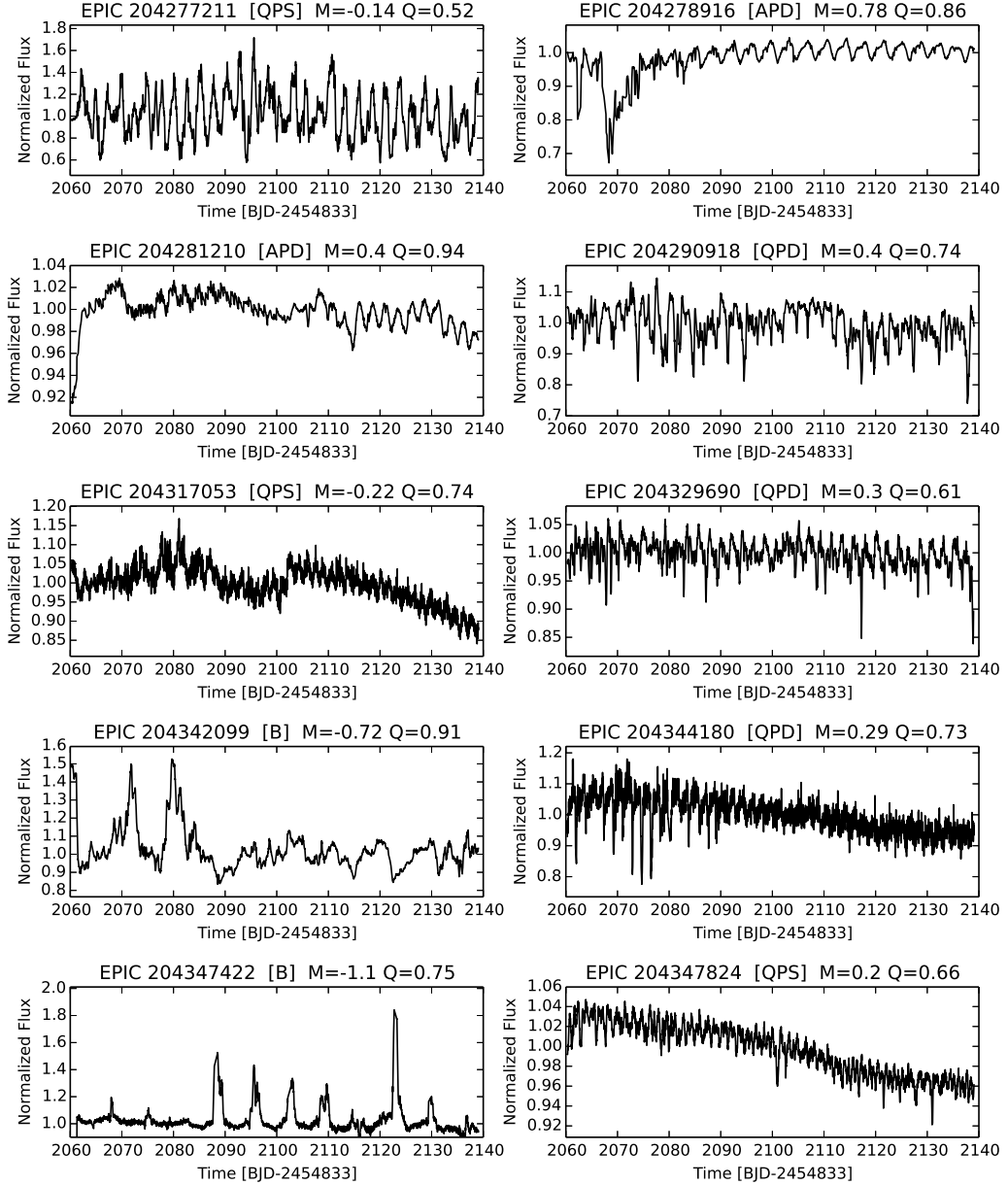


FIG. 14.— Cont.

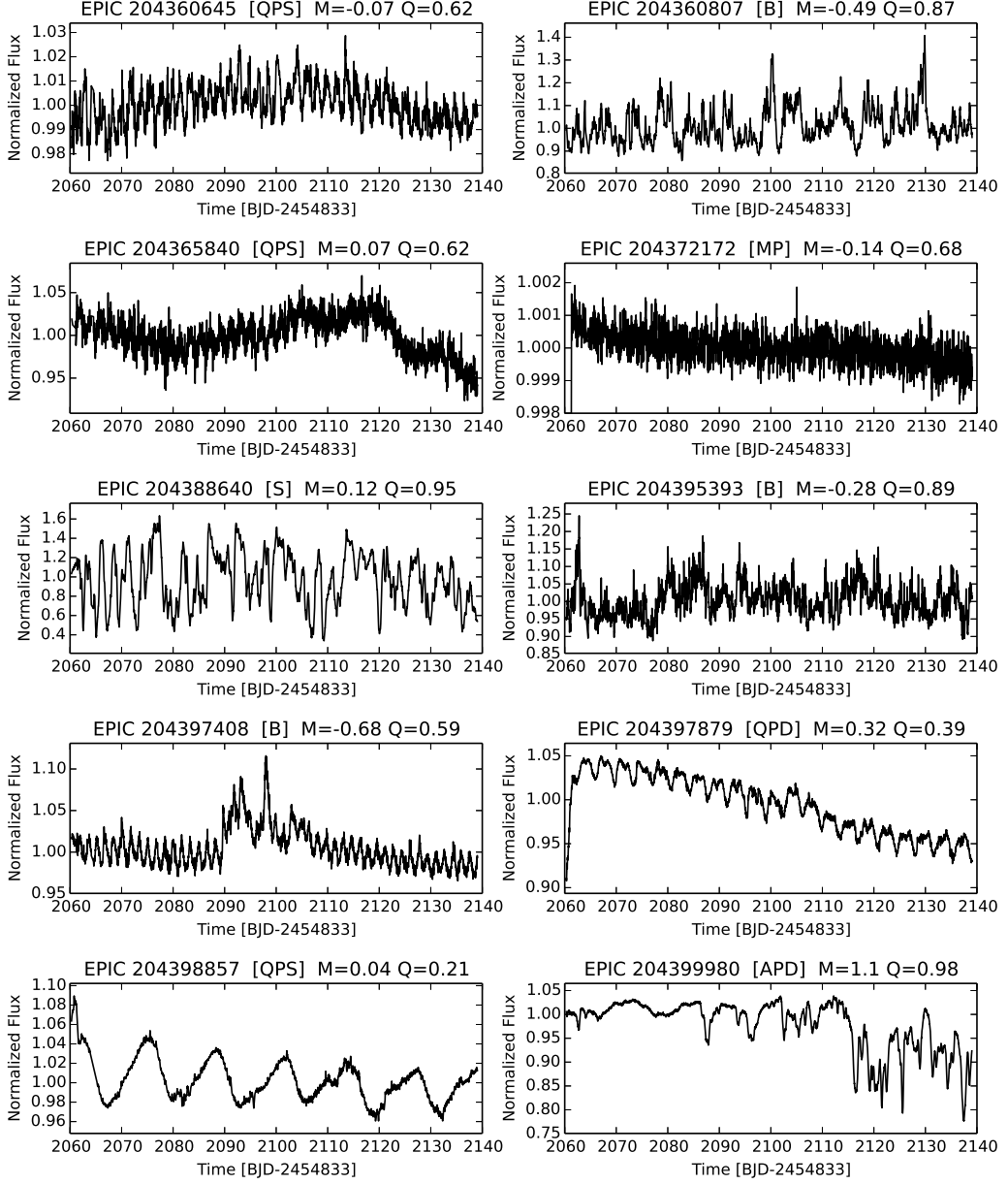


FIG. 14.— Cont.

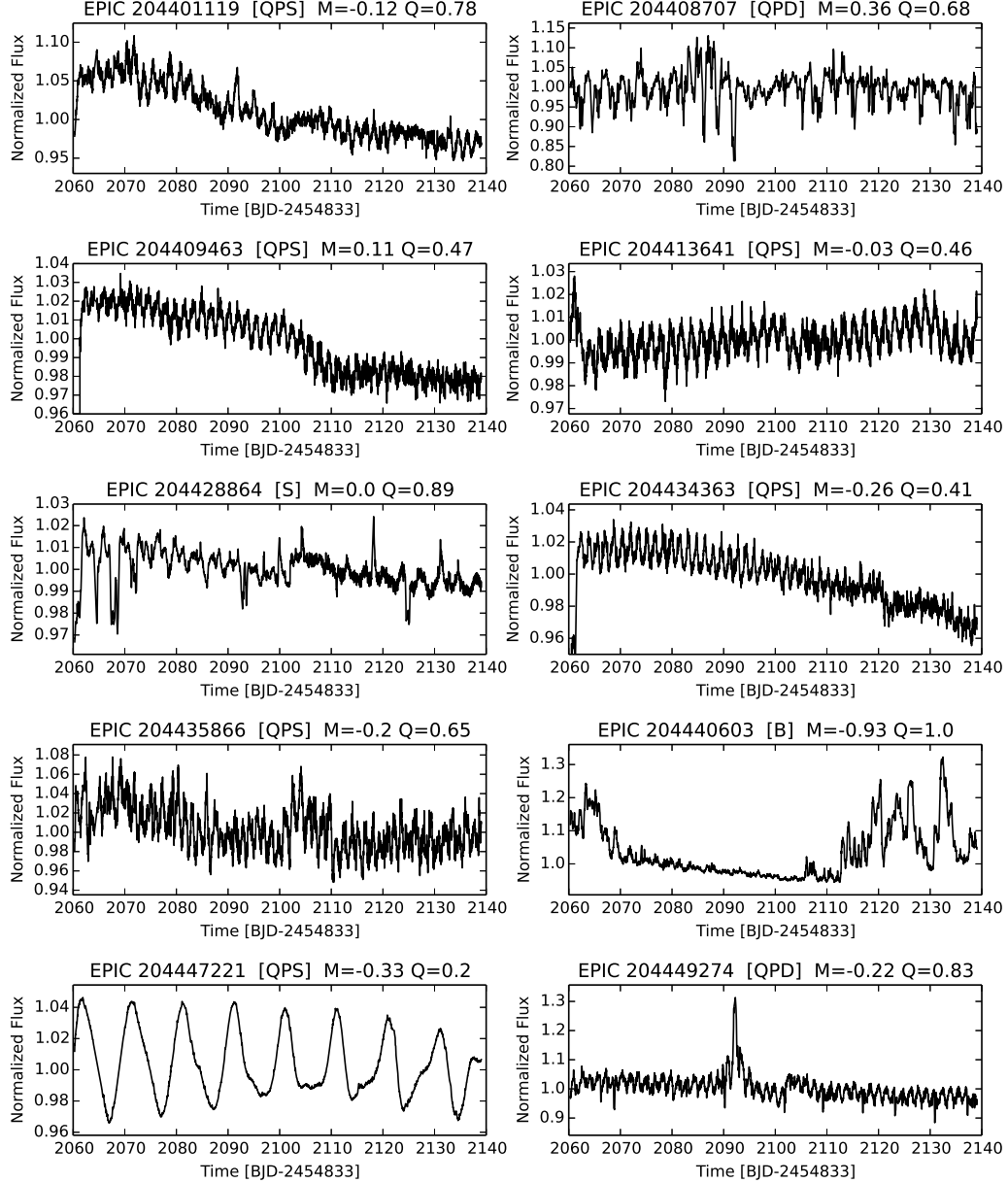


FIG. 14.— Cont.

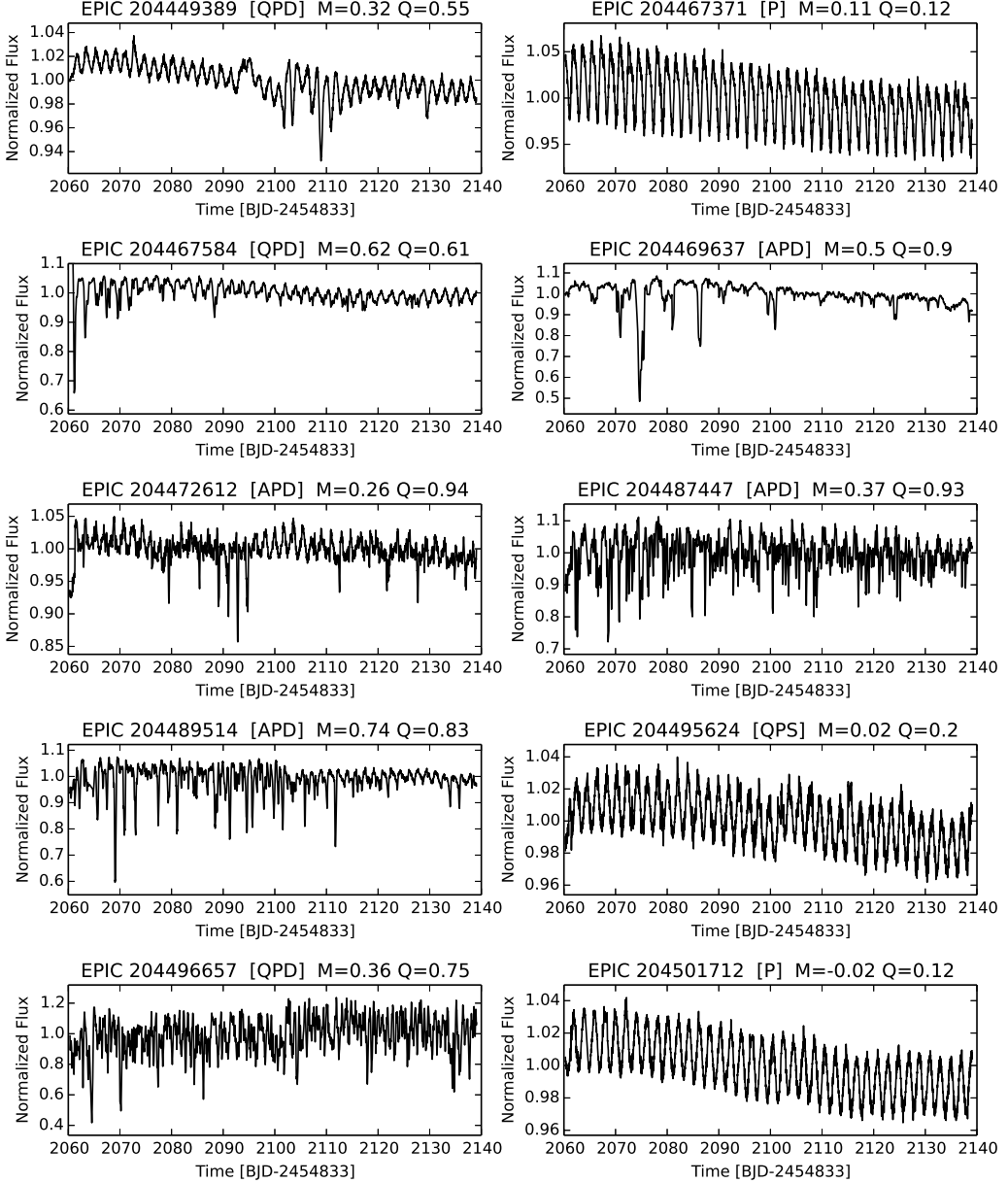


FIG. 14.— Cont.

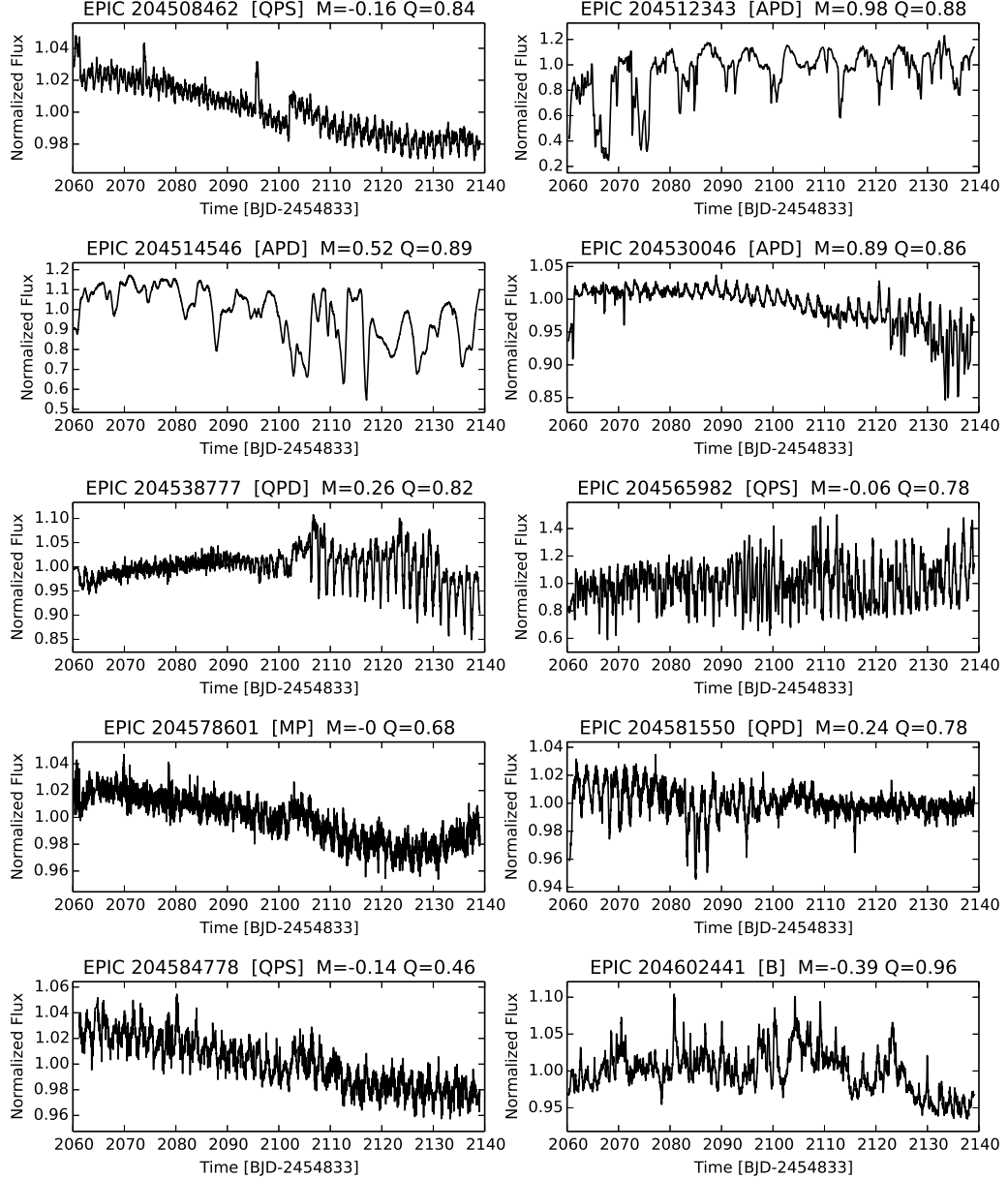


FIG. 14.— Cont.

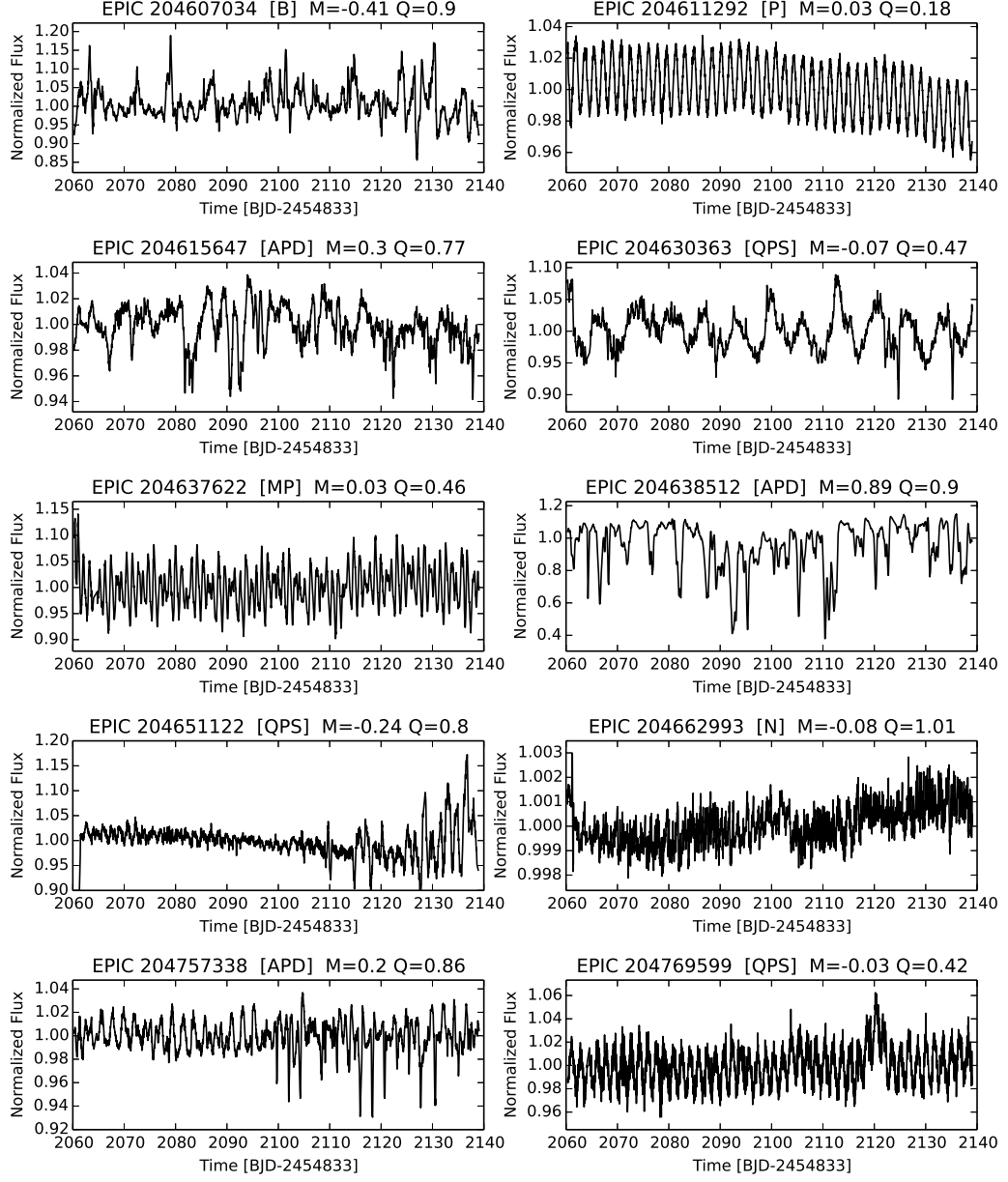


FIG. 14.— Cont.

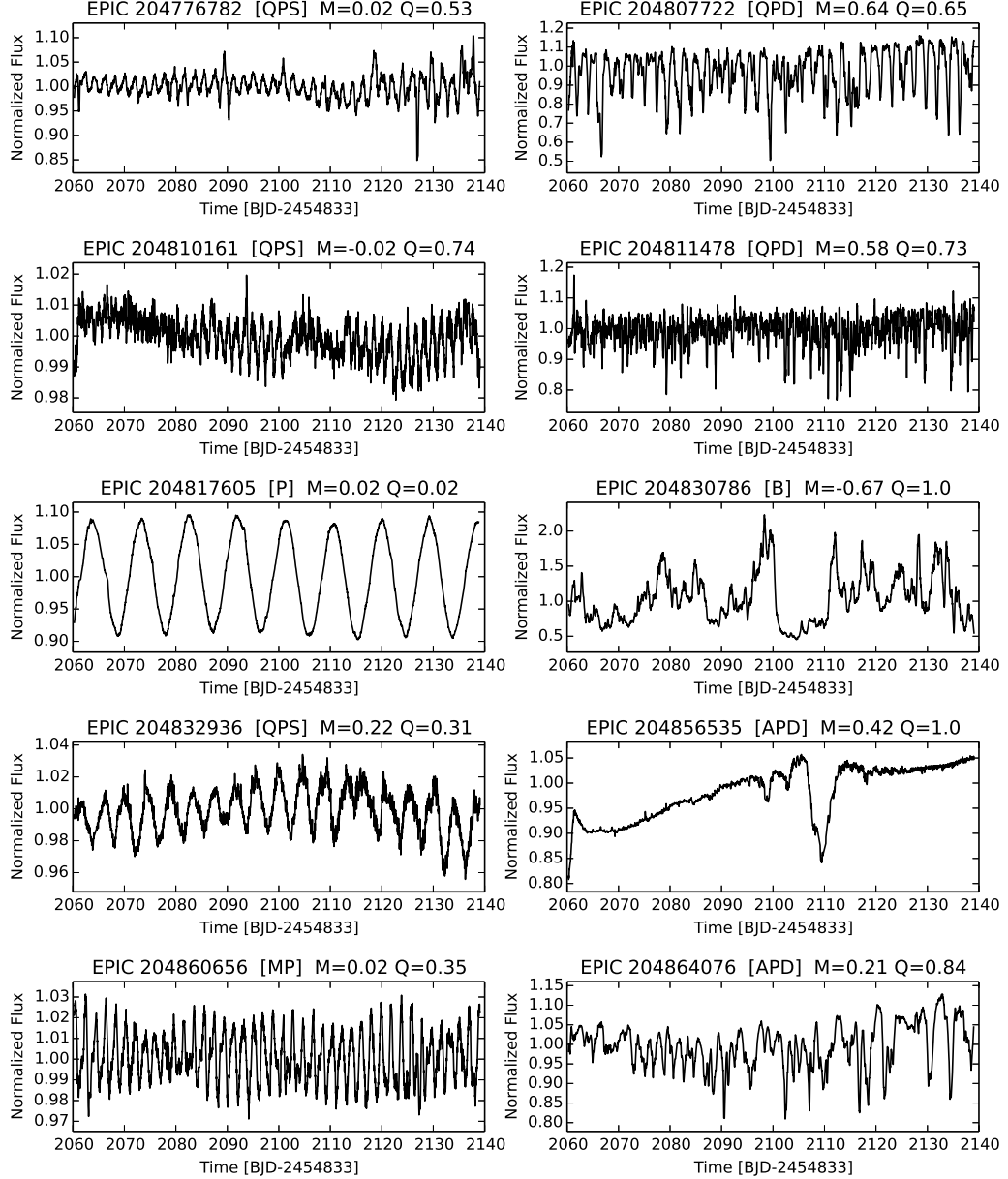


FIG. 14.— Cont.

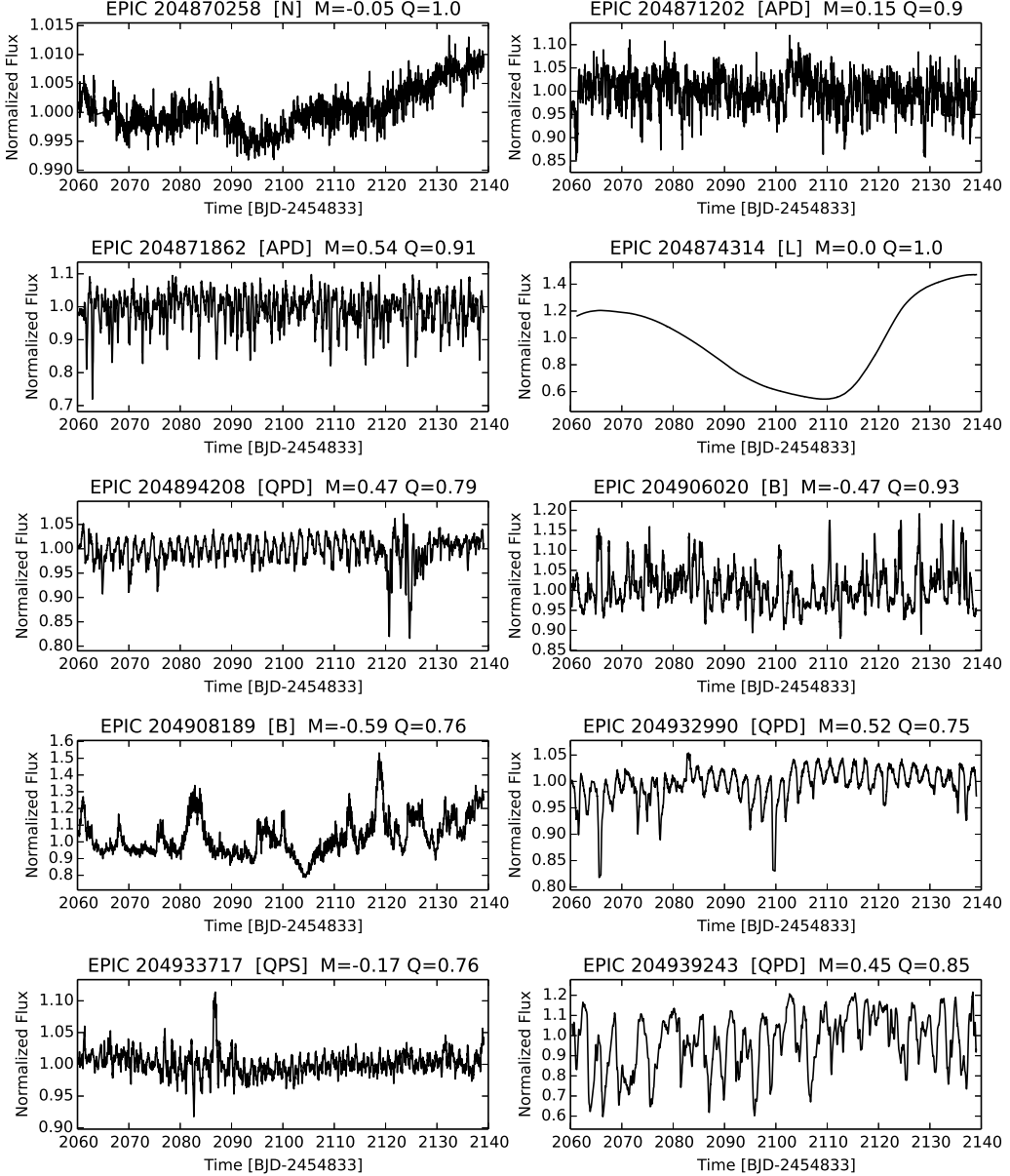


FIG. 14.— Cont.

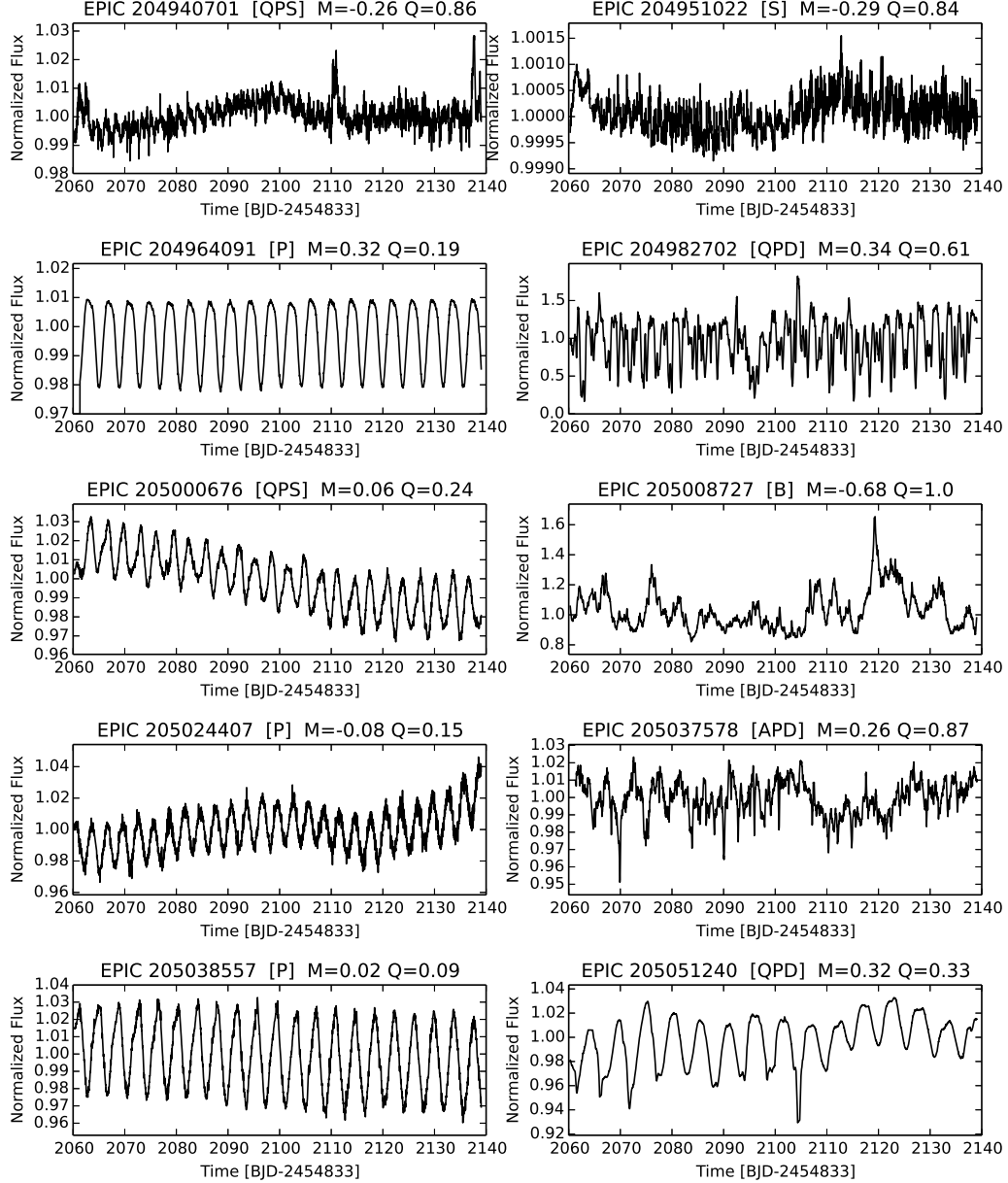


FIG. 14.— Cont.

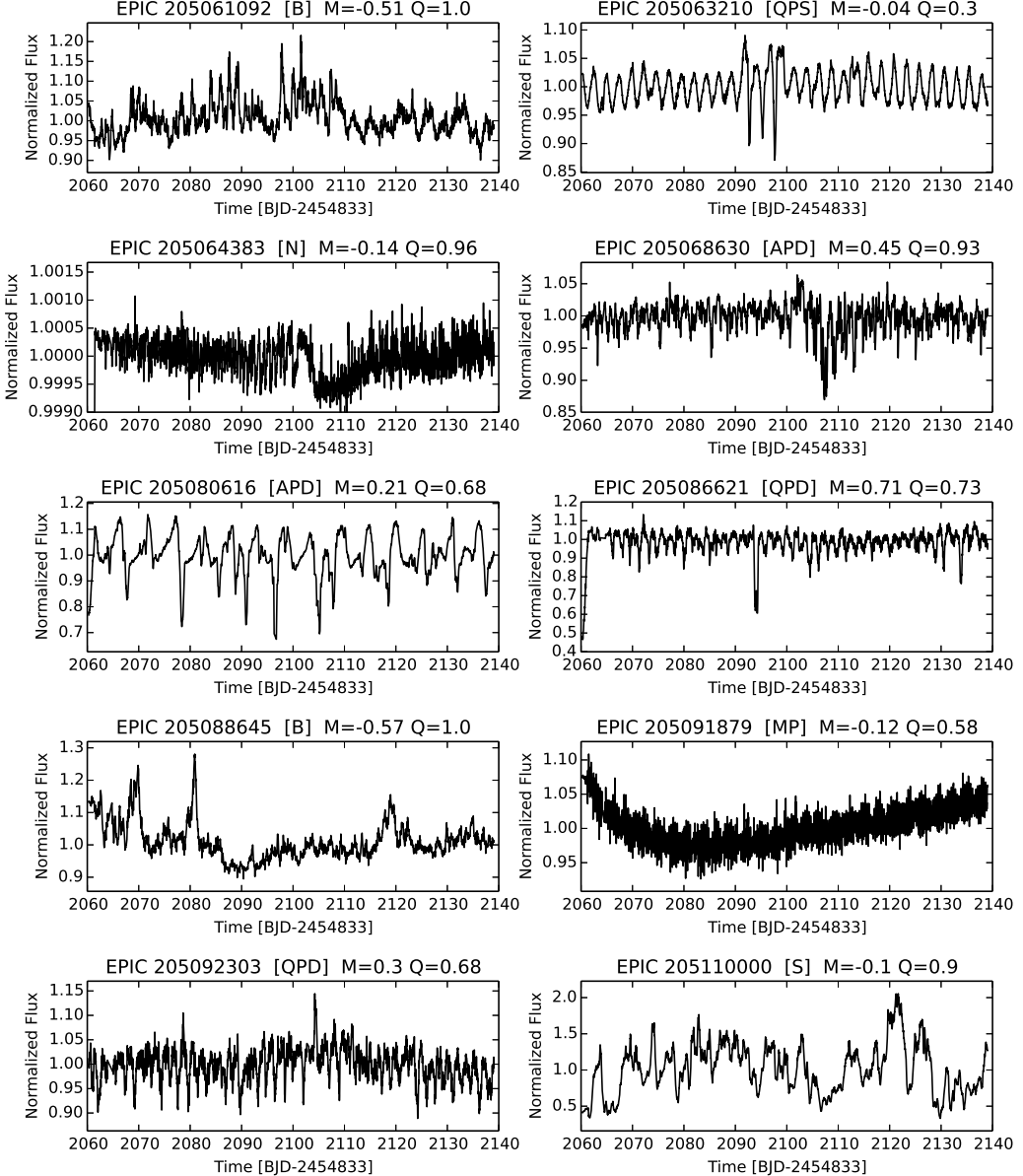


FIG. 14.— Cont.

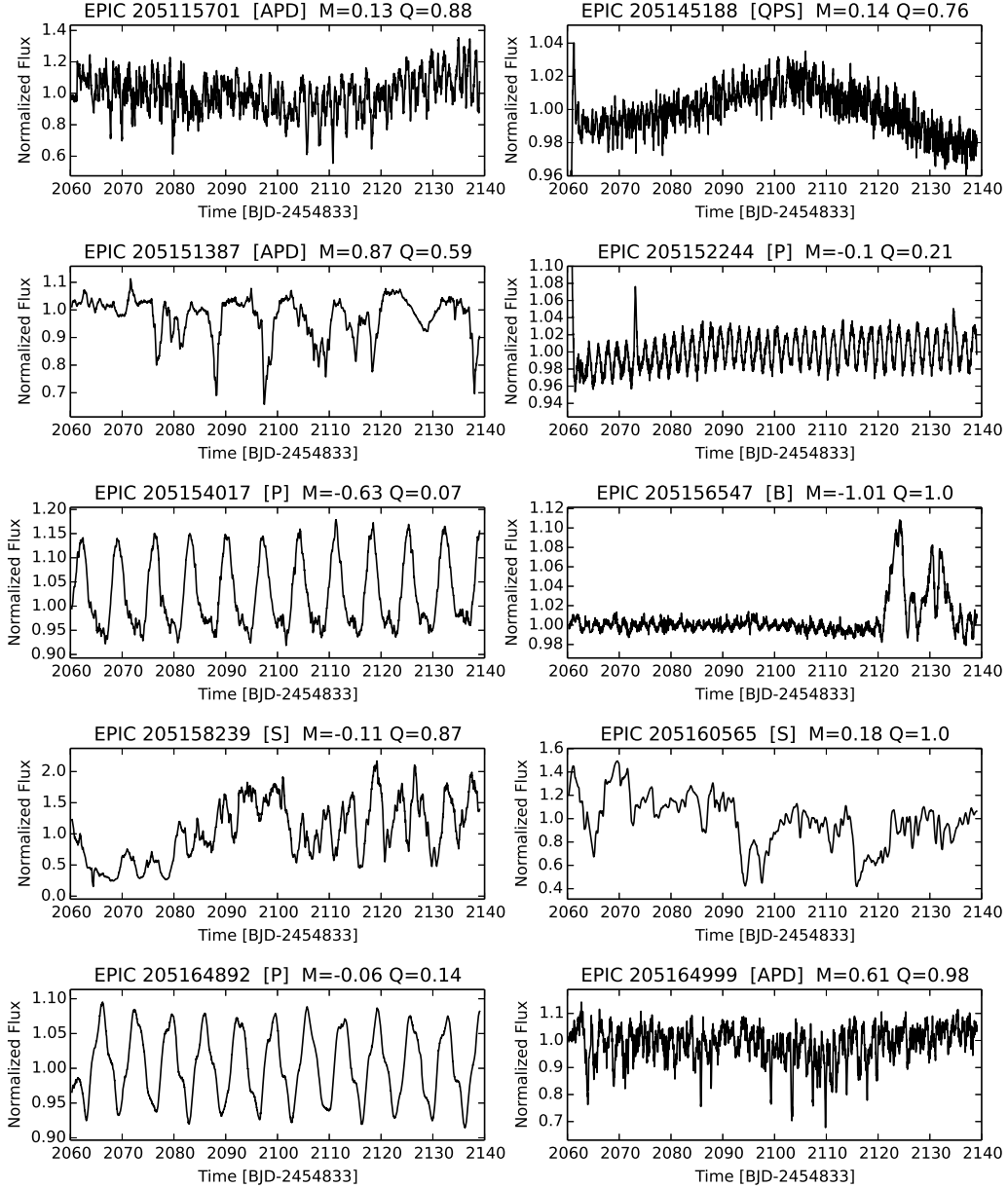


FIG. 14.— Cont.

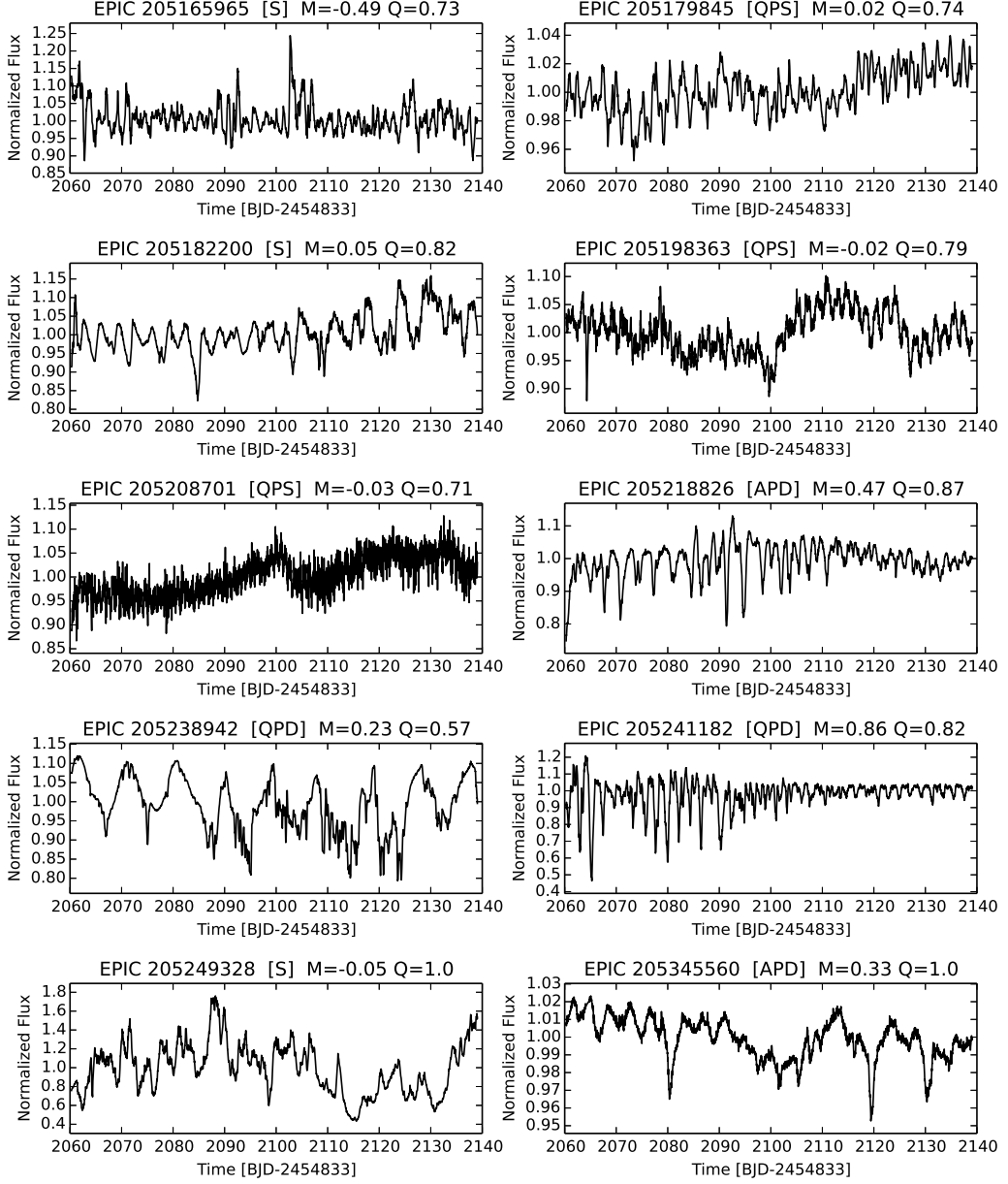


FIG. 14.— Cont.

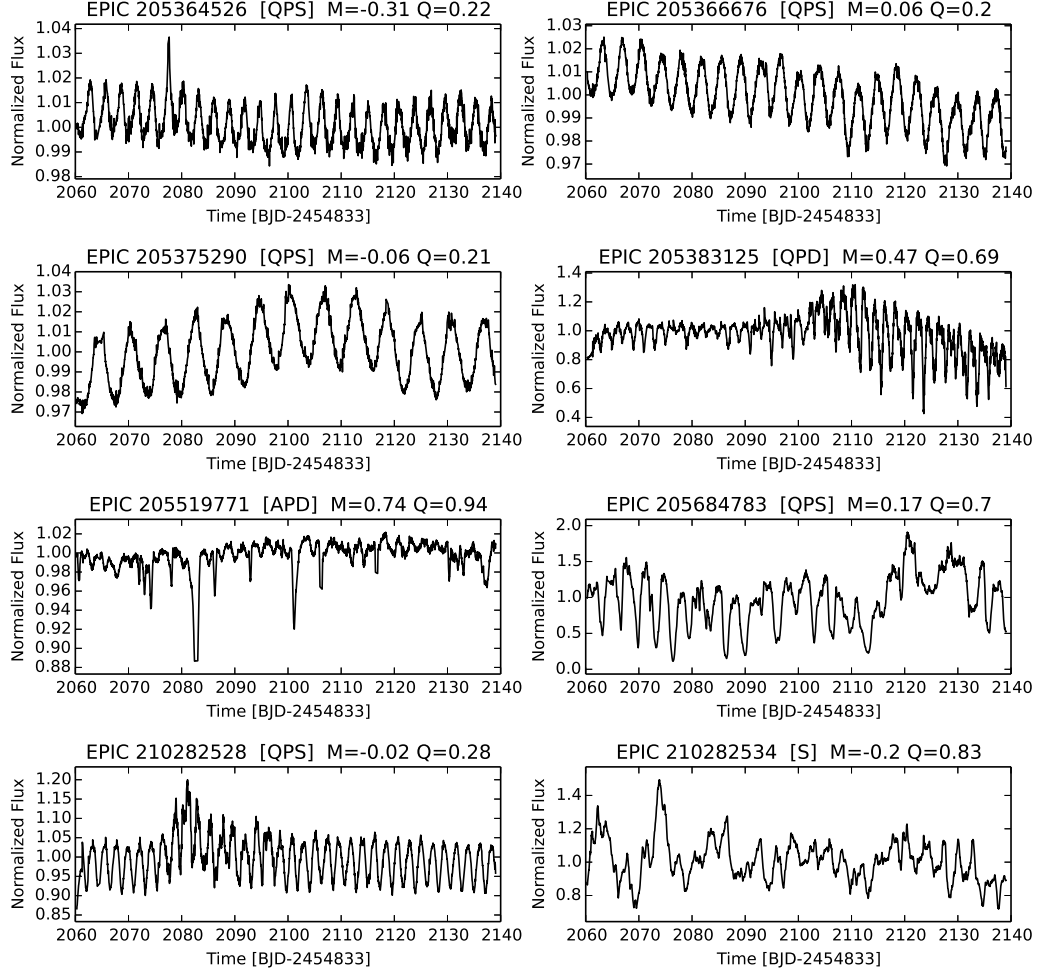


FIG. 14.— Cont.